Forschungszentrum Karlsruhe
in der Helmholtz-Gemeinschaft

Wissenschaftliche Berichte
FZKA 7075

Coupled Monte Carlo-Discrete Ordinates Computational Scheme for Three-Dimensional Shielding Calculations of Large and Complex Nuclear Facilities

Y. Chen

Institut für Rektorsicherheit
Programm Kernfusion

April 2005

Forschungszentrum Karlsruhe

in der Helmholtz-Gemeinschaft

Wissenschaftliche Berichte

FZKA 7075

Coupled Monte Carlo-Discrete Ordinates Computational Scheme for Three-Dimensional Shielding Calculations of Large and Complex Nuclear Facilities*

Yixue Chen

Institut für Reaktorsicherheit

Programm Kernfusion

* Von der Fakultät für Maschinenbau
der Universität Karlsruhe (TH)
genehmigte Dissertation

Forschungszentrum Karlsruhe GmbH, Karlsruhe

2005

Impressum der Print-Ausgabe:

Als Manuskript gedruckt

Forschungszentrum Karlsruhe GmbH
Postfach 3640, 76021 Karlsruhe

Mitglied der Hermann von Helmholtz-Gemeinschaft
Deutscher Forschungszentren (HGF)

ISSN 0947-8620

urn:nbn:de:0005-070752

Coupled Monte Carlo-Discrete Ordinates Computational Scheme for Three-Dimensional Shielding Calculations of Large and Complex Nuclear Facilities

Zur Erlangung des akademischen Grades eines

Doktors der Ingenieurwissenschaften

von der Fakultät für Maschinenbau der Universität Karlsruhe (TH)

genehmigte

Dissertation

von

Yixue Chen, M.S.

aus Shandong (V.R. China)

Tag der mündlichen Prüfung:	21.12.2004
Hauptreferent:	Prof. Dr.rer.nat. Dr.h.c. Dan G. Cacuci
Korreferent:	Prof. Dr. Edith Borie

Coupled Monte Carlo-Discrete Ordinates Computational Scheme for Three-Dimensional Shielding Calculations of Large and Complex Nuclear Facilities

Abstract

Shielding calculations of advanced nuclear facilities such as accelerator based neutron sources or fusion devices of the tokamak type are complicated due to their complex geometries and their large dimensions, including bulk shields of several meters thickness. While the complexity of the geometry in the shielding calculation can be hardly handled by the discrete ordinates method, the deep penetration of radiation through bulk shields is a severe challenge for the Monte Carlo particle transport simulation technique. This work proposes a dedicated computational approach for coupled Monte Carlo – deterministic transport calculations to handle this kind of shielding problems. The Monte Carlo technique is used to simulate the particle generation and transport in the target region with both complex geometry and reaction physics, and the discrete ordinates method is used to treat the deep penetration problem in the bulk shield.

To enable the coupling of these two different computational methods, a mapping approach has been developed for calculating the discrete ordinates angular flux distribution from the scored data of the Monte Carlo particle tracks crossing a specified surface. The approach has been implemented in an interface program and validated by means of test calculations using a simplified three-dimensional geometric model. Satisfactory agreement was obtained for the angular fluxes calculated by the mapping approach using the MCNP code for the Monte Carlo calculations and direct three-dimensional discrete ordinates calculations using the TORT code.

In the next step, a complete program system has been developed for coupled three-dimensional Monte Carlo- deterministic transport calculations by integrating the Monte Carlo transport code MCNP, the three-dimensional discrete ordinates code TORT and the mapping interface program. Test calculations with two simple models have been performed to validate the program system by means of comparison calculations using the Monte Carlo technique directly. The good agreement of the results obtained demonstrates that the program system is suitable to treat three-dimensional shielding problems with satisfactory accuracy.

Finally the program system has been applied to the shielding analysis of the accelerator based IFMIF (International Fusion Materials Irradiation Facility) neutron source facility. In this application, the IFMIF-dedicated Monte Carlo code McDeLicious was used for the neutron generation and transport simulation in the target and the test cell region using a detailed geometrical model. The neutron/photon fluxes, spectra and dose rates across the back wall and in the access/maintenance room were calculated and are discussed. The comparison to the results of shielding analyses conducted previously for IFMIF on the basis of approximate methods and models shows severe discrepancies. These are due to the poor geometry representation and the approximate treatment of the neutron source simulation employed in those calculations. The successful application to IFMIF thus demonstrates the suitability of the program system for the analysis of shielding problems of large and complex nuclear facilities based on coupled Monte Carlo – discrete ordinates calculations.

Programmsystem für gekoppelte probabilistisch-deterministische Abschirmrechnungen von großen und komplexen nuklearen Anlagen in dreidimensionaler Geometrie.

Kurzfassung

Abschirmrechnungen zu fortgeschrittenen nuklearen Anlagen, wie etwa beschleunigergetriebenen Neutronenquellen oder Fusionsreaktoren des Tokamaktyps, sind durch deren komplexe Geometrie und die großen Abmessungen mit Abschirmdicken von mehreren Metern erschwert. Die komplexe Geometrie kann in deterministischen Transportrechnungen, die auf dem Verfahren der diskreten Ordinaten (S_N-Verfahren) beruhen, nur schwer dargestellt werden. Der Strahlungstransport durch dicke Abschirmungen stellt andererseits eine ernste Herausforderung für das (probabilistische) Monte-Carlo-Transportverfahren dar. Zur Behandlung von Abschirmproblemen dieser Art wird in dieser Arbeit ein dezidiertes Rechenverfahren vorgeschlagen, das auf einer Kopplung von probabilistischen und deterministischen Transportrechnungen beruht. Das Monte-Carlo-Verfahren wird für die Beschreibung der Teilchenerzeugung und des Teilchentransports im Bereich der Teilchenquelle eingesetzt, wo sowohl die Geometrie als auch die Reaktionsphysik im allgemeinen komplexer sind, während das S_N-Verfahren für die Behandlung des Strahlungstransports durch die dicke Abschirmung genutzt wird.

Um eine Kopplung dieser beiden Rechenverfahren zu ermöglichen, wurde ein Abbildungsverfahren entwickelt, mit dessen Hilfe die winkelabhängigen Flussdichteverteilungen für die S_N-Transportrechnung über die Auswertung von Monte-Carlo-Trajektorien, die eine festgelegte Fläche durchqueren, gewonnen werden. Das Verfahren wurde in ein Schnittstellenprogramm implementiert und mittels Testrechnungen für eine vereinfachtes dreidimensionales geometrisches Modell validiert. Es konnte eine zufriedenstellende Übereinstimmung für die nach dem Abbildungsverfahren und dem deterministischen S_N-Verfahren berechneten winkelabhängigen Flussdichten erreicht werden. Dabei wurde der MCNP-Code für die im Rahmen des Abbildungsverfahrens durchgeführten Monte-Carlo-Rechnungen eingesetzt und der TORT-Code für die deterministischen, dreidimensionalen Vergleichsrechnungen.

Im nächsten Schritt wurde ein vollständiges Programmsystem zur Durchführung gekoppelter probabilistisch-deterministischer Transportrechnungen entwickelt. Dieses Programmsystem umfasst im wesentlichen den Monte-Carlo-Transport-Code MCNP, das dreidimensionale S_N-Transportprogramm TORT und das erwähnte Schnittstellenprogramm zur Abbildung der winkelabhängigen Flussdichteverteilungen aus den Resultaten der Monte-Carlo-Rechnung. Testrechnungen wurden für zwei einfache Modelle durchgeführt, um das Programmsystem anhand von Vergleichsrechnungen nach dem direkten Monte-Carlo-Verfahren zu validieren. Die gute Übereinstimmung der dabei erzielten Ergebnisse zeigt, dass das Programmsystem geeignet ist, dreidimensionale Abschirmproblem mit befriedigender Genauigkeit behandeln zu können.

Das Programmsystem wurde schließlich zur Analyse von Abschirmproblemen der beschleunigergetriebenen IFMIF-Neutronenquelle eingesetzt. Für diese Anwendung wurde das speziell für IFMIF entwickelte Monte-Carlo-Programm McDeLicious zur Simulation der Neutronenerzeugung im Target und des Neutronentransports innerhalb der Testzelle eingesetzt. Dabei wurde ein detailliertes Geometriemodell der IFMIF-Testzelle benutzt. Die Neutronen- u. Photonenflussdichten, Spektren und die Dosisratenprofile wurden für die Rückwand der Testzelle sowie den angrenzenden Handhabungsraum berechnet und diskutiert. Der Vergleich mit den Ergebnissen von Abschirmanalysen, die bereits früher für IFMIF auf der Basis von vereinfachten Verfahren und Modellen durchgeführt worden waren, zeigen starke Diskrepanzen. Diese sind auf die grob vereinfachte Geometriedarstellung sowie die sehr approximative Beschreibung der Neutronenerzeugung in jenen Abschirmrechnungen zurückzuführen. Die erfolgreiche Anwendung für IFMIF demonstriert somit die Eignung des entwickelten Programmsystem zur Analyse von Abschirmproblemen großer und komplexer nuklearer Anlagen auf der Basis gekoppelter probabilistisch-deterministischer Transportrechnungen.

CONTENTS

LIST OF FIGURES

LIST OF TABLES

LIST OF ABBREVIATIONS AND SYMBOLS

IFMIF	International Fusion Materials Irradiation Facility
WWG	Weight Window Generator
ITER	International Thermo-nuclear Experimental Reactor
D-Li	Deuteron-Lithium
MC-S_N	Monte Carlo-Discrete Ordinates
SSW/SSR	Surface Source Writing/Source Source Reading
DEMO	Fusion Demonstration Reactor
CW	Continuous Wave
IEA	International Energy Agency
KEP	Key Element Technology Phase (KEP) of IFMIF
EVEDA	Engineering Validation and Engineering Design Activity of IFMIF
CSA/CSB	Common Surface A/Common Surface B
$\vec{r}$	position vector
E	particle energy
$\vec{\Omega}$	flight direction
$\psi(\vec{r},E,\vec{\Omega})$	angular flux about $\vec{r}$, E and $\vec{\Omega}$
$\Sigma_t,\Sigma_s,\Sigma_f$	total, scattering, and fission cross section
υ,χ	total fission yield of secondary particles and the corresponding energy distribution
$q(\vec{r},E,\vec{\Omega})$	external source term about $\vec{r}$, E and $\vec{\Omega}$
$\Phi(\vec{r},E)$	scalar flux about $\vec{r}$, E
$J_\xi(\vec{r},E)$	current with respect to the ξ-coordinate about $\vec{r}$, E
i, *j*, *k*	mesh intervals in the three dimensional space of S_N solution

m	one of an ordered set of directions
w_m	weight associated with discrete direction m
μ_m, ξ_m, η_m	cosines of the angles between the particle flight m and first, second and three dimension axis
A, B, C	cell face areas perpendicular to the axes from which μ, ξ and η are measured
V, S	volume and source in a given mesh cell
$P(l)$	probability density distribution of collision about the distance of l
$\psi_{i,j,k,m,g}$	angular flux in a mesh cell (i, j, k) with direction m and energy group g
$\Phi_{i,j,k}^{S_N}$	scalar flux for a mesh cell (i, j, k) in S_N solution
N	total number of source particles simulated in the Monte Carlo run
ΔA	area of the given surface element in Monte Carlo geometric model
$J_n^{MC}\left(\Delta A, \Delta E, \Delta\vec{\Omega}\right)$	contribution of an individual particle n to the current in a given surface element ΔA with energy range ΔE and direction range $\Delta\vec{\Omega}$ in Monte Carlo simulation
$\Phi_n^{MC}\left(\Delta A, \Delta E, \Delta\vec{\Omega}\right)$	contribution of an individual particle n to the scalar flux in a given surface element ΔA with energy range ΔE and direction range $\Delta\vec{\Omega}$ in Monte Carlo simulation
$weight_n$	the Monte Carlo weight of particle n
λ_n	cosine of angle between surface normal and particle n's trajectory in Monte Carlo simulation

1. INTRODUCTION

In the field of nuclear engineering, the discrete ordinates (DO) and the Monte Carlo (MC) methods are well established computational techniques used routinely for shielding and design calculations. In the last few decades, advanced nuclear facilities such as tokamak fusion reactors and accelerator based neutron sources have been developed. Shielding calculations for such facilities are complicated due to their complex geometries and their large dimensions, including bulk shields of several meters thickness. While the complexity of the geometry in the shielding calculation is nearly impossible to handle by the discrete ordinates method, the deep penetration of radiation through bulk shields are a severe challenge for the Monte Carlo particle transport simulation technique. This work aims to develop a dedicated combined MC-DO computational approach for shielding calculations of advanced nuclear facilities to better cope with both the complex geometry and the deep penetration radiation transport. In this chapter, the conventional methods for shielding calculations are briefly reviewed; then the challenges to the existing approaches are presented and a potential solution is discussed. Finally the objectives of this work, which will be discussed in subsequent chapters, are presented.

1.1 Survey of methods for shielding calculations

The discrete ordinates (DO) method (S_N method) [1] is the most widely-used deterministic method for the solution of the neutron transport equation. The S_N method attempts to solve the Boltzmann transport equation by discretizing the independent variables. One of its main application areas is the calculation of neutron and photon transport in deep penetration problems. Various one- and multi-dimensional S_N codes (e.g. one-dimensional codes: ANISN [2], ONEDANT [3] and DTF-II [4], two-dimensional codes: DORT [5] and TWODANT [6]) were developed and are widely used in the field of radiation shielding.

Recently, with the great progress of computer technology as well as the availability of advanced multi-dimensional S_N methods, the application of three-dimensional S_N codes to practical shielding problems has become of increasing interest. The successful solutions of some difficult shielding problems [7, 8] have demonstrated the capability of three-

dimensional S_N codes such as TORT [9]. In addition, the capability for parallel computing has become available with the three-dimensional code PENTRAN [10] and applied to practical shielding problems [11]. However, the S_N method still suffers from the limited geometry representation when dealing with complex three-dimensional problems. Furthermore, the existing discrete ordinates codes are not capable of treating charged particle transport problems, although there are no principle obstacles for the implementation of this feature.

The Monte Carlo (MC) method is increasingly preferred for transport calculations due to its powerful capabilities to accurately model the physics of particles in complicated three-dimensional problems. A number of Monte Carlo transport codes (e.g. MCNP/MCNPX [12, 13], TRIPOLI [14], MCBEND [15], and MORSE [16]) have been developed by different scientific and industrial institutions over the last half century. In spite of the dramatic improvement of computer speed, the application of the Monte Carlo method for deep-penetration-relevant problems (oil well-logging, radiation shielding, etc.) is still constrained due to its inherent limitations. By extracting flux results from tracks of a limited sample size of particles, it is often difficult to obtain a sufficient population far away from the source with many mean free paths of material to penetrate.

To improve the computing efficiency of Monte Carlo simulations, many variance reduction techniques, such as energy cut-off, geometry splitting with Russian roulette, weight cut-off, weight window (WW), have been developed and implemented [12]. Among these variance reduction techniques, the WW technique has been widely used and proved to be very powerful. However, it is not easy to apply the WW technique properly in complex problems, because it usually requires a lot of experience, intuition, and iterations from the side of the user. Additionally, the subdivision of geometrical cells of the model is generally required and this work is usually time-consuming and cumbersome. To alleviate the difficulties in the determination of the WW parameters, the Monte Carlo code MCNP provides a standard Weight Window Generator (WWG) [6] for the conventional cell-based or superimposed mesh-based WW. However this WWG, while useful, is still complex and cannot overcome a bad set of initial WW parameters. If a region is sampled poorly, unreliable WW might be generated.

During the past decades, great efforts have been made to develop automatic WW generators based on the solution of an adjoint transport calculation. The CADIS (Consistent Adjoint Driven Importance Sampling) methodology has been developed by using a three-dimensional discrete ordinates adjoint function for source biasing and consistent transport

biasing with the WW technique [17, 18]. The AVATAR (Automatic Variance And Time of Analysis Reduction) method [19] was proposed by using the basic inverse relation between statistical weight and importance to calculate space-, energy-, and angular-dependent weight windows from a three-dimensional adjoint calculation using the three-dimensional S_N code THREEDANT [20].

The implementation of these new variance reduction techniques significantly improves the performance of Monte Carlo codes. However, for deep-penetration-relevant problems, in particular for difficult shielding problems arising in the development of advanced nuclear systems such as accelerator-based neutron source and tokamak fusion reactor, Monte Carlo methods are still not able to provide complete solutions with sufficient accuracy, even with the implementation of these new techniques.

1.2 Challenges in shielding design

Within the last few decades, the development of next-generation nuclear systems has achieved considerable progress. For instance, the International Thermo-nuclear Experimental Reactor (ITER) [21] has completed the engineering design phase and will be constructed in the near future. Shielding calculations for fusion reactors are very difficult because of the complex geometry of the tokamak machine, the thick bulk shields, and the large dimensions of the building housing the reactor. It is thus impossible to use a single model, or code, to accurately calculate the transport of neutrons from the plasma zone out into the rest of the building. However, an accurate estimation of the radiation field around the machine is very important from the safety point of view.

The International Fusion Materials Irradiation Facility (IFMIF) [22, 23] is an accelerator-based Deuteron-Lithium (D-Li) neutron source designed to produce an intense neutron field that will simulate the neutron environment of a D-T fusion reactor for material testing. The geometry of the lithium target within the test cell is very complex and the shielding walls around the target are very thick (up to 3 meters). It is extremely difficult to conduct direct shielding calculations with sufficient accuracy by using the existing Monte Carlo or S_N techniques.

Accelerator driven spallation neutron sources are expected to play an important future role for various applications as well as fundamental research studies. Therefore several such facilities (e.g. ESS [24], SNS [25], and JSNS [26]) are being planned or are currently under

construction at different sites around the world. Shield design for this kind of neutron sources has proved to be a difficult task since it is difficult to make reliable estimations by using the conventional approaches for shielding calculations.

Shield design and analyses of these advanced nuclear facilities have been demonstrated to be a challenge to the conventional methods for shielding calculations. In summary, the shielding problems of these advanced nuclear systems have the following features:

1. The geometry configuration of the target/source region is complex.
2. The source modeling is non-standard.
3. There is a thick bulk shield around the target/source region.
4. Charged particle transport is involved for accelerator based systems.

As it is well known, Monte Carlo transport codes are best suited for modelling the geometrical details of the target and the physical complexity of the particle (neutral and/or charged particles) interactions and tracking. In addition to these general advantages, some Monte Carlo codes such as MCNP allow the implementation of an arbitrary source model. When the internal source descriptions are not sufficient, a dedicated source module can be inserted with as many details as required. Therefore, it is a natural choice to use the Monte Carlo method to deal with the complex geometry, the complicated source modelling and the charged particle transport. As mentioned above, the Monte Carlo method is not able to provide a complete solution of the whole shielding problem, especially for deep penetration calculations because it is very difficult or even impossible to get a sufficient number of particles in the deep part of bulk shield due to the statistical nature of the particle tracking simulation. For discrete ordinates method, among its numerous advantages, the capability for treating deep penetration problems is the most distinguished one. Discrete ordinates methods have, however, limitations in treating complex geometries and an accurate source modelling. In addition, the existing discrete ordinates codes are not able to handle charged particle transport which is of special interest in accelerator based nuclear systems.

A coupling scheme which combines the advantages of both the MC and the S_N approaches would be very beneficial for analyses of shielding problems of advanced nuclear facilities. By using such a coupling scheme, the shielding problem can be separated into two parts: the source region with its complex geometry and the bulk shield region with a relatively simple geometry. The Monte Carlo method can be used for particle transport in the source region with the complex geometry involved. The S_N method is used to treat the deep penetration

problem in the bulk shield region with relatively simple geometry. Hence, the shielding problem can be solved on the basis of the coupled Monte Carlo-Discrete Ordinates (MC-S_N) computational scheme.

Several MC-S_N coupling schemes have already been developed and used for shielding calculations of the accelerator based nuclear systems. A set of interface utilities [27] has been created to allow coupled MC-S_N shielding analyses. This toolset includes two interfaces: MTA and MTD. MTA provides a linkage between the Monte Carlo code MCNP4B/MCNPX and the one dimensional discrete ordinates code ANISN. MTD provides a coupling between MCNP4B/MCNPX and the two-dimensional discrete ordinates code DORT. This coupling toolset was tested by two simple sample problems and satisfactory agreement was obtained. In addition, a procedure to couple the Monte Carlo code HETC96 [28] with the one-dimensional code ANISN was developed and used for the Spallation Neutron Source (SNS) project [25] to treat the radiation shielding problem [29, 30]. A similar computational scheme [31] was developed to couple the Monte Carlo code system HERMES [32] and ANISN for the shielding design of the European Spallation Source (ESS) project [24].

1.3 Objective of this work

Based on the review of previous work, it is obvious that the conventional methods, i.e. the Monte Carlo or the discrete ordinates methods, are not able to meet the challenge arising from the shielding design of advanced nuclear systems by themselves. Therefore, a coupling scheme which combines the advantages of each method is a natural choice to treat such shielding problems. The Monte Carlo method is used to model the complicated geometry, source and particle physics, and the discrete ordinates method is used to solve the deep-penetration problem in the bulk shield. As mentioned above, several coupling procedures have been developed and used for the shielding design of accelerator based nuclear systems. However, these procedures only allow the coupling of the Monte Carlo codes and one- or two-dimensional discrete ordinates codes. Full three-dimensional MC-S_N coupled calculations are not supported by these procedures. In order to improve the quality of the shielding design, the development of a coupled MC-S_N computational scheme for full three-dimensional shielding calculations is thus required.

The objective of this work is to develop a computational tool which allows full three-dimensional coupled MC-S_N shielding calculations for large and complex nuclear facilities.

To this end, a mapping approach is required which allows to calculate the discrete ordinates angular flux distribution from the scored data of the Monte Carlo particle tracks crossing a specified surface. By integrating the Monte Carlo transport code, the three-dimensional S_N code and the coupling program for the angular flux mapping process, a program system is to be developed for shielding calculations of large and complex nuclear facilities. After a brief review of neutron transport theory to provide the basis for the coupling scheme, in chapter 2 of this work, a mapping approach is described in chapter 3 for the three-dimensional MC-S_N coupling scheme along with numerical validation calculations. The development of the program system for the coupled shielding analysis is presented and test calculations are discussed in chapter 4. Chapter 5 presents the application of the developed coupling scheme to the shielding analysis of the accelerator based IFMIF neutron source as an illustrative example. Chapter 6 summarizes the work with potential directions of future research.

2. NEUTRON TRANSPORT THEORY

For shielding analysis of nuclear facilities, the most essential topic is the calculation of neutron transport and interaction with matter. In this chapter the governing equation of neutron transport is presented, and the discrete ordinates method and the Monte Carlo method which are the most widely-used approaches for neutron transport solution are briefly described. Codes used for each method are introduced.

2.1 Neutron transport equation

The process of neutron transport and interaction with matter can be represented by the Boltzmann transport equation. This equation is, in principle, a balance equation for neutron losses due to leakage, absorption and scattering processes and neutron gains through in-scattering processes and the direct emission of source neutrons in an infinitesimal phase-space element. The steady-state transport equation can be expressed as follows [33]:

$$\begin{aligned}&\vec{\Omega}\cdot\nabla\psi\left(\vec{r},E,\vec{\Omega}\right)+\Sigma_t\left(\vec{r},E,\vec{\Omega}\right)\psi\left(\vec{r},E,\vec{\Omega}\right)=\\&\iint\Sigma_s\left(\vec{r},E'\rightarrow E,\vec{\Omega}'\cdot\vec{\Omega}\right)\psi\left(\vec{r},E',\vec{\Omega}'\right)d\vec{\Omega}'dE'\\&+q\left(\vec{r},E,\vec{\Omega}\right)\ ,\end{aligned}\qquad(2.1)$$

where

$\psi\left(\vec{r},E,\vec{\Omega}\right)$ = angular flux density

$\vec{r}$ = position vector

E = particle energy

$\vec{\Omega}$ = flight direction

Σ_t, Σ_s = total and scattering cross section

$q\left(\vec{r},E,\vec{\Omega}\right)$ = external source term.

The boundary conditions for Eq. (2.1) are generally specified by the physical situation in the application. The scalar flux is the product of the total number of neutrons in a differential volume, which is the integral over direction of the number of neutrons with direction within $d\vec{\Omega}$ about $\vec{\Omega}$, times the speed:

$$\Phi(\vec{r},E)=\int_0^{4\pi}\psi(\vec{r},E,\vec{\Omega})d\vec{\Omega} \tag{2.2}$$

and the current with respect to the ξ-coordinate is the net flow of neutrons in the positive ξ-direction:

$$J_\xi(\vec{r},E)=\vec{n}_\xi\int_0^{4\pi}\psi(\vec{r},E,\vec{\Omega})d\vec{\Omega}(\vec{n}_\xi\cdot\vec{\Omega}). \tag{2.3}$$

2.2 The Discrete Ordinates method

The discrete ordinates method [1], also called S_N method, is the most widely-used deterministic method for the solution of neutron transport problems. The discrete ordinates method is based on a conceptually straightforward evaluation of the transport equation at a few discrete angular directions, or ordinates, and the use of quadrature sets to replace the angular integrals by summations over the discrete ordinates. The essence of the method is the choice of ordinates, quadrature weights, difference schemes, and iterative solution procedures.

In one-dimensional slab and spherical geometries, only one angular coordinate is required to define the direction of the particle motion. In multi-dimensional geometries, as well as the one-dimensional cylindrical geometry, two angular coordinates are required to specify the direction of motion. With reference to Fig. 2.1, the direction cosines of the neutron flight direction $\vec{\Omega}$ with respect to the x_1-, x_2-, and x_3-coordinate axes are denoted by μ, ξ and η, respectively. Only two of these directions are independent since $\vec{\Omega}$ is a unit vector:

$$\mu^2+\xi^2+\eta^2=1. \tag{2.4}$$

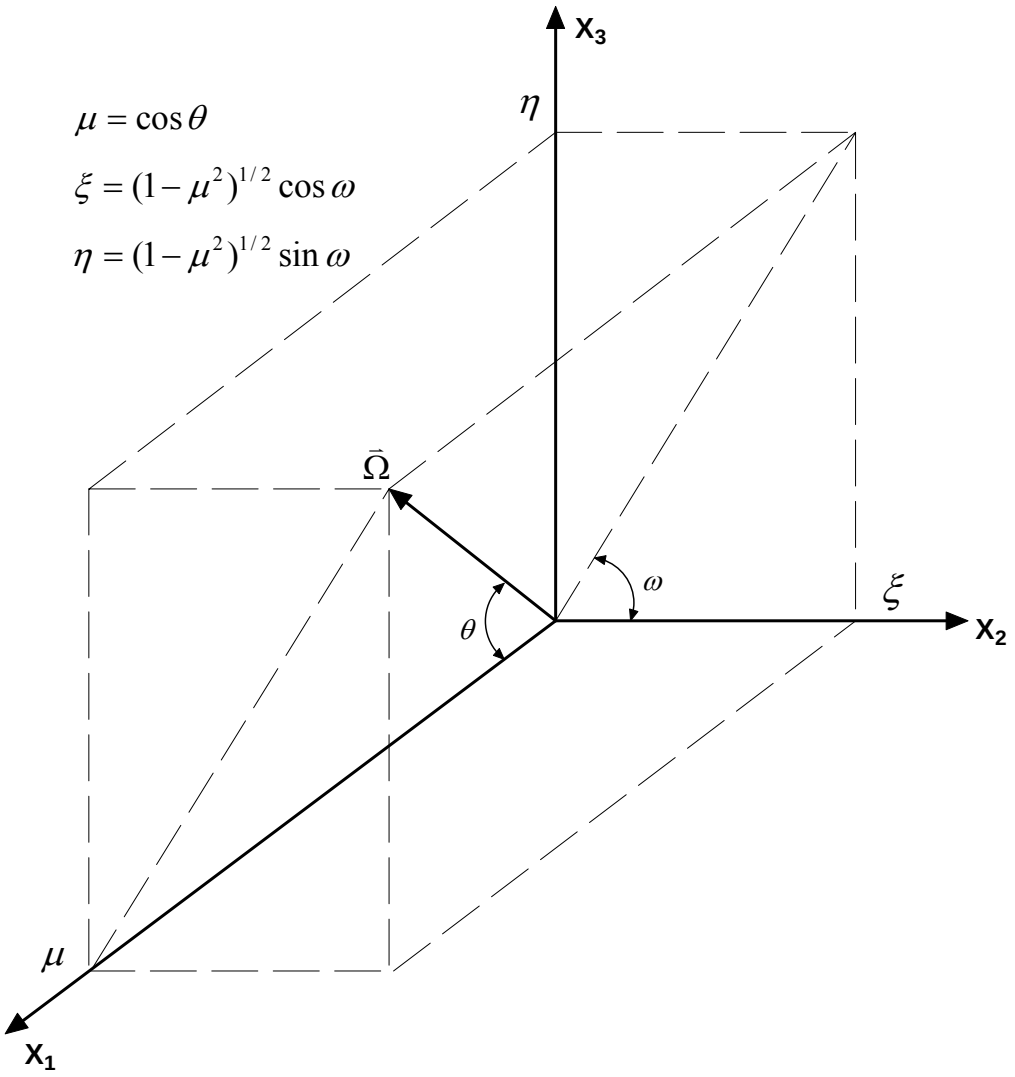

Fig. 2.1 Coordinate system for multidimensional discrete ordinates

The particle flux is determined in all eight octants of the unit sphere over which $\vec{\Omega}$ varies in three-dimensional problems. It is convenient to use a set of ordinates that are symmetric in the eight octants. If the ordinates and weights are constructed for a set of direction cosines satisfying the relationship of Eq. (2.4) in one octant with the direction cosine set (μ_n, ξ_n, η_n), the ordinates and weights for the other octants with direction cosine sets $(-\mu_n, \xi_n, \eta_n)$, $(\mu_n, -\xi_n, \eta_n)$, $(\mu_n, \xi_n, -\eta_n)$, $(-\mu_n, -\xi_n, \eta_n)$, $(-\mu_n, \xi_n, -\eta_n)$, $(\mu_n, -\xi_n, -\eta_n)$ and $(-\mu_n, -\xi_n, -\eta_n)$ are obtained simply by changing the signs of one or more direction cosines.

The level symmetric quadratures as shown in Fig. 2.2 use the same set of N/2 positive values of the direction cosines with respect to each of the three axes (i.e., $\mu_n = \xi_n = \eta_n, n = 1, \cdots, N/2$). The rotational symmetry of the level symmetric quadrature set

and the requirement of Eq. (2.4) determine all the direction cosines except one. Once μ_1 is selected, the other can be obtained from

$$\mu_n = \mu_1^2 + 2(n-1)\frac{1-3\mu_1^2}{N-2} \tag{2.5}$$

and $\mu_n = \xi_n = \eta_n$. The choice of μ_1 can be determined according to the problem to be solved. But it is required that $\mu_1^2 \leq \frac{1}{3}$.

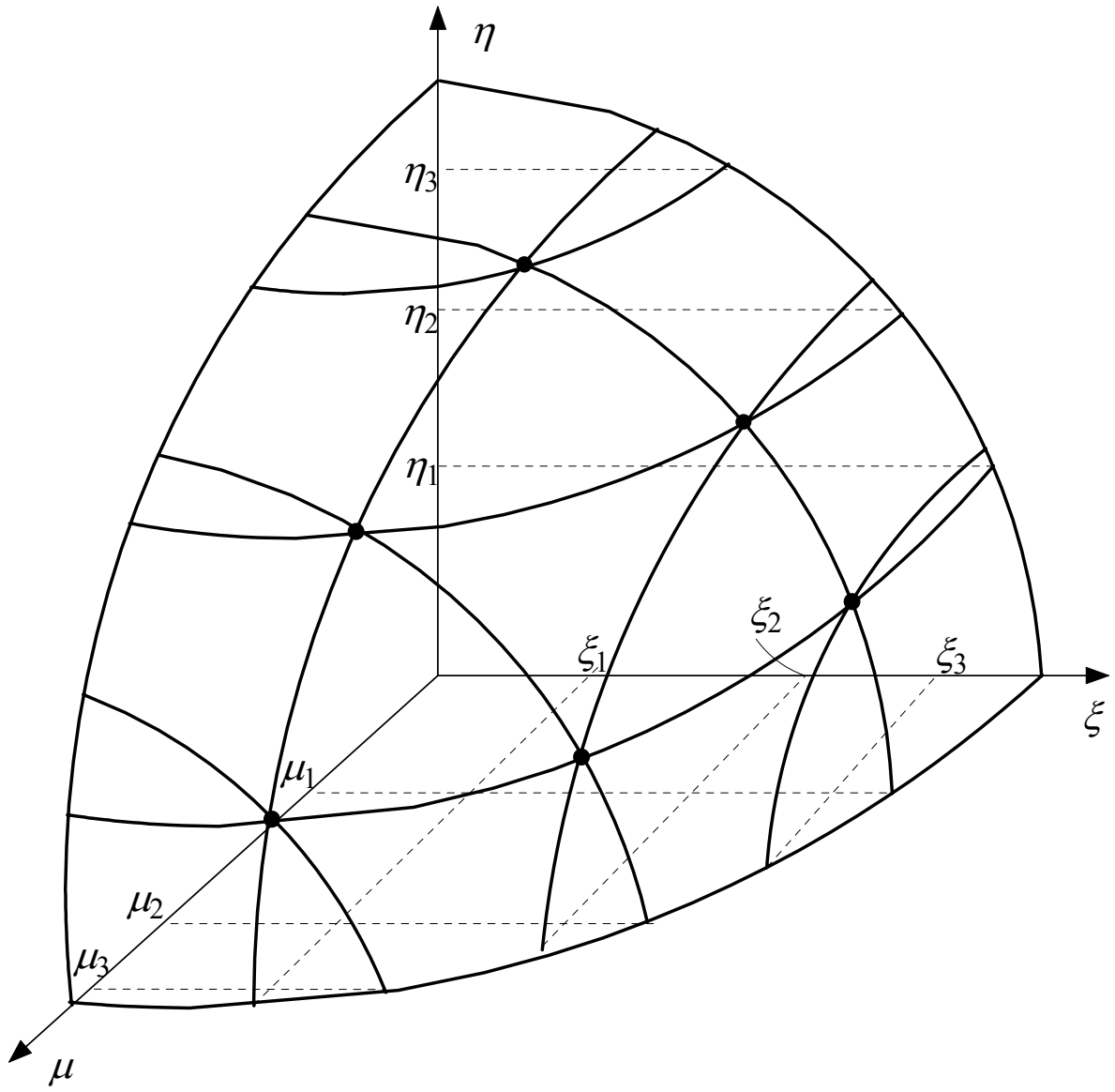

Fig. 2.2 Level symmetric S_6 discrete ordinates quadrature set

In three-dimensional geometry, the formulation used for the discrete ordinates solution for either RθZ or XYZ geometry might be written as:

$$
\begin{aligned}
& w_m \mu_m \left[A_{i+\frac{1}{2},j,k} \psi_{i+\frac{1}{2},j,k,m,g} - A_{i-\frac{1}{2},j,k} \psi_{i-\frac{1}{2},j,k,m,g} \right] \\
& + w_m \xi_m \left[B_{i,j+\frac{1}{2},k} \psi_{i,j+\frac{1}{2},k,m,g} - B_{i,j-\frac{1}{2},k} \psi_{j-\frac{1}{2},k,m,g} \right] \\
& + w_m \eta_m \left[C_{i,j,k+\frac{1}{2}} \psi_{i,j,k+\frac{1}{2},m,g} - C_{i,j,k-\frac{1}{2}} \psi_{i,j,k-\frac{1}{2},m,g} \right] \\
& + \left[A_{i+\frac{1}{2},j,k} - A_{i-\frac{1}{2},j,k} \right] \left[\alpha_{m+\frac{1}{2}} \psi_{i,j,k,m+\frac{1}{2},g} - \alpha_{m-\frac{1}{2}} \psi_{i,j,k,m-\frac{1}{2},g} \right] \\
& + \sum_{i,j,k,g}^{t} w_m V_{i,j,k} \psi_{i,j,k,m,g} = w_m V_{i,j,k} S_{i,j,k,m,g} \quad .
\end{aligned}
\tag{2.6}
$$

In this notation, the subscripts *i*, *j* and *k* represent mesh intervals in the three dimensional space. The subscript *m* refers to one of an ordered set of directions along which the angular flux is to be evaluated. Each direction has an associated weight, w_m. Quantities involving integrals over all directions are to be evaluated by sums with w_m as the weighting function. ψ represents the angular flux. The ordered set of directions of particle flight is characterized by their direction cosines (μ_m, ξ_m, η_m), where μ is the cosine of the angle between the particle flight and the first dimension axis, i.e., X or R, η is the cosine of the angle with the Z axis, and ξ is the cosine with the remaining direction vector, either the Y axis or the azimuthal axis in the case of RθZ geometry. The coefficients *A, B, C* are cell face areas perpendicular to the axes from which μ, ξ and η are measured. *V* and *S* are the volume and source in a given mesh cell, respectively. Σ^t is the macroscopic total cross section.

The geometric unit cells used in XYZ and RθZ geometry are illustrated in Fig. 2.3. The faces corresponding to the geometric parameters *A*, *B* and *C* are labelled. Table 2.1 gives the values of the coefficients in terms of cell dimensions. It should be noted that the θ dimension is measured in units of rotations in this notation. Thus, θ varies from 0 to 1 during a full rotation. $\overline{R}$ represents the value of *R* midway between faces.

Table 2.1 Geometric coefficients in three-dimensions

Geometry	XYZ	RθZ
A	$\Delta Y \bullet \Delta Z$	$2\pi R \bullet \Delta\theta \bullet \Delta Z$
B	$\Delta X \bullet \Delta Z$	$\Delta R \bullet \Delta Z$
C	$\Delta X \bullet \Delta Y$	$2\pi \overline{R} \bullet \Delta R \bullet \Delta\theta$
V	$\Delta X \bullet \Delta Y \bullet \Delta Z$	$2\pi \overline{R} \bullet \Delta R \bullet \Delta\theta \bullet \Delta Z$

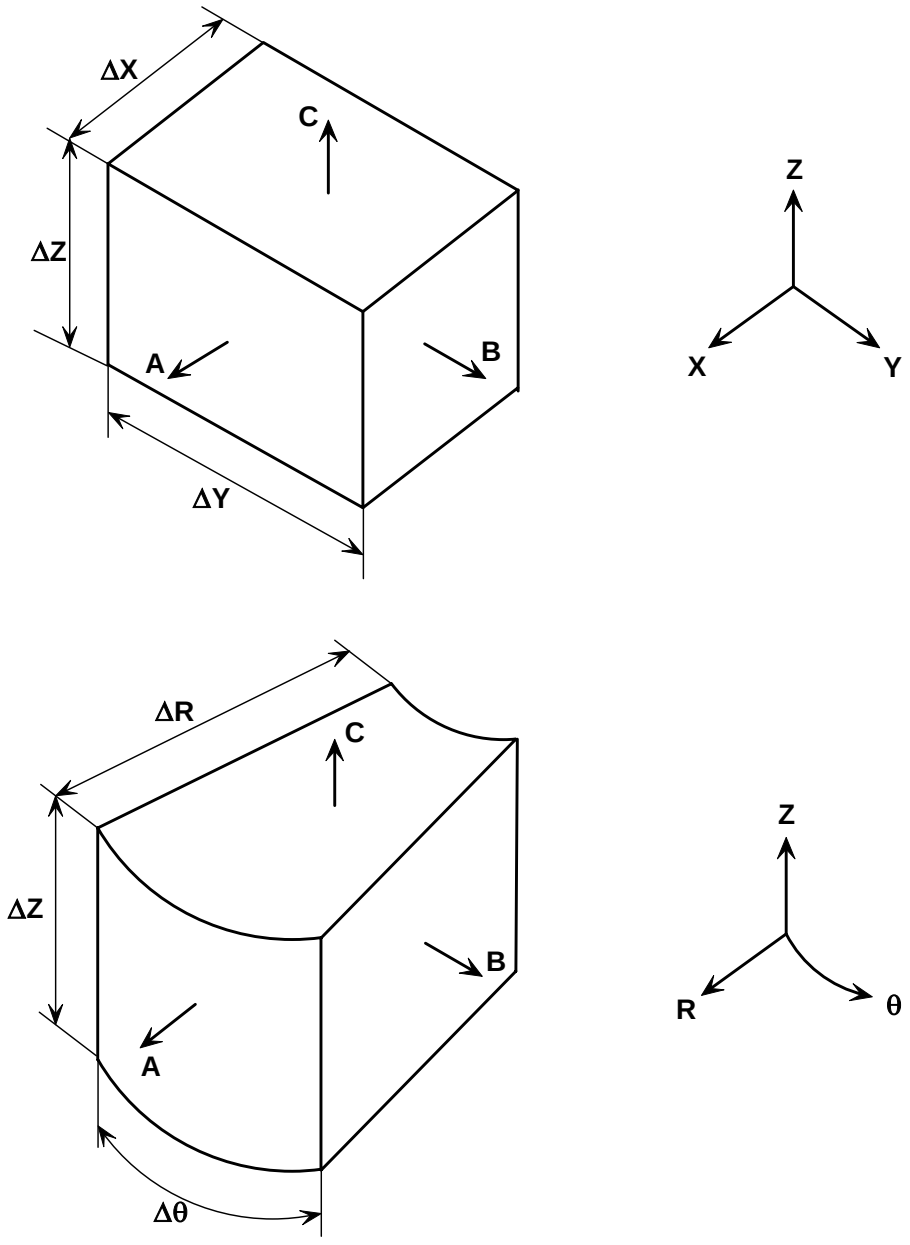

Fig. 2.3 Three-dimensional unit cells in XYZ and RθZ geometries

Among numerous one- and multi-dimensional discrete ordinates codes or code systems, the code package DOORS [34] which was developed in ORNL is one of the most used discrete ordinates code systems. The code package includes the transport codes TORT [9], DORT [5], ANISIN [2], GBANISN [35] and FALSTF [36] and additional utility programs for various purposes such as cross section preparation, post-processing and visualization of results. The code TORT is able to calculate neutron and/or photon fluxes in two- or three-dimensional systems. Due to its powerful capability, TORT is used as the reference code in this work for three-dimensional discrete ordinates solution of the coupled MC-S_N calculations. The discrete ordinates codes included in DOORS read ANISN-formatted [34] cross section libraries. Users may use one or several appropriate data processing codes, such as NJOY [37], TRANSX [38] or SCAMPI [39], to generate ANISN-format cross section from various data libraries.

2.3 The Monte Carlo method

The Monte Carlo method is a stochastic approach and very different from the deterministic transport method. The deterministic methods, as described above, solve the transport equation for the average particle behavior. The Monte Carlo method describes particle transport on the microscopic level by simulating individual particle histories from birth in the source to death by absorption or leakage. The transport of particles and their interaction with matter is thus treated as a stochastic process instead of solving any kind of transport equation. The true random pathway of a particle - as it is in reality - is simulated on the basis of stochastic laws with the interaction probability of particles and nuclei included in the nuclear cross-sections. When taking into account a large number of particle histories, their simulated behavior on average approaches the average behavior in reality.

For Monte Carlo methods, there are two important concepts: particle weight and particle track. The particle weight is a number carried along with each particle, representing the particle's relative contribution to the final tallies (estimators). The particle track represents the individual pathway of a source particle during its history. When a particle starts from a source, a particle track is created. If that track is split into 2 at a splitting surface, a second track is created and there are now two tracks from the original source particle, each with half of the single particle weight. The track length in a given cell can be used to determine a

quantity of interest, such as flux, fluence or energy deposition. Tracks crossing surfaces are used for surface flux and current estimations. Tracks undergoing collisions are used to calculate reaction rates.

In a cell with fixed material composition, the methodology of sampling a neutron collision along the track can be determined using the following theory. The source neutron will travel in a straight line in the matter until it undergoes a collision. The probability of a first collision for a particle between l and $l+dl$ along its flight path is

$$P(l)dl = \Sigma_t \exp\left(-\Sigma_t l\right)dl \,, \tag{2.7}$$

where Σ_t is the macroscopic total cross section of the medium and is interpreted as the probability per unit length of a collision. Setting λ as the random number on [0, 1), it can be written as

$$\lambda = \int_0^l P(s)ds = \int_0^l \Sigma_t \exp\left(-\Sigma_t s\right)ds = 1 - \exp\left(-\Sigma_t l\right); \tag{2.8}$$

it follows that

$$\ln(1-\lambda) = -\Sigma_t l \,. \tag{2.9}$$

Since $(1-\lambda)$ and λ are distributed in the same manner, we obtain the expression for the distance to collision by

$$l = -\frac{\ln(\lambda)}{\Sigma_t} \,. \tag{2.10}$$

Having determined the distance to the next collision, the type of reaction, the direction of flight, and the energy of out-coming particle(s) has to be determined based on the rules (physics) and probabilities (transport data). Fig. 2.4 shows schematically the random history of an incident neutron in a slab. The neutron collides with matter at event 1 and then is scattered in the direction as shown, which is selected randomly from the physical scattering distribution. A photon is also generated and is temporarily stored, or banked, for later analysis. At event 2, a certain reaction occurs, resulting in the termination of the incoming neutron and the birth of two outgoing neutrons and one photon. One neutron and the photon are banked for later analysis. The first generated neutron leaks out of the slab at event 3. The banked neutron is retrieved and, by random sampling, captured at event 4 with a photon generated. Then this photon is followed and captured at event 5 by random sampling. The banked photon which was generated at event 2 is captured at event 6. The remaining photon

generated at event 1 is now followed and has a collision at event 7 and escapes from the slab at event 8.

The neutron history is now completed. As more and more such histories are followed, the neutron and photon distributions become better known. The quantities of interest are tallied, along with estimates of the statistical precision of the results.

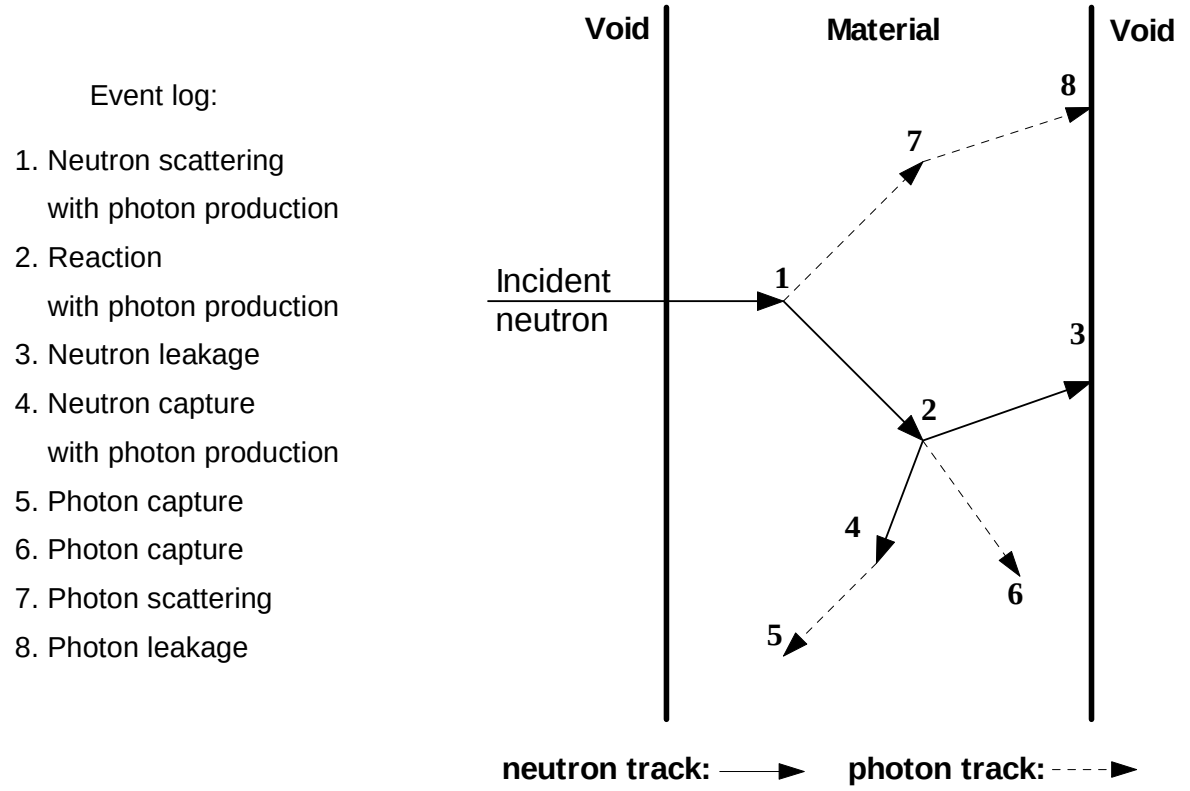

Fig. 2.4 Typical neutron history in the Monte Carlo simulation

The Monte Carlo method as described above is well suited for solving complicated three-dimensional neutral and/or charged particle transport problems. The Monte Carlo method does not rely on approximations in describing the interaction of the particles with the nuclei. Thus there is no inherent limitation of the accuracy of the Monte Carlo calculation once a sufficient large number of particle histories has been followed for scoring specified events and, eventually, deriving macroscopic quantities such as the fluence and reaction rates. For this reason, as well as the great advance of modern computer technology, the Monte Carlo technique is increasingly preferred for the solution of particle transport problems [12, 13, 14, etc.].

Among numerous Monte Carlo transport codes, MCNP [12], developed by LANL for more than half century, is one of most preferred MC codes. MCNP is a general-purpose Monte Carlo N-Particle code that can be used for neutron, photon, electron, or coupled neutron/photon/electron transport, including the capability to calculate eigenvalues for critical systems. The code treats an arbitrary three-dimensional configuration of materials in geometric cells. Point-wise cross section data are used. In addition, the capability for a general source definition, a rich collection of variance reduction techniques, and a flexible tally structure make MCNP very versatile and easy to use. In this work, MCNP and the extension versions of MCNP are used in the coupling scheme for Monte Carlo simulations.

3. THE MAPPING APPROACH

In this chapter, the general methodology for the coupled MC-S_N calculations is presented. A mapping approach is derived to compute the discrete ordinates angular flux distribution from the information of the Monte Carlo particle tracks crossing a specified surface. The theoretical basis of this mapping approach is described. The implementation of the mapping approach enables the coupling of the three-dimensional Monte Carlo and discrete ordinates codes. Specific functional modules have been developed for the implementation and validation of the mapping approach. Numerical validation of the mapping approach is discussed.

3.1 General methodology for MC-S_N coupling

The purpose of the coupling scheme is to combine the advantages of the Monte Carlo codes and the discrete ordinates codes to treat shielding problems such as for advanced nuclear systems. Fig. 3.1 shows the schematic model for the coupled MC-S_N shielding calculations.

To perform a coupled calculation, the whole model of the shielding problem should be separated into two parts: the source/target region and the bulk shield region. The geometry of the source/target region is in general complex. In addition, for the accelerator based nuclear system charged particle transport usually plays a significant role in the shielding design. Therefore, the Monte Carlo method is the natural choice to simulate particle transport in this region. In the part of bulk shield region, the geometry is in general relatively simple. The nature of the deep penetration, however, makes the shielding calculation in this region difficult. Therefore, the discrete ordinates method is the best choice to find a reliable shielding solution in this region. In order to couple these two different methods, a suitable mapping approach is necessary to pass over the particle information from the Monte Carlo simulation to the discrete ordinates calculation.

In the coupled MC-S_N calculation, a link between the Monte Carlo geometric model and the discrete ordinates mesh model must be specified. In general, a common surface or a volume can be used as a geometric link. Since an anisotropic volume source option is currently not available for the current S_N code systems (e.g., DOORS [34], DANTSYS [40]), a common surface is used as geometric link between the models of these two methods. The

Monte Carlo simulation is performed to obtain the information of particle tracks (e.g., particle type, weight, flight direction, spatial position, energy) which cross the geometric link. The discrete ordinates angular flux can then be evaluated by using a mapping approach based on the recorded Monte Carlo particle tracks. In general, the following steps are followed in a coupled MC-S_N calculation:

1. Separation of the model of the shielding problem into two parts: the target/source region for the Monte Carlo simulation and the bulk shield region for the discrete ordinates calculation;
2. Specification of a geometric link between the target/source region (Monte Carlo model) and the bulk shield region (S_N mesh model);
3. Monte Carlo simulation to score particle tracks crossing the specified geometric link;
4. Mapping of the Monte Carlo particle tracks to discrete ordinates angular fluxes;
5. Creation of an angular flux source file for use by the discrete ordinates codes;
6. Discrete ordinates calculations using the source file created in the preceding step.

To enable such a coupled MC-S_N calculation, a program system is necessary. Chapter 4 describes the program system which has been developed in the framework of the present work. It has to be noted that the key problem for conducting the coupled calculation is to develop an approach for calculating the discrete ordinates angular flux distribution from the recorded information of the Monte Carlo particle tracks crossing the specified common surface. A mapping approach for this purpose was developed and is described in the following sections.

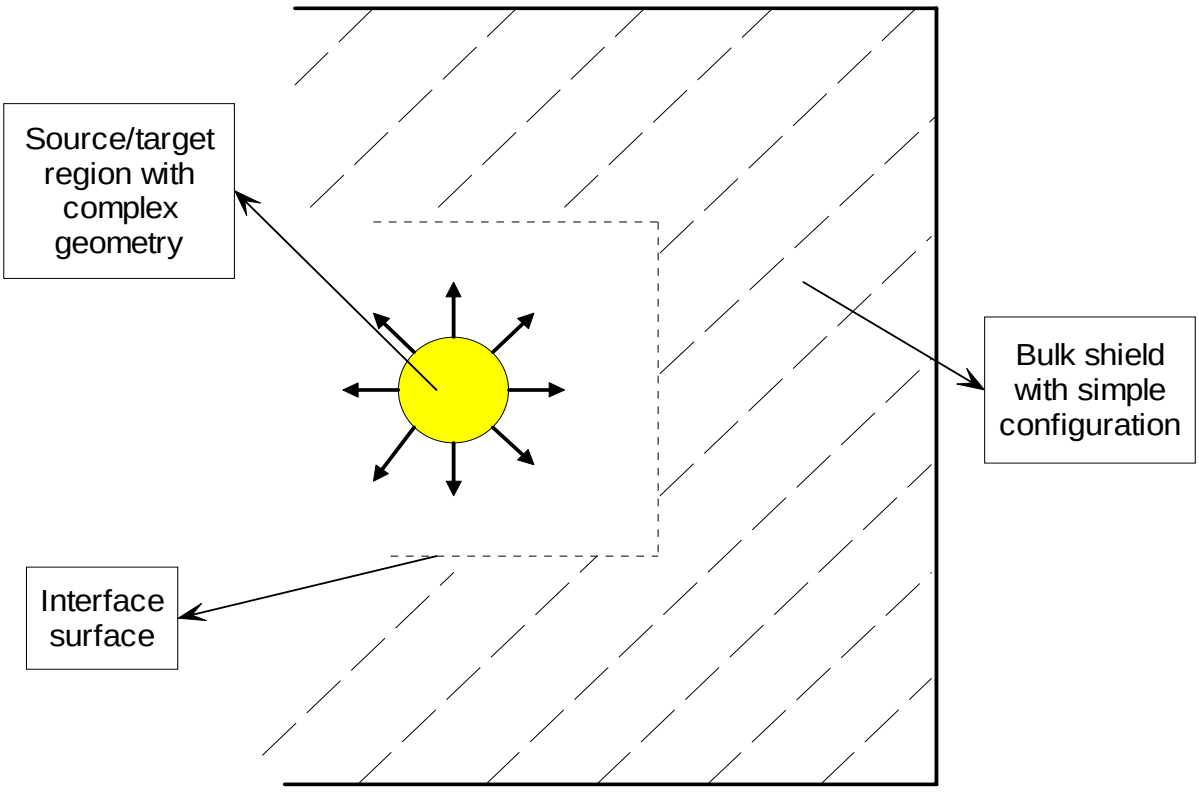

Fig. 3.1 Schematic model for the coupled Monte Carlo-Discrete Ordinates shielding calculation

3.2 Theoretical basis

In developing a mapping approach, there are two key problems: the mapping of Monte Carlo particle tracks to discrete ordinates angular fluxes and the relating of the Monte Carlo particle flight directions to discrete ordinates quadrature directions. In the following sections, the mathematical basis to map the Monte Carlo particle tracks to the discrete ordinates angular flux distribution is derived, and the methodology to relate the Monte Carlo particle flight direction to the discrete ordinates quadrature direction is presented.

3.2.1 Mapping MC particle track to S_N angular flux

In order to couple the Monte Carlo and S_N methods, the key problem is to establish a suitable relationship between Monte Carlo particle track and discrete ordinates angular flux.

In discrete ordinates transport codes like TORT, the Boltzmann transport equation is solved using the method of discrete ordinates to treat the directional variable and the method

of finite differences to treat the spatial variables. Energy dependence is treated by a multi-group formulation.

In three dimensions, the formulation used for discrete ordinates solution might be written as in Eq. (2.6) for either RθZ or XYZ geometry. The angular flux in a mesh cell (*i, j, k*) with direction *m* and energy group *g* is represented by $\psi_{i,j,k,m,g}$. The scalar flux in the cell (*i, j, k*) is given by:

$$\Phi_{i,j,k}^{S_N} = \sum_m \sum_g w_m \psi_{i,j,k,m,g} \quad . \tag{3.1}$$

In a Monte Carlo transport calculation, a particle weight represents the partial current across a given surface element. The contribution of an individual particle *n* to the current is

$$J_n^{MC}\left(\Delta A, \Delta E, \Delta\vec{\Omega}\right) = weight_n \int_{\Delta E} dE \int_{\Delta A} d\vec{r} \int_{\Delta\vec{\Omega}} d\vec{\Omega}\delta(E, E_n)\delta(\vec{r}, \vec{r}_n)\delta(\vec{\Omega}, \vec{\Omega}_n), \tag{3.2}$$

where $J_n^{MC}\left(\Delta A, \Delta E, \Delta\vec{\Omega}\right)$ represents the current in a given surface element ΔA with energy range ΔE and direction range $\Delta\vec{\Omega}$. $weight_n$ represents the Monte Carlo weight of particle *n*. E_n, $\vec{r}_n$ and $\vec{\Omega}_n$ define the particle's energy, spatial position, and flight direction, respectively. The integral over the delta function gives the contribution of one, if the particle falls within the energy range ΔE, the surface element ΔA, and the range of the flight direction $\Delta\vec{\Omega}$.

The contribution of a particle to the scalar flux per source particle about $(\Delta A, \Delta E, \Delta\vec{\Omega})$ can be written as:

$$\Phi_n^{MC}\left(\Delta A, \Delta E, \Delta\vec{\Omega}\right) = \frac{J_n^{MC}\left(\Delta A, \Delta E, \Delta\vec{\Omega}\right)}{N\Delta A \mid \lambda_n \mid} \ , \tag{3.3}$$

where *N* is the total number of source particles simulated in the Monte Carlo run and ΔA represents the area of the given surface element. λ_n is the cosine of the angle between the surface normal and the particle's trajectory.

By summing up the contribution from each individual particle, the total scalar flux about $(\Delta A, \Delta E, \Delta\vec{\Omega})$ is given by

$$\Phi^{MC}(\Delta A, \Delta E, \Delta\vec{\Omega}) = \sum_n \Phi_n^{MC}(\Delta A, \Delta E, \Delta\vec{\Omega}) . \tag{3.4}$$

And the total scalar flux for the surface element ΔA can be written as:

$$\Phi^{MC}(\Delta A) = \sum_{\Delta E}\sum_{\Delta\vec{\Omega}} \Phi^{MC}(\Delta A, \Delta E, \Delta\vec{\Omega}) . \tag{3.5}$$

In order to relate the discrete ordinates angular flux to the Monte Carlo particle track, we specify ΔA, ΔE and $\Delta\vec{\Omega}$ in Eq. (3.5) to be equivalent to one face surface of a mesh cell (i, j, k), an energy group *g*, and a direction *m* in Eq. (3.1), respectively. Then we can set

$$\Phi^{MC}(\Delta A) = \Phi^{S_N}_{i,j,k} . \tag{3.6}$$

Based on Eqs. (3.1, 3.5, 3.6), it follows that:

$$w_m \psi_{i,j,k,m,g} = \Phi^{MC}(\Delta A, \Delta E, \Delta\vec{\Omega}) . \tag{3.7}$$

Introducing Eqs. (3.2, 3.3, 3.4) to Eq. (3.7) leads to:

$$\begin{aligned} w_m \psi_{i,j,k,m,g} &= \sum_n \Phi^{MC}_n(\Delta A, \Delta E, \Delta\vec{\Omega}) \\ &= \sum_n \frac{J^{MC}_n\left(\Delta A, \Delta E, \Delta\vec{\Omega}\right)}{N\Delta A\,|\,\lambda_n\,|} \\ &= \sum_n \frac{weight_n}{N\Delta A\,|\,\lambda_n\,|} \int_{\Delta E} dE \int_{\Delta A} d\vec{r} \int_{\Delta\vec{\Omega}} d\vec{\Omega}\,\delta(E, E_n)\delta(\vec{r}, \vec{r}_n)\delta(\vec{\Omega}, \vec{\Omega}_n), \end{aligned} \tag{3.8}$$

Then we obtain

$$\psi_{i,j,k,m,g} = \sum_n \frac{weight_n}{w_m N\Delta A\,|\,\lambda_n\,|} \int_{\Delta E} dE \int_{\Delta A} d\vec{r} \int_{\Delta\vec{\Omega}} d\vec{\Omega}\,\delta(E, E_n)\delta(\vec{r}, \vec{r}_n)\delta(\vec{\Omega}, \vec{\Omega}_n) . \tag{3.9}$$

Eq. (3.9) establishes the relationship between the Monte Carlo particle tracks and the discrete ordinates angular flux.

3.2.2 Relating MC Particle Direction to S_N Quadrature Direction

In order to evaluate the angular flux distribution from Monte Carlo particle tracks based on Eq. (3.9), the location of a Monte Carlo track in the discrete ordinates phase space (*i, j, k, m, g)* should be first determined. It is straightforward to relate the variables of energy and spatial position of the Monte Carlo track to the corresponding phase space variables in discrete ordinates approach. But for the variable of the particle flight direction, the relationship is not so obvious.

In the discrete ordinates method, an angular integral (e.g. scalar flux) is approximated by the weighted sums of angular fluxes evaluated in particular directions:

$$\Phi_{i,j,k,g} = \int_{4\pi} \psi_{i,j,k,g}(\vec{\Omega}) d\vec{\Omega} \approx \sum_{m=1}^{M} w_m \psi_{i,j,k,g,m} \tag{3.10}$$

The quadrature set is defined by the M particular pairs of weights and directions, $(w_m \Omega_m)$, with the weights adding up to the width of the domain of the integral. The weight may be interpreted as the area around the discrete direction on a unit sphere. Usually angular fluxes are normalized so that the domain of the integral is one:

$$\sum_m w_m = 1. \tag{3.11}$$

Because the Monte Carlo particle directions are assigned as continuous variable, a method must be devised to determine the discrete ordinates quadrature direction in which the Monte Carlo particle is travelling. By using this method, the quadrature direction is assigned based on the proximity of the particle's direction of flight to a discrete angle in the quadrature set. Accordingly, the unit sphere is divided into M parts of directional regions which are associated with the M quadrature directions. The octant in which the particle is travelling is determined, and then the region within the octant is determined based on the technique described in the following sections.

To illustrate the technique, an example for the symmetric level S_6 quadrature set is presented. Fig. 3.2 displays the segmentation of the directional regions for the first octant of a unit sphere S_6 quadrature set. The black dots in Fig. 3.2 represent the discrete directions $\Omega_m(\mu_m, \xi_m, \eta_m)$ in which the deterministic transport solution is computed. The directional regions are bordered by normal latitudinal and longitudinal lines (thick lines) as shown in Fig. 3.2. Each region corresponds to one S_N quadrature direction.

The level-symmetric quadratures in which discrete directions are grouped into η-levels (where η is the cosine of the angle with the Z axis) are often used in S_N solutions. The unit sphere is first divided into strips for each η-level by parallel latitudinal lines as indicated in Fig. 3.2. The area fraction of each η-level strip is required to be equal to the sums of the weights of the quadrature directions in the corresponding η-level. The strip for each η-level is further divided into mesh grids by longitudinal lines and each grid corresponds to a discrete ordinates quadrature direction. Similarly, the area fraction of each grid is kept equal to the

weight associated to its corresponding quadrature direction. In this way, the area fraction of each directional region is equal to the weight of its corresponding quadrature direction:

$$S_m = w_m , \tag{3.12}$$

where S_m is the area fraction of the directional region on a unit sphere corresponding to the discrete ordinates quadrature direction (μ_m, ξ_m, η_m).

The segmentation of the directional regions on a unit sphere is achieved as shown in Fig. 3.2. For the angular variable, the link between the Monte Carlo particle track and the discrete ordinates angular flux can be established as follows:

$$\Delta_n \psi_m = \frac{weight_n}{w_m N \Delta A |\lambda_n|} \int_{\Delta\mu_m} d\mu \int_{\Delta\xi_m} d\xi \int_{\Delta\mu_m} d\eta \delta(\mu, \mu_n)\delta(\xi, \xi_n)\delta(\eta, \eta_n) , \tag{3.13}$$

where $\Delta_n \psi_m$ represents the Monte Carlo particle track's contribution to the discrete ordinates angular flux in the quadrature direction (μ_m, ξ_m, η_m) with the ranges of direction cosine $\Delta\mu_m$, $\Delta\xi_m$ and $\Delta\eta_m$. The integral over the delta functions is one if the particle track's direction cosines fall within the ranges of $\Delta\mu_m$, $\Delta\xi_m$ and $\Delta\eta_m$, and zero otherwise. The total angular flux about the direction (μ_m, ξ_m, η_m) can be obtained by summing over the contributions from all Monte Carlo particle tracks, as given by:

$$\psi_m = \sum_n \Delta_n \psi_m . \tag{3.14}$$

In this way, the relationship between the Monte Carlo particle track and the discrete ordinates angular flux is established for the angular variable.

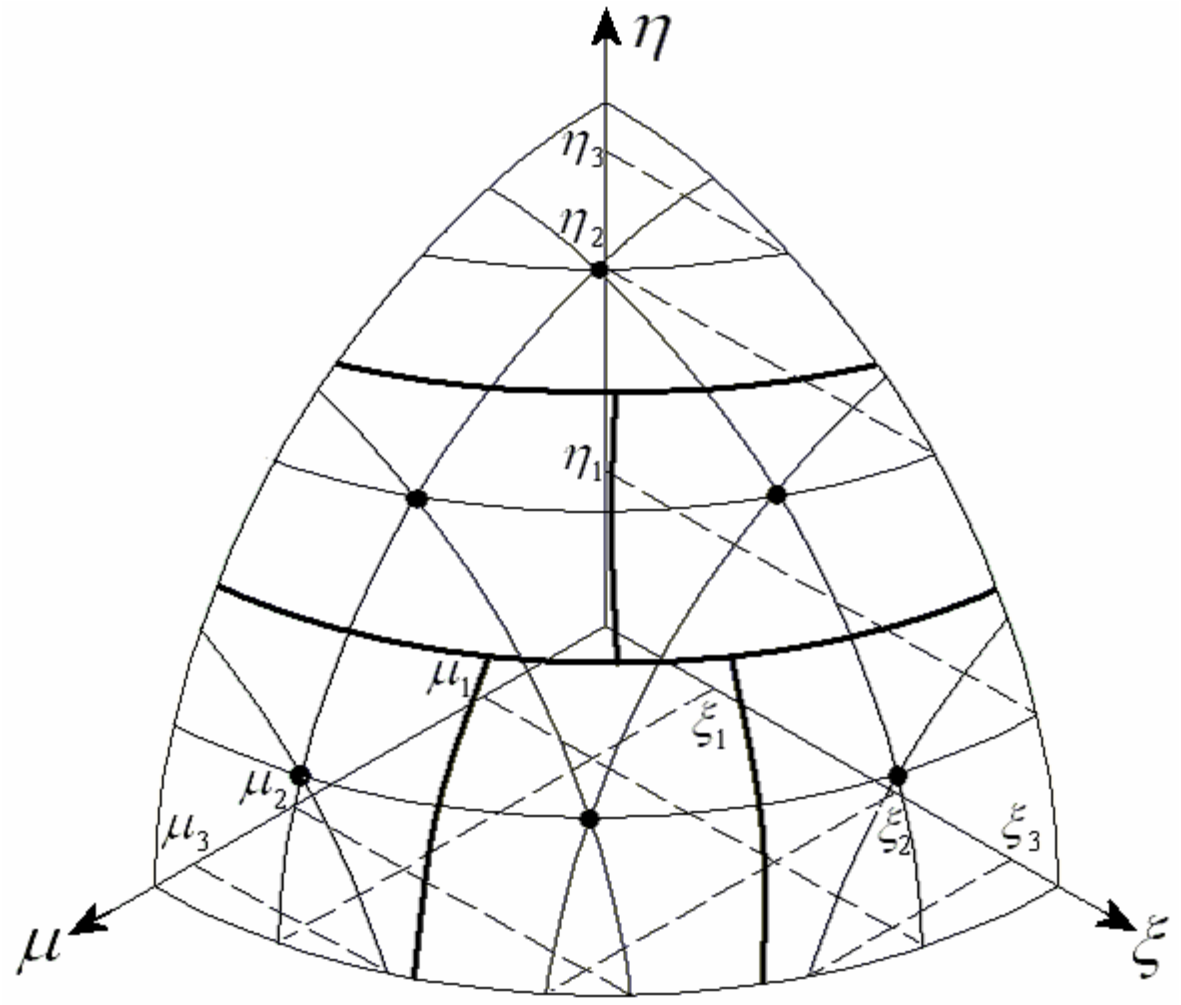

Fig. 3.2 Segmentation of directional regions for quadrature directions in the first octant of unit sphere for S_6 quadrature set

3.3 The coupling interface program

The mapping approach described above was implemented into an interface program used to couple the Monte Carlo transport code MCNP and the three-dimensional discrete ordinates code TORT. The interface program is able to calculate the discrete ordinates angular flux distribution using the mapping approach based on the particle data from the Monte Carlo simulation. The calculated angular fluxes are used to generate the boundary source file for the TORT code. The interface program is integrated into a code system for three-dimensional coupled MC-S_N shielding calculations.

The flow chart of the interface program is displayed in Fig. 3.3. Five modules, i.e. MCPROC, SNPROC, USERINP, MAPPING and SNSRC, are included in the program. The module MCPROC is designed to read and process the particle data from the preceding Monte Carlo calculations. SNPROC and USERINP process the discrete ordinates data and user-provided input file, respectively. The data from these modules are transferred to the module MAPPING. The mapping calculations are then performed to obtain the discrete ordinates angular flux distribution on the specified common surface. According to the user requirement, the boundary source file for the code TORT can then be generated from the angular flux distribution by the module SNSRC. In addition, a module FLXPROC is developed to process TORT results which are extremely difficult to handle manually for a big calculation.

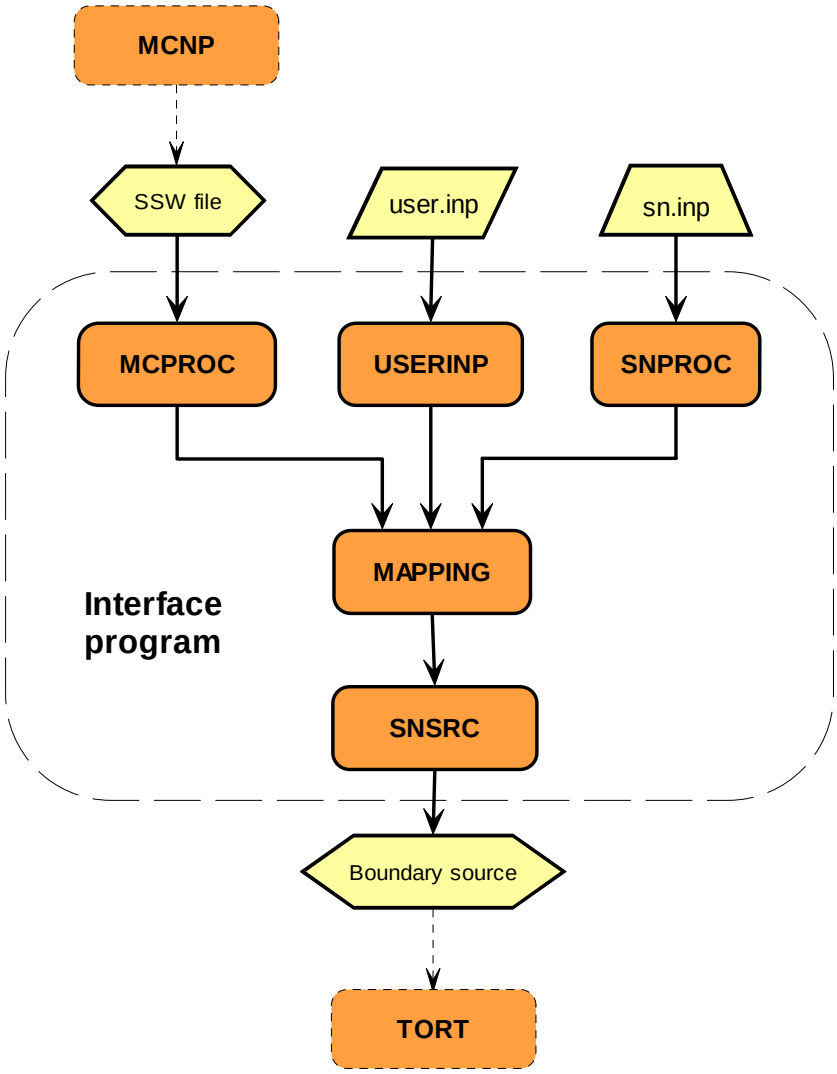

Fig. 3.3 Flow chart of the interface program

3.3.1 MC and S_N data processing

Most Monte Carlo transport codes provide various estimators to obtain particle fluxes or currents over a surface. However, most estimators only give the averaged and/or integral results. For the coupled scheme, accurate and complete information of individual Monte Carlo particle tracks (e.g., position, direction vector, energy, weight, particle type) is required in order to avoid uncertainties while mapping from Monte Carlo tracks to discrete ordinates angular fluxes. MCNP provides a standard capability of surface source writing (SSW) and reading (SSR) to allow particle tracks crossing a surface in one problem to be used as a source input for a subsequent problem. The SSW feature of MCNP offers the possibility to accurately record the particle tracks across the specified surface. By using the SSW capability, the data of the particles crossing the specified surface(s) are recorded accurately in SSW-format in a binary file.

The module MCPROC reads the SSW binary file to extract the following particle track data: history number, particle type, weight, energy, spatial location, and cosines of the angles between the flight direction and the X and Y coordinate axes. The cosine of the angle between the flight direction and the Z coordinate axis is calculated by MCPROC according to the relation given by Eq. (2.4). All the required particle data are stored in a temporary file and ready for the use by the module MAPPING.

The SNPROC module reads the TORT input files (i.e. sn.inp, see Appendix A.2) to get the data about the geometric model, energy group structure, and quadrature set. These data are processed for use by the MAPPING module in the next step. The SNPROC module includes the following sub-modules: VALUE, QUADR and DIRECT for dedicated purposes. VALUE is used to rebuild digital values from the input file. QUADR is used to calculate the second-direction cosines because only the first- and third-direction cosines of the quadrature set are provided in the TORT input file. As discussed in Section 3.2.2, the relationship between the Monte Carlo particle flight direction and the discrete ordinates quadrature direction can not be established directly. Therefore, the sub-module DIRECT segments the unit sphere into directional regions corresponding to the quadrature directions by means of the method presented in Section 3.2.2. Monte Carlo particle flight directions are easily arranged into the directional regions of the unit sphere and then the corresponding quadrature direction is determined by the module MAPPING.

3.3.2 The mapping module

The module MAPPING was developed to perform the mapping process by using the approach described in Section 3.2. Based on the data provide by MCPROC, SNPROC and USERINP, the angular flux distribution on the specified common surface are calculated. In the calculation, the corresponding spatial location and the energy group in the discrete ordinates solution of each Monte Carlo track are determined. Then, by arranging the flight direction of the Monte Carlo track to the directional region of the unit sphere, the corresponding quadrature direction of the Monte Carlo track is assigned. The contribution of each particle track to the angular flux in the corresponding phase space is calculated sequentially. By summing over the contributions from all the particles, the angular flux distribution is obtained. This module is applicable not only to the mapping process of neutron or photon problems, but also to coupled neutron/photon problems.

In principle, the module can also be used for the mapping of charged particle fluxes. Charged particle transport, however, is not considered in this work since the mean free path of the charged particles is too small compared to the thickness of the bulk shield. As a consequence, charged particles do not contribute to the dose caused by the radiation penetrating the bulk shield.

3.3.3 Peripheral modules

The module USERINP reads and processes a user-provided input file (i.e. user.inp, see Appendix A.1) to obtain the specified names of the input files of the Monte Carlo SSW source file, the S_N input file and the output boundary source file. In addition, USERINP processes messages such as the type of the S_N mesh geometry, the type and format of the S_N boundary source etc.

The module SNSRC is used to generate the specified boundary source file for the S_N code based on the angular flux distribution calculated by the MAPPING module. For the TORT code, the boundary source file is written in VARBND-format (see Appendix B.3) into a binary file. Source files for the other S_N codes can also be generated.

The post-processing of the TORT results for a big problem is usually difficult due to the huge size of the output files. The angular flux results of TORT calculations are stored in a binary file in the DIRFLX format (see APPENDIX B.1). The FLXPROC module is developed to read and manage the angular flux results in the DIRFLX format. The angular

fluxes can be edited and printed according to user requirements. This module is used for the numerical validation calculations in the following section.

It should be noted that any Monte Carlo transport code of the MCNP-family and any TORT-like discrete ordinates transport code can be used in this mapping approach with only minor modifications of the dedicated modules. All modules are written in the standard FORTRAN-90.

3.4 Numerical validations

Numerical validations of the mapping approach were performed with a simplified test model. The angular flux distribution on a given surface was calculated with the Monte Carlo code MCNP using the coupling interface program. For the purpose of comparison, the angular flux distribution was also calculated by using the TORT code and processed by the module FLXPROC. A fairly good agreement was obtained between the results from these two different approaches.

3.4.1 Model geometry

Validation calculations were performed with a simplified test model as shown in Fig. 3.4. The model is a 20×20×40 cm rectangular block with a slab neutron source on one side. The source emits 14 MeV neutrons isotropically. A surface for the neutron flux calculation and MC particle tracks scoring is located at 30 cm from the source as indicated in Fig. 3.4. The shielding material is a mixture of stainless steel and water (60a% SS316L + 40a% Water). This test model is used in both the MCNP and TORT calculations.

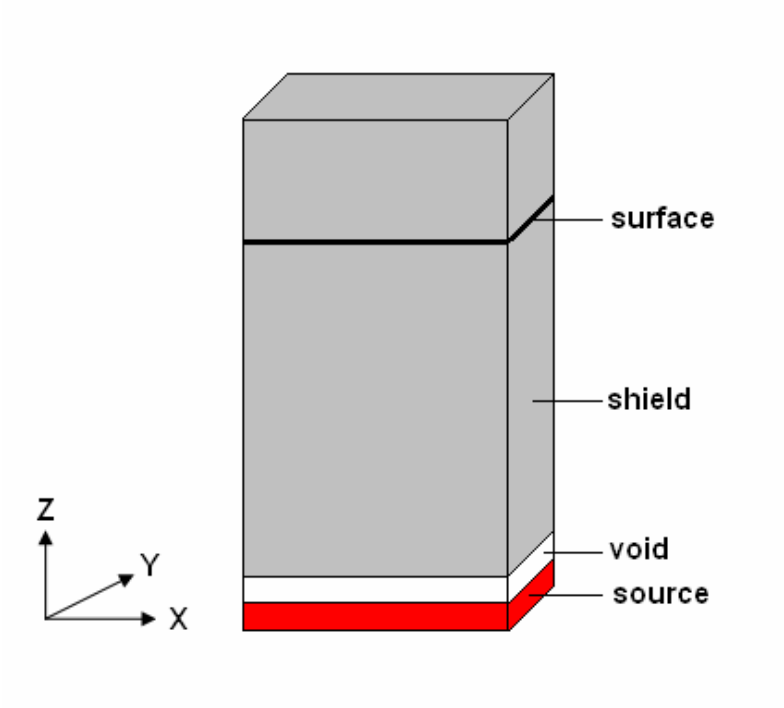

Fig. 3.4 Geometric model for validation calculation

3.4.2 Nuclear data

In MCNP calculations, point-wise cross section data in ACE format generated from the ENDF/B-VI [41] data library are used. The files are included in the MCNP code package and are ready to use. In TORT calculations, an ENDF/B-VI based fine-group cross section library VITAMIN-B6 [42] is used. The VITAMIN-B6 library has a multi-group structure consisting of 199 neutron groups (10^{-5} eV ≤ E ≤ 20.0 MeV) and 42 gamma-ray groups (1.0 keV ≤ E ≤ 14.0 MeV) in AMPX master library format. The library structure has 36 thermal-neutron groups with up-scattering.

The VITAMIN-B6 library is a general purpose master library and cannot be used in the TORT calculations directly. In order to generate a problem-dependent cross section file for TORT from the VITAMIN-B6 library, the code system SCAMPI [43] is used. SCAMPI (Scale and Ampx Processing Interface) is able to create problem-dependent cross sections for discrete ordinates transport codes from a problem-independent multi-group master library in AMPX format. It consists of modules derived from the code systems AMPX-77 [44] and SCALE [45].

The SCAMPI computational flow to create problem-dependent multi-group cross section data for TORT is shown in Fig. 3.5. This computational procedure is used in this work to

process all cross section data from the AMPX-format master libraries for the code TORT in the validation calculations of the mapping approach, the test calculations of the program system in chapter 4, and the IFMIF shielding calculations in chapter 5. In the validation calculations, only the neutron transport is considered. Therefore, a 199 neutron-group cross section file containing 36 thermal groups with up-scattering was generated for TORT.

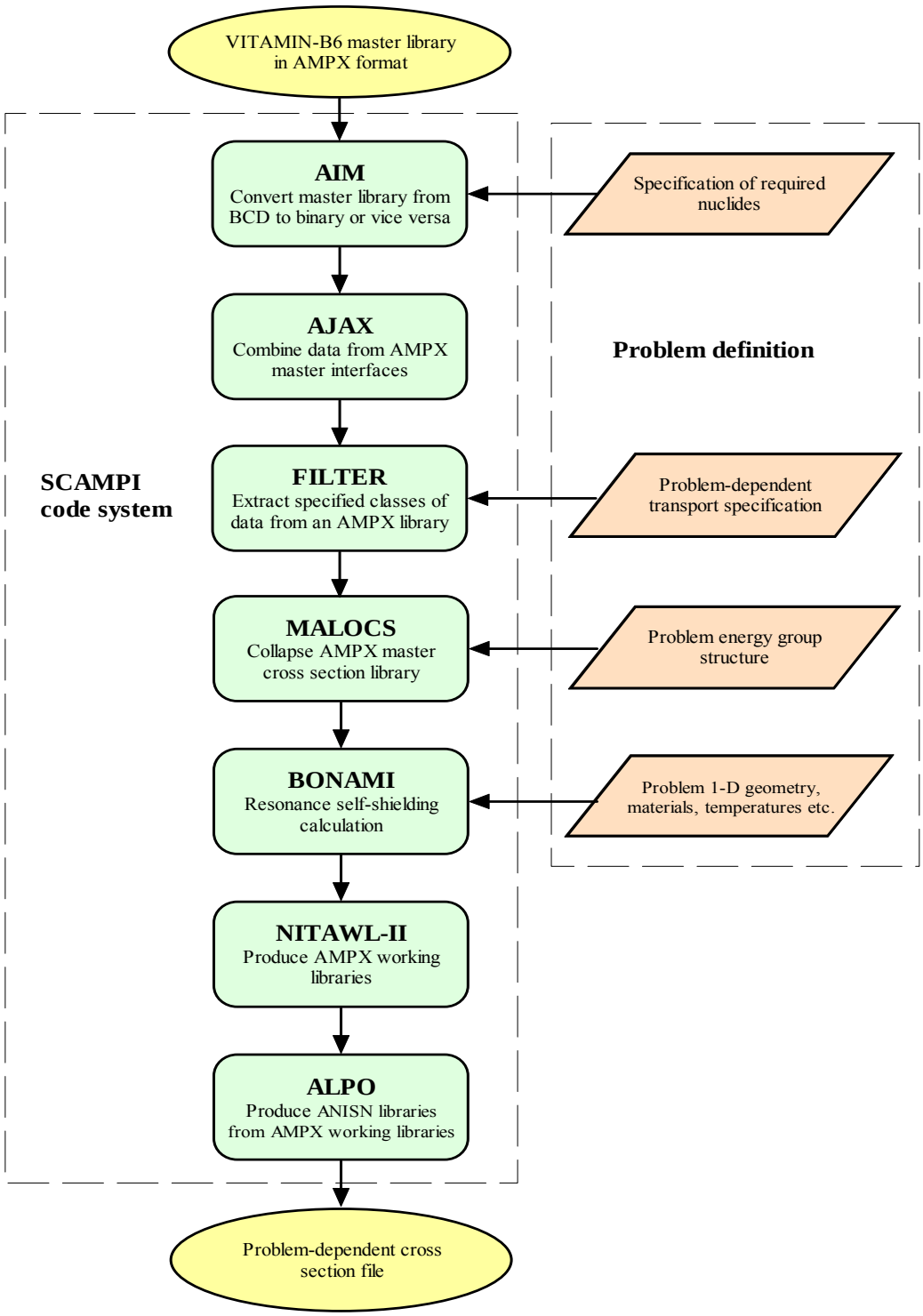

Fig. 3.5 Computational flow for generating problem-dependent cross section data libraries from AMPX format master libraries

3.4.3 Results and discussions

MCNP calculations were performed to obtain the neutron scalar fluxes on the specified surface shown in Fig. 3.4. All the particle tracks crossing the surface were recorded in the binary surface source file using the SSW option. The angular flux distribution on the surface is then evaluated using the interface program.

With the same geometric model and source representation, TORT calculations were performed. The mesh grid of the TORT geometric model is 20×20×40 and the Legendre expansion of the scattering kernel is P_3. The difference between the total scalar fluxes at the central part of the given surface calculated by MCNP and TORT is less than 1% for a S_{12} angular quadrature set used by TORT. Fig 3.6 shows the comparison of the neutron spectra at the center of the given surface calculated by MCNP and TORT using S_4, S_8 and S_{12} angular quadrature sets. The results confirm that the neutron flux is correctly calculated by both MCNP and TORT.

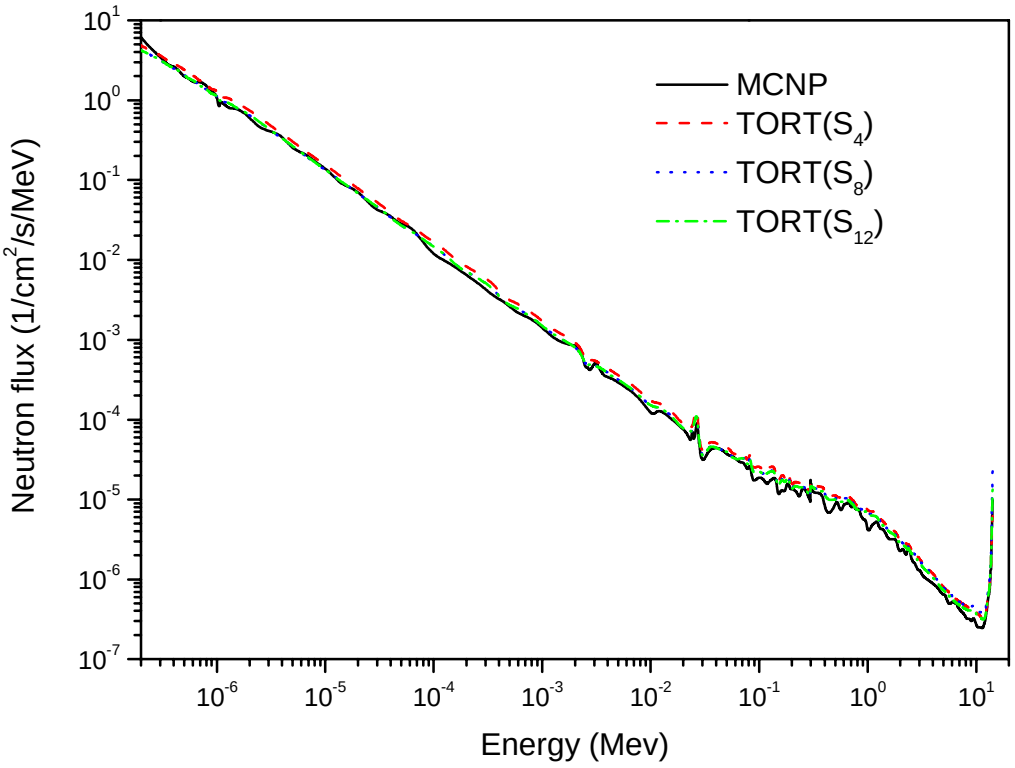

Fig. 3.6 Neutron spectra calculated by MCNP and TORT with quadrature sets S_4, S_8 and S_{12}

The angular flux distribution on the surface shown in Fig. 3.4 was calculated by the mapping approach based on the SSW surface source file generated in MCNP calculation, and directly by TORT, respectively. In the MCNP calculation, 20 million source particles were tracked. Comparisons of the results are performed in a mesh cell at the center of the surface and are discussed in the following.

Fig 3.7 compares the angular fluxes in specific directions calculated by these two different approaches with different angular quadrature sets S_4, S_8 and S_{12}. For all considered quadrature sets, satisfactory agreement can be obtained. In the thermal energy range, a minor discrepancy appears. The reason is that only a limited number of neutrons are slowed down into this energy range in the Monte Carlo simulation of this specific model with relatively high-energy neutron source and relatively small dimensions of the shielding zone. In addition, differences are observed in the source energy range in the case of S_4. This has to be expected because the number of discrete directions for this angular quadrature set is insufficient for this application. By using high order quadrature sets such as S_8 and S_{12}, the differences disappear.

Fig. 3.8 shows the ratios of angular fluxes calculated by the mapping approach and directly by TORT using the different angular quadrature sets. The results of three different MCNP runs with different numbers of neutron source histories are compared. The differences between the results of the two approaches are highlighted. The oscillation of the ratios around unity is due to the stochastic character of the recorded Monte Carlo particle tracks which are used by the mapping approach to calculate the angular flux distribution. As the number of considered Monte Carlo source particles increases, the differences decrease. Therefore, although the surface for mapping can be specified arbitrarily, in a practical application the surface should be specified so that a sufficient number of Monte Carlo particle tracks can cross it within a reasonable computing time and be recorded for use by the mapping approach.

Figs. 3.9, 3.10 and 3.11 compare the angular fluxes as a function of energy and direction in the case of 20 million Monte Carlo source particles with different angular quadrature sets. An overall satisfactory agreement is obtained. Minor discrepancies in different phase-spaces are caused by statistical fluctuations due to low probabilities of the neutron population in those phase-spaces. In summary, the results demonstrate that the mapping approach is properly implemented and functions in the interface program. The program thus can be used for the three-dimensional coupled MC-S_N shielding calculations as described in chapter 4.

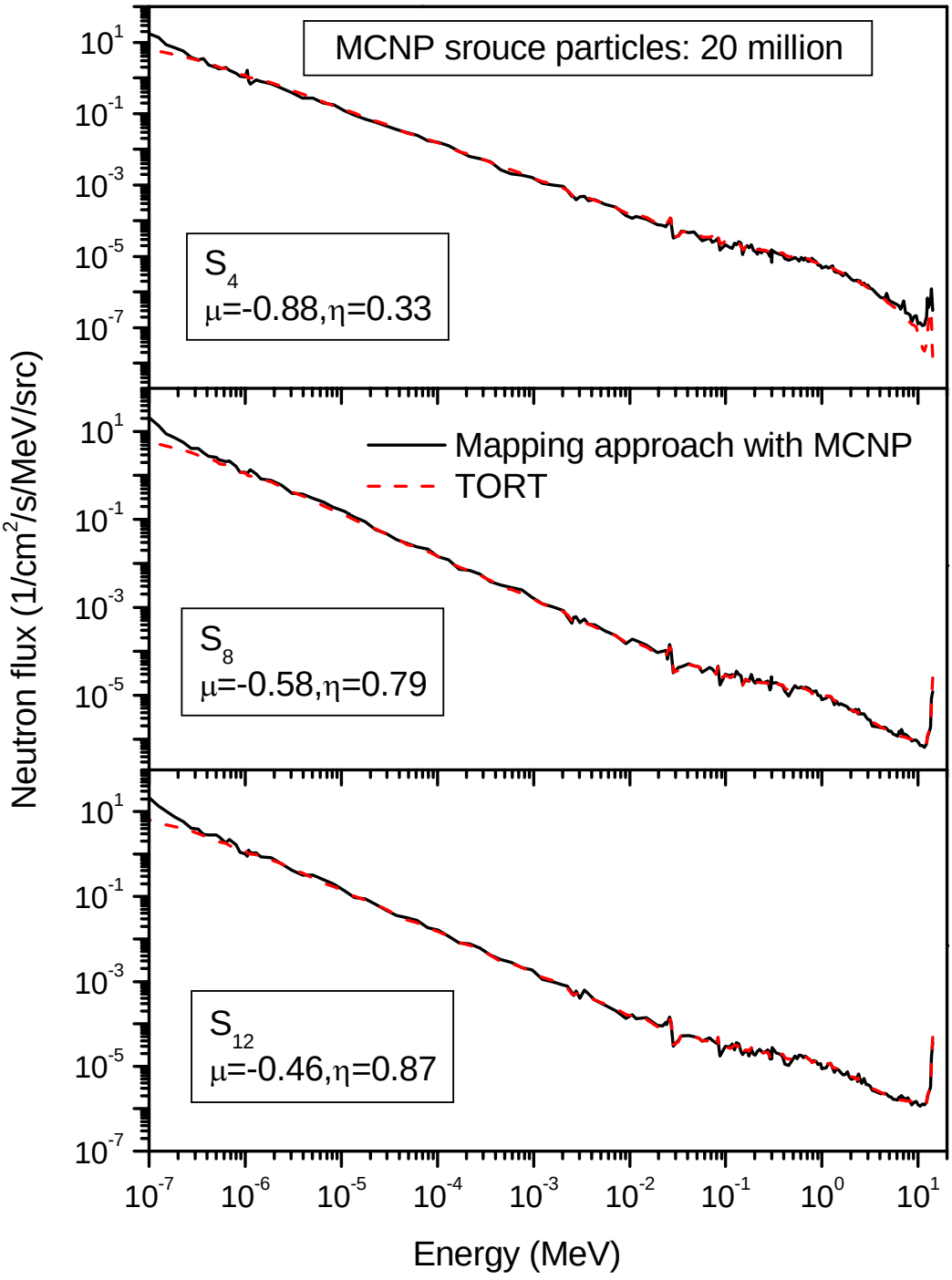

Fig. 3.7 Comparison of angular fluxes calculated by the mapping approach and TORT

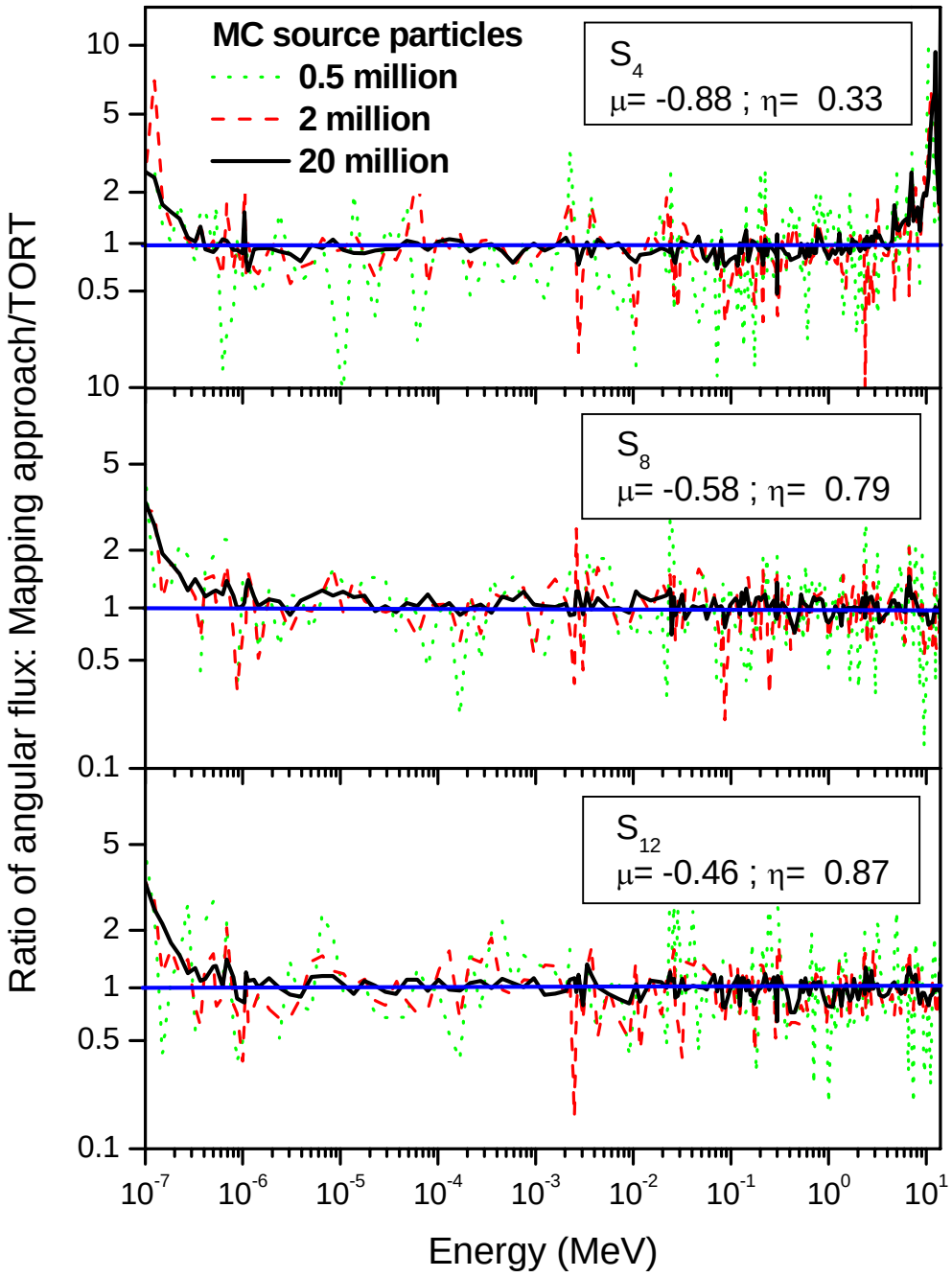

Fig. 3.8 Comparison of angular fluxes as a function of energy calculated by the mapping approach and TORT

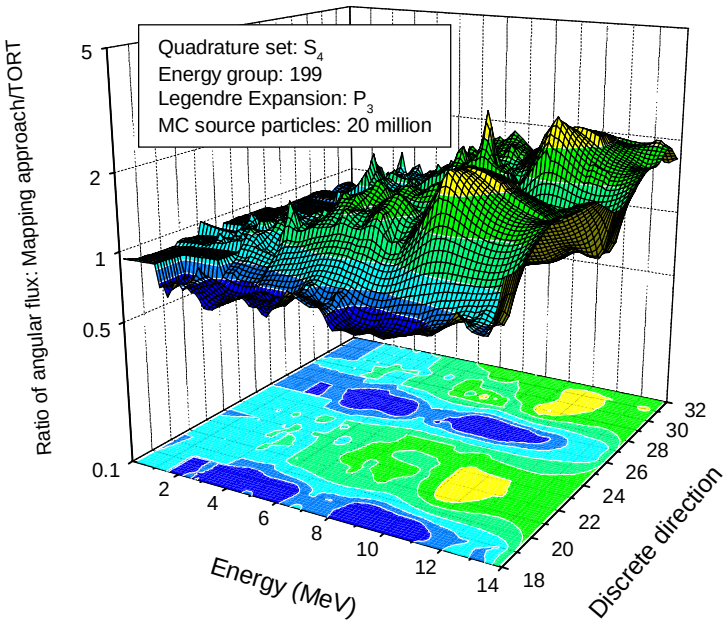

Fig. 3.9 Comparison of angular fluxes as a function of energy and direction calculated by the mapping approach and TORT with S_4 angular quadrature set

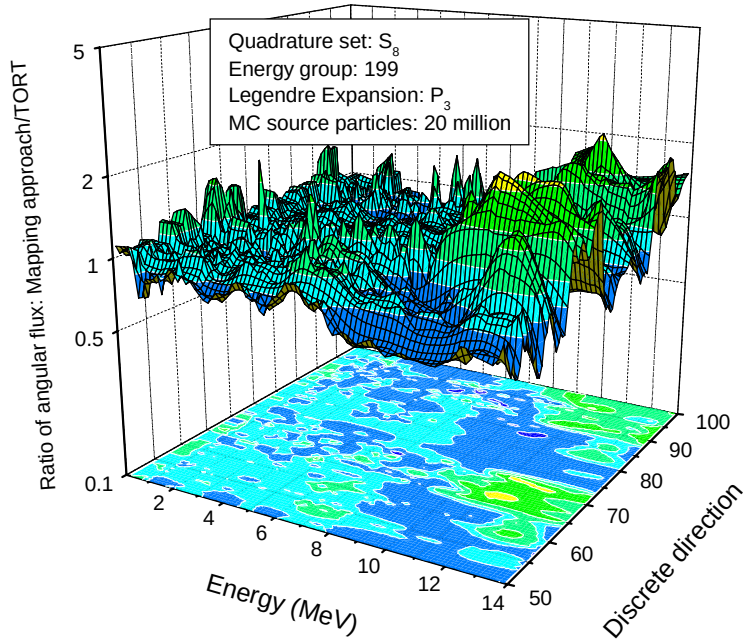

Fig. 3.10 Comparison of angular fluxes as a function of energy and direction calculated by the mapping approach and TORT with S_8 angular quadrature set

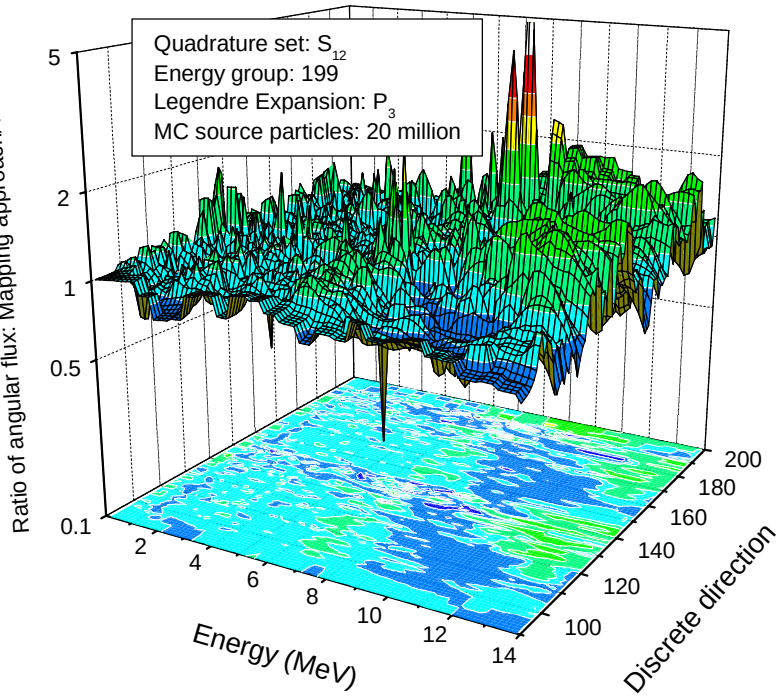

Fig. 3.11 Comparison of angular fluxes as a function of energy and direction calculated by the mapping approach and TORT with S_{12} angular quadrature set

4 THE PROGRAM SYSTEM FOR COUPLED SHIELDING CALCULATIONS

This chapter describes the program system for the three-dimensional coupled Monte Carlo-Discrete Ordinates shielding calculations. The Monte Carlo transport code MCNP, the three-dimensional discrete ordinates code TORT and the coupling interface program with the relevant nuclear data and additional modules are loosely integrated in the program system. Test calculations with two test models are performed. The results are compared with that from direct Monte Carlo calculations.

4.1 The program system

The underlying method for coupled Monte Carlo-Discrete Ordinates shielding calculations was discussed in chapter 3. The mapping approach, which is the key part for the coupling of these two different methods, was presented and validated in chapter 3. In this chapter, a program system for the coupled shielding analysis is described. The program system integrates the Monte Carlo transport code MCNP, the three-dimensional discrete ordinates code TORT, and the interface program system which implements the mapping approach. The flow chart of the program system is displayed in Fig. 4.1.

For a practical application to a large and complex nuclear facility, the problem geometry is first separated into two parts: the source/target region with a complex geometry for the Monte Carlo simulation and the bulk shielding region with a relatively simple geometry for the discrete ordinates treatment. A common surface is specified between these two parts to link the Monte Carlo model and the deterministic mesh model.

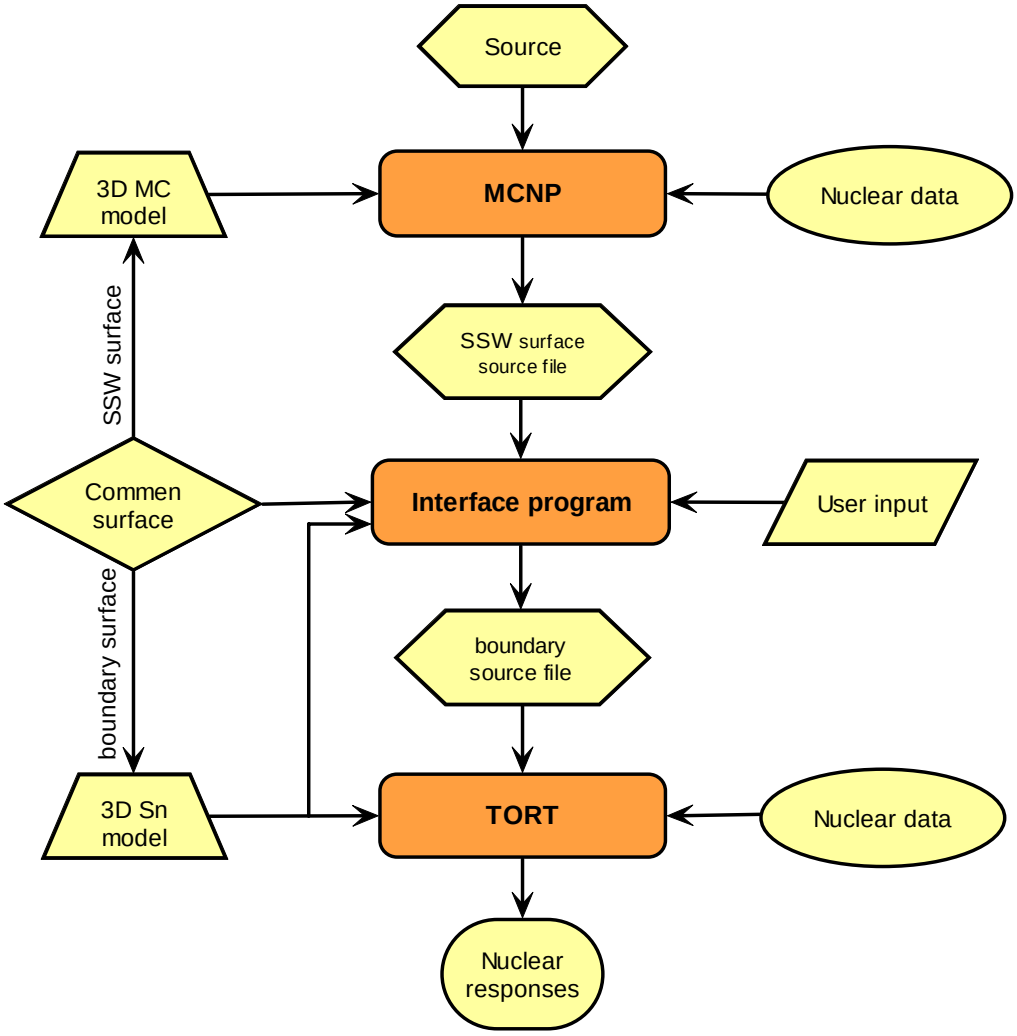

Fig. 4.1 Flow chart of the coupled Monte Carlo/Deterministic computational scheme

In the Monte Carlo calculation, the particle tracks of interest crossing the link surface are recorded in a binary file in SSW-format. For the deterministic model, the link surface is specified as a boundary for source input. The interface program reads and process the SSW file, the TORT input file including the meshes, the energy group structure, and the angular quadrature sets. In addition, a user input file is required for the definition of some additional parameters. The mapping process is then applied and the boundary source file is generated for the use in TORT calculations.

The program system is aimed at dealing with complex shielding problems, in particular with complex three-dimensional geometries and large dimensions. Both Cartesian (X, Y, Z) and Cylindrical (R, θ, Z) geometry can be used in the discrete ordinates solution of the coupled analysis. The system can also be modified to couple one and/or two-dimensional deterministic codes to Monte Carlo codes.

4.2 Test calculations

In order to verify the program system for the coupled shielding analysis, test calculations are performed with two test models. Neutron and photon fluxes and spectra are calculated and compared with those from direct MCNP calculations.

4.2.1 Nuclear data and test models

Point-wise cross section files generated from the ENDF/B-VI [40] data library are used in the MCNP calculations. By using the computational procedure described in Chapter 3, a 199 neutron groups and 42 gamma-ray groups problem-dependent cross section file was generated for TORT from the library VITAMIN-B6 [42]. The cross section file includes 36 thermal-neutron groups with up-scattering.

Since the purpose of these calculations is to test the program system instead of an actual application, the test models were prepared to be well suited for direct MCNP calculations. Figs. 4.2 and 4.3 display the two test models. Test model 1 is a 20×20×40 cm rectangular block with a cylinder source (height: 6 cm, radius: 2 cm) on one side and a detector cell on the other side. Test model 2 is a 20^{o} sector of a cylinder (radius: 40 cm, height: 40 cm) with reflecting boundary condition in the azimuthal direction. The radius of the source zone is 6 cm. The sources for both test models are 14 MeV neutrons with isotropic distribution. The shielding material for both models is a mixture of stainless steel and water (60a% SS316L + 40a% Water). As indicated in Figs. 4.2 and 4.3, the common surface was specified in each test model to separate the whole geometry into two parts: source zone and bulk shield zone with detector.

The complete test models are considered in the MCNP calculations while only the parts of bulk shield are needed in the TORT calculations. Two TORT mesh models are created, one in Cartesian (X, Y, Z) geometry for test model 1 and another in Cylindrical (R, θ, Z) geometry for test model 2. The specified common surface is used for the particle data scoring in the Monte Carlo simulation and as boundary for the surface source input in the TORT calculation.

It is noted that in practical applications the common surface is specified so that all complex components around the source are on one side for the Monte Carlo calculations and

the parts with relatively simple geometry are on the other side for the discrete ordinates calculations. The common surface should not be too far from the source zone in order to get a statistically accurate Monte Carlo estimation of the angular flux distribution on the common surface within a reasonable computing time. To check the statistical accuracy of the angular flux distribution on the common surface, several dedicated surface tallies are used in the Monte Carlo calculations. Additionally, it should be noted that sufficient shielding outside the specified common surface must be included in the Monte Carlo model in order to properly take into account the back-scattered particles.

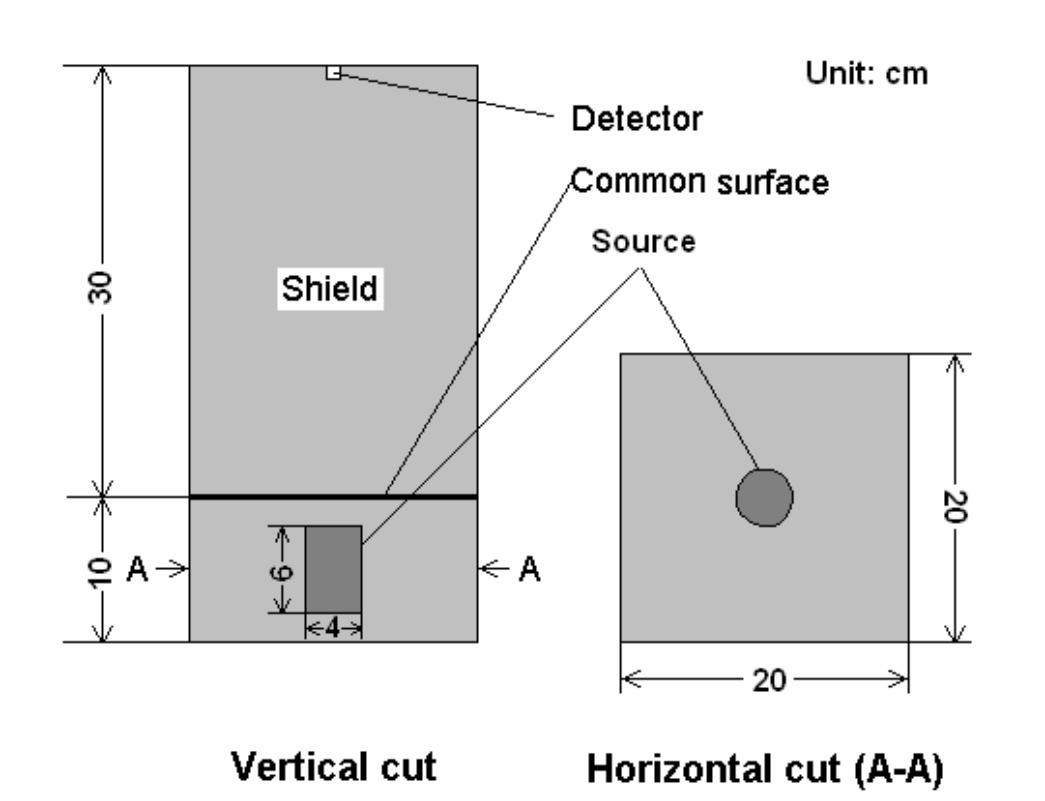

Fig. 4.2 Test model 1

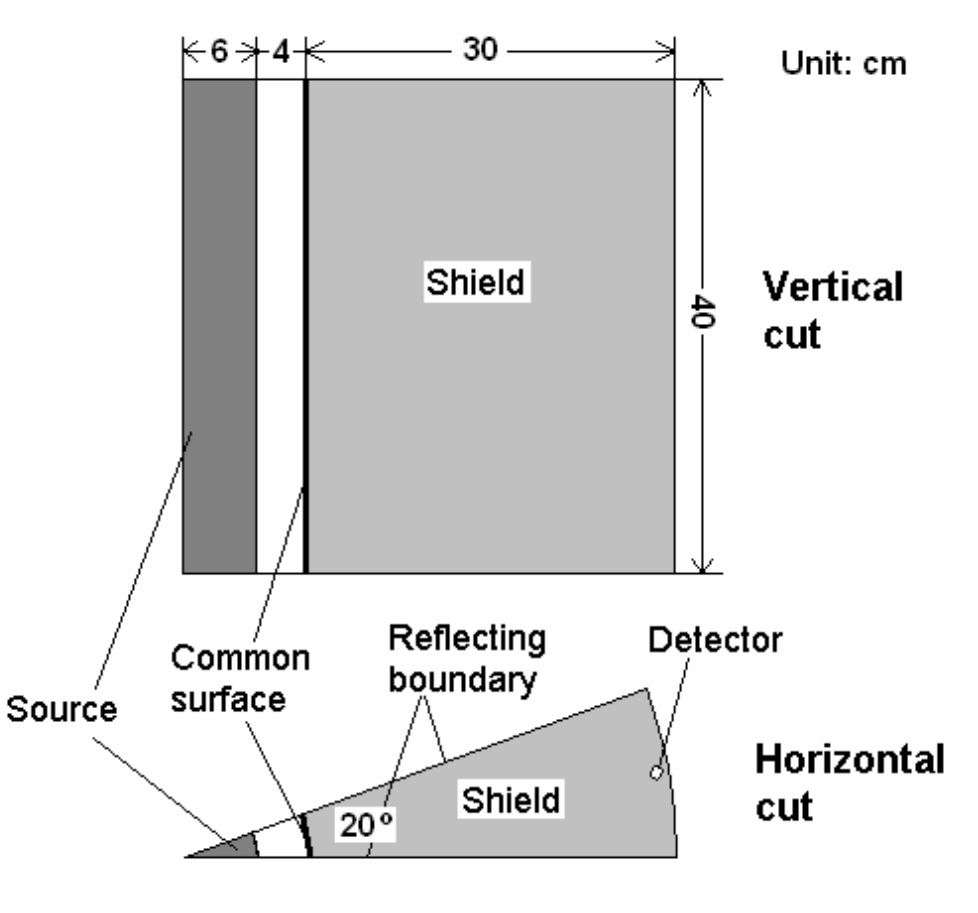

Fig. 4.3 Test model 2

4.2.2 Calculations with test model 1

MCNP calculations were performed to obtain the neutron and photon scalar fluxes and spectra at the detector location (see Fig. 4.2) for test model 1. In addition, each Monte Carlo track crossing the specified common surface was recorded in a binary file in SSW-format with its detailed information. The interface program generates the angular flux boundary source file of TORT. For the TORT calculations, the order of angular quadrature was set to S_8 and the order of Legendre expansion to P_3.

Based on the generated surface source file, a series of TORT calculations with various spatial meshes were performed to calculate the neutron and photon scalar fluxes and spectra. Table 4.1 shows the comparison of neutron and photon scalar fluxes at the detector calculated by the coupled MCNP-TORT approach and directly by MCNP. The agreement of the neutron

fluxes is improved as the number of the geometry meshes increased. This is because the accuracy of the representation of the particle distribution on the common surface employed in the mapping process improves as the number of geometry meshes increases. For the most detailed TORT mesh grid, the discrepancy in neutron fluxes is less than 0.5%.

For the results of the photon flux, the difference between these two approaches becomes considerable as shown in Table 4.1. This is due to the fact that these two approaches employ different photon physics treatments. MCNP can handle the photon transport with a detailed or simple physics model. While the electron transport is turned off for the problem of photon transport, a thick-target bremsstrahlung model (TTB) is used. In contrast, the existing S_N codes are not capable of handling the problem of electron transport and do not consider the bremsstrahlung effect as well. Consequently, electron-induced photons are ignored in the TORT calculations, which results in an underestimation of the photon flux by TORT compared to MCNP. As shown in Table 4.1, the discrepancy of the photon fluxes is reduced from ~15% to ~6% when MCNP uses the simple photon physics model and does not take into account the bremsstrahlung effect.

Fig 4.4 shows a comparison of the neutron spectra for the specified detector calculated directly by MCNP and by the coupled scheme. Fairly good agreement between these two methods is obtained. Within the energy range of thermal neutrons, slight disagreement appears as the neutrons are slowed down. The reason for this discrepancy might be that the thermal neutron treatments used in MCNP and in TORT are different. MCNP uses a thermal treatment based on the free gas approximation to account for the thermal motion of the atom. It also has an explicit *S(a, b)* capability that takes into account the effects of chemical binding and crystal structure for thermal neutrons. In the discrete ordinates solution, up-scattering cross section data for thermal groups are usually employed to treat the thermal neutron transport problems. The TORT cross section file used in this problem was generated from the library VITAMIN-B6 and includes 36 thermal-neutron groups with up-scattering. The different treatment of the thermal neutron transport in these two approaches might explain the minor difference in thermal energy range. In addition, for the VITAMIN-B6 library several problems such as insufficient self-shielding corrections and inadequate scattering matrices have been reported recently [46, 47], and these also might contribute to the slight disagreement. It has to be mentioned that this slight disagreement is not important in shielding problems with high energy neutrons since thermal neutrons do not contribute to the dose rate. For shielding problems in which thermal neutrons are of interest, the related deficiencies in the VITAMIN-B6 library have to be fixed or other appropriate data must be applied.

The comparison of photon fluxes calculated by MCNP and the coupling scheme for test model 1 is displayed in Fig. 4.5. It is observed that fairly good agreement can be obtained in the high energy range (> 0.1 MeV). For low energy photons (< 0.1 MeV), the coupled scheme underestimates the flux due to the absence of electron-induced photons in the TORT calculations when compared with the MCNP calculations with the detailed photon model. As mentioned above, satisfactory agreement between these two approaches can be achieved when MCNP uses the simple photon model without considering the bremsstrahlung effect. This confirms that the disagreement between the results from these two approaches is mainly due to the different physics models employed in the Monte Carlo code and the S_N code instead of resulting from the mapping process of the coupled scheme. In addition, it should be noted that for most practical shielding problems low energy photons are not important due to their minor contribution to the dose rate.

Table 4.1 Comparison of the total neutron/photon flux calculated by MCNP and the coupled MCNP-TORT approach

Method	TORT meshes	Neutron flux ($1/cm^2/s$)	Photon flux ($1/cm^2/s$)
MCNP	-	(1.93±0.002)E-05[a]	(2.13±0.002)E-05[b]/ (1.94±0.002)E-05[c]
3-D coupled MCNP-TORT	20×20×30	1.92E-05	1.82E-05
	10×10×15	2.07E-05	1.93E-05
	6×6×10	2.26E-05	2.08E-05

[a] Read as $(1.93\pm0.002) \times 10^{-5}$,

[b] Calculated with detailed photon model and bremsstrahlung effect,

[c] Calculated with simple photon model without bremsstrahlung effect.

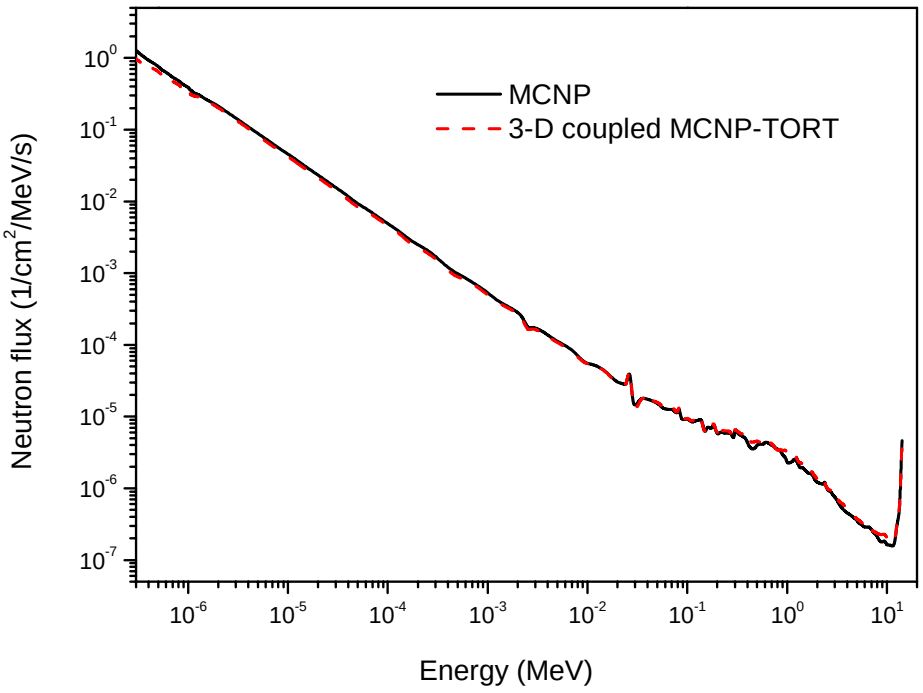

Fig. 4.4 Comparison of the neutron spectrum of model 1

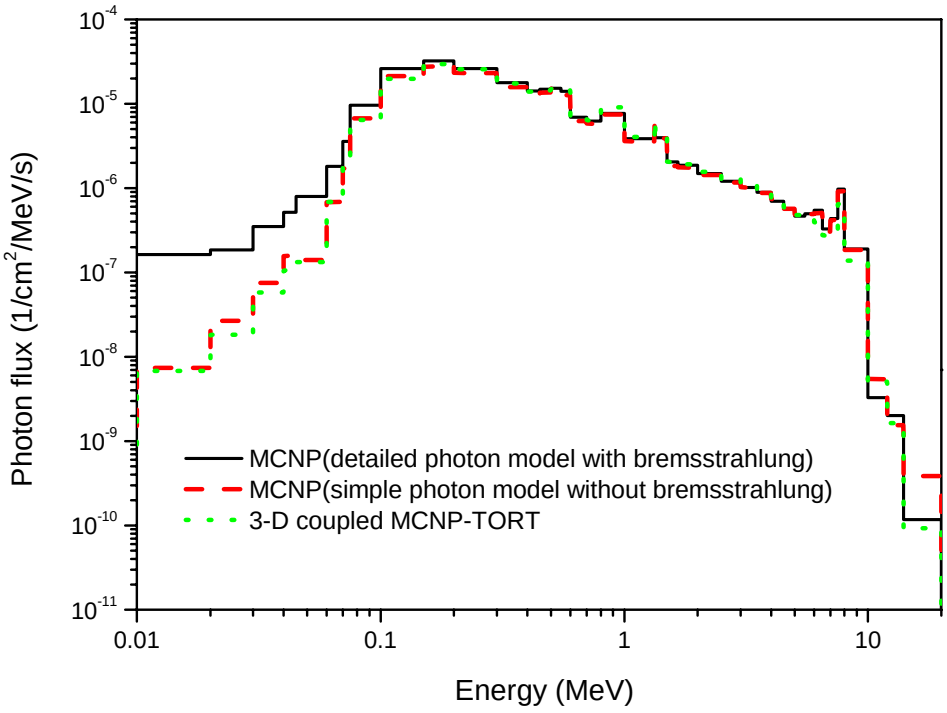

Fig. 4.5 Comparison of the photon spectrum of model 1

4.2.3 Calculations with test model 2

The neutron/photon scalar fluxes and spectra were calculated using directly MCNP and the MC-S_N coupled code system. A S_8 angular quadrature set and a P_3 order of scattering expansion were used in the TORT calculations. A set of TORT calculations with various spatial meshes were performed. Table 4.2 gives the comparison of neutron and photon scalar fluxes at the detector (see Fig. 4.3) calculated by MCNP and the coupled approach. As already observed for test model 1, the agreement of neutron fluxes between these two approaches improves as the number of geometry meshes of the TORT model increases. The discrepancy is less than 0.7% in the case of the finest TORT mesh grid. For the comparison of photon fluxes, again a considerable discrepancy is obtained. The discrepancy is about 15% when using detailed photon physics models in MCNP and about 6% when the bremsstrahlung effect is turned off.

Comparisons of the neutron and photon spectra are displayed in Figs. 4.6 and 4.7, respectively. For neutron spectra, there is again good agreement over the whole energy range above ~1 eV, and a slight disagreement below ~1 eV. The comparison of photon spectra shows again that the coupling scheme underestimates the photon flux below 0.1 MeV due to the absence of electron-induced photons in TORT calculations.

Table 4.2 Comparison of the total neutron/photon flux calculated by MCNP and the coupled MCNP-TORT approach

Method	TORT meshes	Neutron flux ($1/cm^2/s$)	Photon flux ($1/cm^2/s$)
MCNP	-	(3.07 ± 0.003)E-04[a]	(3.77±0.004)E-04[b]/ (3.42±0.004)E-04[c]
3-D coupled MCNP-TORT	31×11×21	3.09E-04	3.19E-04
	15×7×15	3.31E-04	3.26E-04
	10×5×11	3.64E-04	3.35E-04

[a] Read as $(3.07\pm0.003) \times 10^{-4}$,

[b] Calculated with detailed photon model and bremsstrahlung effect,

[c] Calculated with simple photon model without bremsstrahlung effect.

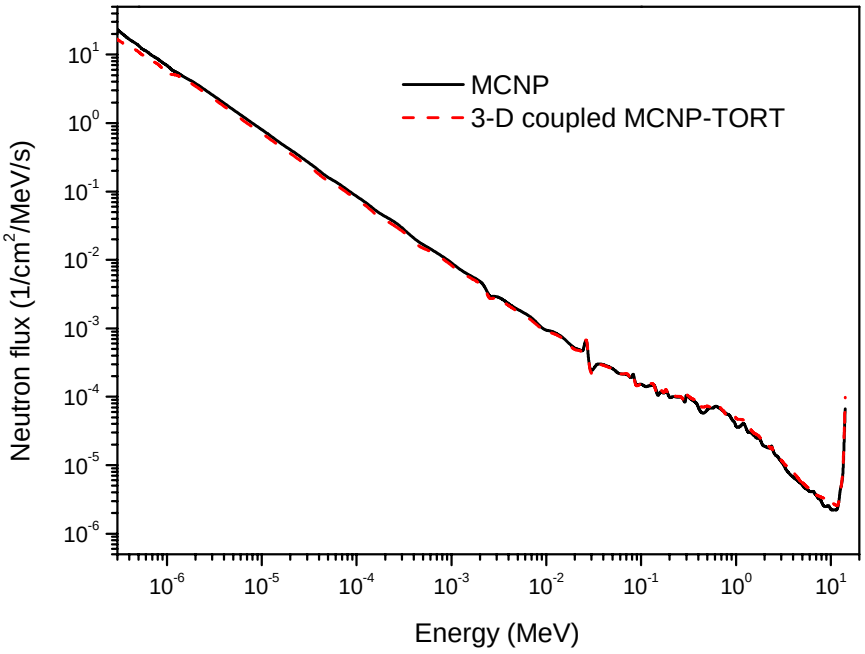

Fig. 4.6 Comparison of the neutron spectrum of model 2

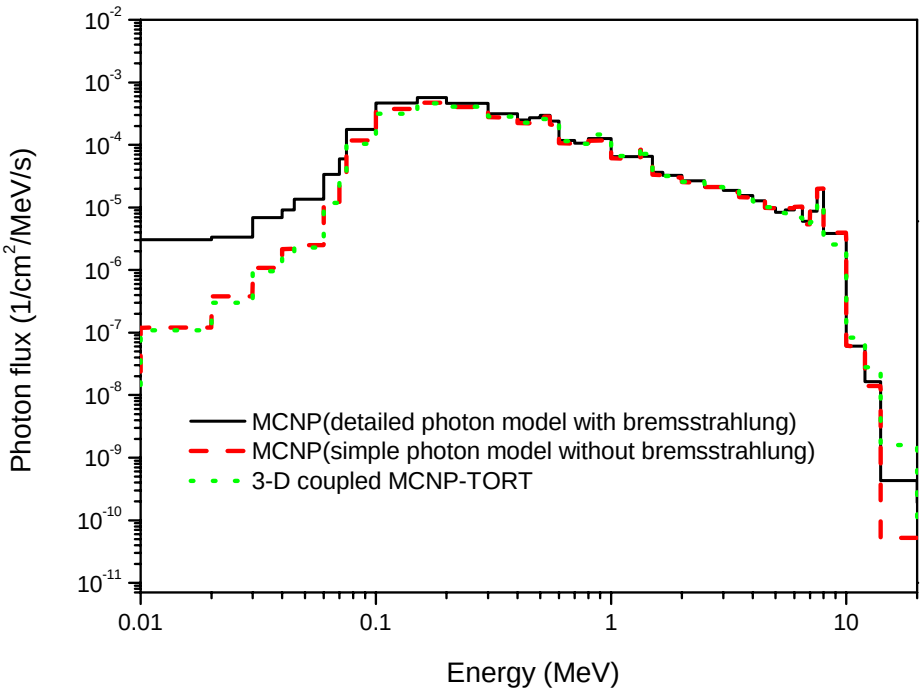

Fig. 4.7 Comparison of the photon spectrum of model 2

4.3 Summary and conclusions

In order to validate the program system for three-dimensional MC-S_N coupled shielding calculations, test calculations with a Cartesian and a Cylindrical geometrical model were performed. The comparisons between the results calculated by MCNP and by the coupled code system show that:

1. Fairly good agreements of neutron fluxes above 1 eV are obtained. The minor discrepancy in the thermal energy range is mostly due to the approximate thermal neutron treatment and inadequate low energy cross section data in the master nuclear library used by TORT. When thermal neutrons are of concern, the related deficiencies in the data library have to be fixed or other qualified data must be used.
2. Good agreements of photon fluxes above 0.1 MeV are obtained. Below 0.1 MeV, the MC-S_N coupled code system slightly underestimates the photon fluxes due to the approximate treatment of photons and the absence of electron-induced photons in S_N calculations. Overall satisfactory agreement can be obtained when the simple photon physics model is used and the generation of electron-induced photons is turned off in MCNP. It is, however, more realistic to apply the detailed photon physics model in MCNP, although low energy electron-induced photons are not important for shielding problems.

The test calculations show that reliable three-dimensional shielding calculations can be performed with the MC-S_N coupled code system, but its distinguished features for handling geometrically complex and dimensionally large nuclear facilities is not yet demonstrated. The next chapter will present such an application.

5 APPLICATION TO IFMIF SHIELDING ANALYSIS

The shielding problem of the accelerator driven IFMIF (International Fusion Materials Irradiation Facility) neutron source [22, 23] is complicated due to the geometric complexity of the test cell with the Deuteron-Lithium (D-Li) source inside and a bulk shield around the test cell. Previous work has shown that conventional methods are not able to provide a complete solution to this shielding problem with satisfactory accuracy. In this chapter the application of the three-dimensional MC-S_N coupled code system to the IFMIF shielding analysis is presented. Comparisons between the results of this work and previous work are also discussed. In this way, the capability of the MC-S_N coupled program system for application to the shielding problem of large and complex nuclear facilities is demonstrated.

5.1 The IFMIF neutron source

IFMIF is an accelerator driven D-Li neutron source designed to produce an intense neutron field that will simulate the neutron environment of a D-T fusion reactor. The primary mission is to generate a materials irradiation database for the design, construction, licensing, and safe operation of a Fusion Demonstration Reactor (DEMO). This will be achieved through testing and qualifying materials under irradiation at the high neutron fluence levels anticipated for the full lifetime of DEMO.

IFMIF consists of three major subsystems: the Test facilities, the Target Facility, and the Accelerator Facility, in addition to the Post-Irradiation Facilities and other conventional facilities as shown in Fig. 5.1. Two Continuous-Wave (CW) linear accelerators produce two 40 MeV, 125 mA deuteron beams. Both beams strike a common flowing lithium target, providing, through the resulting D-Li reactions, an intense neutron flux at the (maximum) level of 10^{19} n/m^2/s with a broad energy peak around 14 MeV.

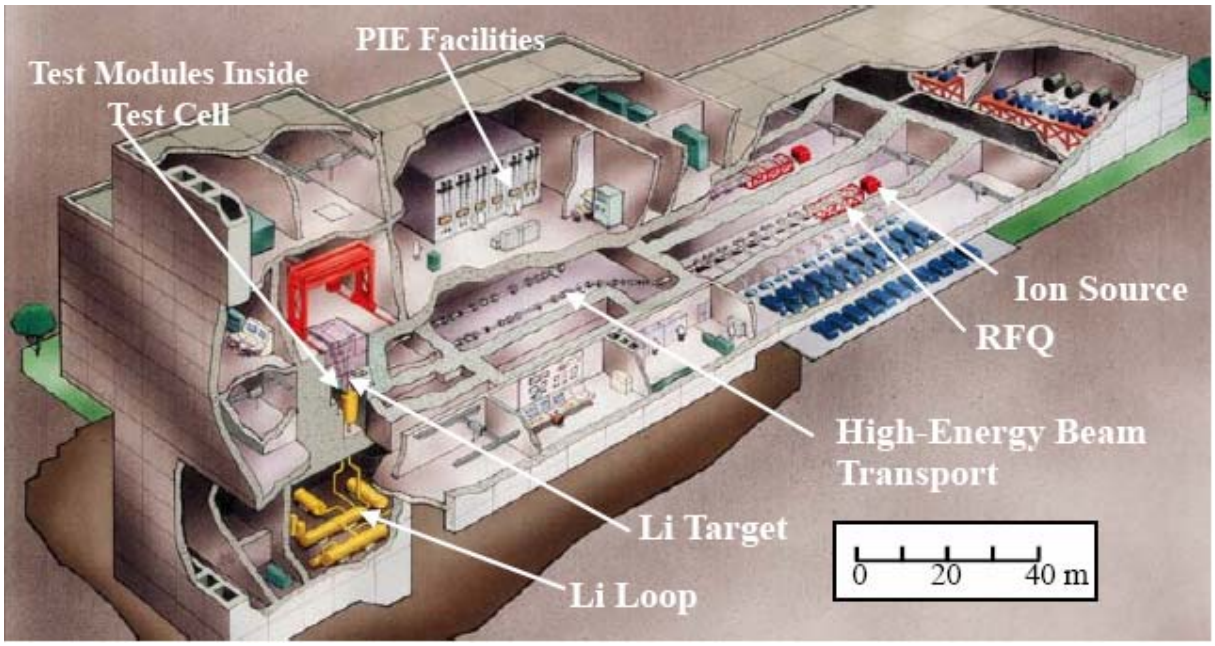

Fig. 5.1 Three-dimensional view of IFMIF

The design activities of IFMIF are performed under the International Energy Agency (IEA) collaboration which began in 1995. In 2000, a three-year Key Element Technology Phase (KEP) of IFMIF was undertaken to reduce the key technology risk factors. It was recognized that some development activities and some detailed preliminary design efforts are still required to provide the basis for deciding about the IFMIF construction. Therefore, a new phase, the Engineering Validation and Engineering Design Activity (EVEDA), is planned to focus on the detailed engineering design and associated prototypical component tests.

At the stage of EVEDA, complete shielding analysis is required to predict the radiation level in each facility room and cell to make sure the safety requirements can be met. The reliability of the shielding calculations will have significant effect on the detailed engineering design, optimization, and cost reduction consideration. However, shielding analyses for IFMIF are complicated due to the complex geometry, especially of the test cell (see Fig. 5.2) with the D-Li neutron source inside, and the large dimensions of the surrounding rooms with concrete shielding walls in the range of 2~3 m. Because of the significant influence of the geometric configuration and the components of the test cell, a detailed computational model of the test cell has to be used in the shielding calculations. In addition, an accurate representation of the D-Li neutron source must be provided in the neutron transport calculations.

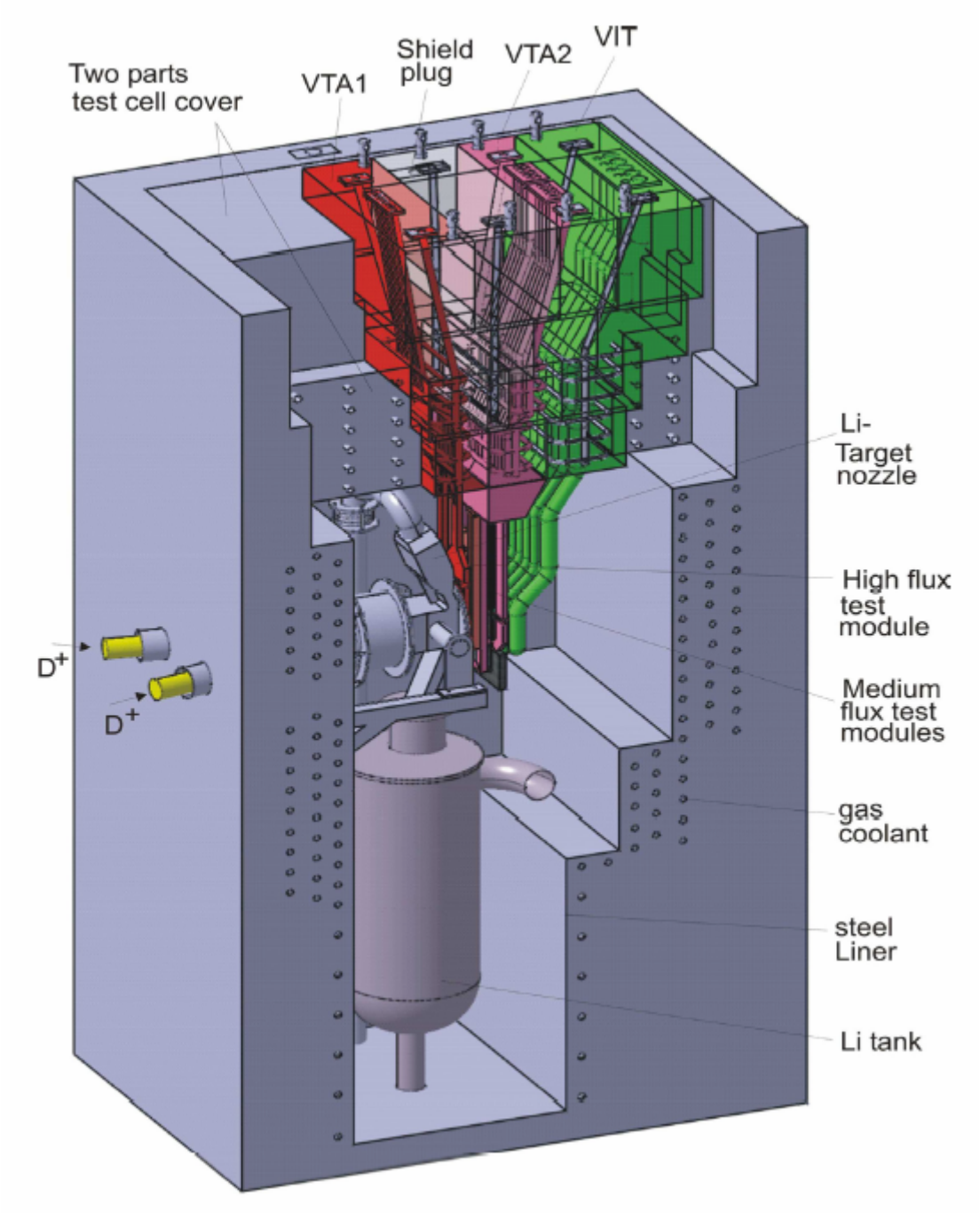

Fig. 5.2 Elevation view of test facilities with the lithium target and all vertical test assemblies

In previous analyses, a series of neutron transport calculations [48, 49, 50] were performed to provide preliminary assessments of the radiation level in the accessible regions around the test cell. In these calculations, very simplified geometrical models and very approximate representations of the neutron source were employed due to the inherent limits of the methods applied. Therefore, significant uncertainties are included in these calculations

which could severely affect the shield design of IFMIF in the future. To improve the reliability of the IFMIF shielding calculations, the complex geometry of the test cell, the large-sized bulk shield (with the associated deep radiation penetration) as well as the accurate description of the D-Li neutron source must be taken into account. Such a task can be accomplished with the three-dimensional coupled MC-S_N program system developed in this work. In the following sections, the application of this program system to the IFMIF shielding analysis is presented and discussed.

5.2 Problem definition

In this application, the neutron and photon fluxes and the resulting dose rate distribution are calculated across the back wall of the test cell (facing the D-Li target and the Test Modules) as well as inside the access/maintenance room behind the back wall. Since the main purpose of this application is to demonstrate the capability of the coupled program system for shielding calculations of large and complex systems, a complete shielding analysis of the IFMIF facility is not included in this work. Yet some valuable conclusions will be derived for the future IFMIF shield design. The coupling scheme and the code system are described in chapters 3 and 4. The basic definition of the shielding problem of IFMIF is presented in the following sections.

5.2.1 Source term and nuclear data

IFMIF is driven by two 40 MeV deuteron CW linear accelerators each with 125 mA beam current delivered to a thick flowing lithium target. Neutrons are produced in a stripping reaction with a broad energy (up to ~55 MeV) maximum peaked at 14-16 MeV. In order to accurately simulate the generation of D-Li source neutrons, the Monte Carlo code McDeLicious [51] has been developed as enhancement to MCNP with the new capability to sample source neutrons on the basis of tabulated d + ^{6,7}Li cross-section data [52]. For the coupled MC-S_N shielding calculation, McDeLicious was used to simulate the neutron and photon generation and transport in the D-Li target region. High energy cross section data from the ENDF/B-VI Release 6 (up to 150 MeV) data library [53] and FZK/INPE (up to 50 MeV) evaluated data files [52] are used with McDeLicious.

The three-dimensional discrete ordinates code TORT is used to treat the deep-penetration problem of the neutron transport in the bulk shield region around the D-Li target. Vitenea-IEF [54], an intermediate energy (up to 150 MeV for neutrons and up to 100 MeV for gammas) coupled 256-neutron and 49-gamma-ray multi-group cross section library in AMPX format, is used with TORT. The library was obtained by processing the LANL evaluated files of ENDF/B-VI release 6 [53] and FZK/INPE files [52] by the NJOY-AMPX-SCALE code systems [37, 43, 44]. The library contains the following materials/isotopes: H-1, H-2, C, O-16, Al-27, Si-28, Si-29, Si-30, P-31, Ca, Cr-50, Cr-52, Cr-53, Cr-53, Fe-54, Fe-56, Fe-57, Ni-58, Ni-60, Ni-61, Ni-62, Ni-64, Cu-63, Cu-65, Nb-93, W-182, W-183, W-184, W-186, Pb-206, Pb-207, Pb-208 from ENDF/B-VI Release 6 and K-39, Li-6, Li-7, V-51 from FZK/INPE nuclear data files. The problem-dependent cross section file for TORT was generated from Vitenea-IEF by using the code system SCAMPI as described in Section 3.4.2.

5.2.2 Geometric model and materials

The three-dimensional geometric model used for the shielding calculations is displayed in Figs. 5.3 and 5.4. The model includes two parts: the test cell and the access/maintenance room. The part of the test cell (the region marked with yellow colour in Figs. 5.3 and 5.4) is a detailed three-dimensional MCNP model [55] developed on the basis of the current reference design of the facility in the framework of the IFMIF project. This model describes accurately the detailed geometry of all subsystems in the test cell such as the beam and target system, the lithium handling system, the high/medium/low flux test modules, the ceiling, the floor, and the walls. The walls and the floor are assumed to consist of 3m thick heavy concrete and a 3cm thick steel liner inside. The innermost 50 and 20 cm (0 cm for the floor) are assumed to contain cooling ducts, comprising 10% of the volume, for the back and side wall. The use of this model in the Monte Carlo simulation enables to take into account the complex configuration of the test cell which would have been a very difficult, if not impossible, task for a deterministic calculation. On the other hand, it is very difficult for the Monte Carlo simulation to transport a sufficient number of particles through the thick concrete wall to the access/maintenance room. Consequently, the discrete ordinates method is used in this part.

The mesh model for TORT calculations includes the test cell back wall and the access/maintenance room. The ceiling, the vertical wall, and the floor of the access/maintenance room are made of ordinary concrete with thicknesses of 0.5m, 0.5m and 1.0m thick, respectively (except the back wall), respectively. In order to enable the use of a

detailed mesh model with a fine energy group structure, a high order of the scattering kernel Legendre approximation and the angular quadrature set, the mesh model is further divided into two parts: the back wall and the access/maintenance room. The mesh grids for the back wall and the room are (64 × 52 × 60) and (62 × 44 × 82) in XYZ geometry, respectively. The code TORSET [56], which is included in the DOORS code package, is used for the splicing and bootstrapping from the part of the back wall to the part of the access/maintenance room in the TORT solution.

In this application, the inner surface (see Figs. 5.3 and 5.4) of the back wall is specified as the common surface (CSA: Common Surface A) for scoring the Monte Carlo particle tracks and acting as boundary surface for the TORT source input. In addition, another plane surface which is 50cm far from the inner surface is also used as the common surface (CSB: Common Surface B) in order to make sure that the results do not depend on the choice of the common surface. The thick concrete walls are included in the geometric model for the Monte Carlo simulation in order to take into account the albedo effect. It is noted that the other surface(s) can also be specified as the common surface according to the specific requirement of the problem to be solved.

The shielding material of the walls, ceiling and floor surrounding the Test Cell is heavy concrete (marked with yellow colour in Figs. 5.3 and 5.4). The material of the walls, ceiling and floor surrounding the access/maintenance room is ordinary concrete (marked with grey colour in Figs. 5.3 and 5.4). Table 5.1 shows the material composition of the heavy concrete and the ordinary concrete. Because the cross section data of Mg, S, Ti and Mn are not included in the Vitenea-IEF library, the contribution of Mg and S are added to Ca in the case of ordinary concrete and the contribution of Mg, S, Ti and Mn are added to Fe in the case of heavy concrete in the TORT calculations. The effect of this material approximation has been investigated by means of McDeLicious calculations and proved to be negligible. In order to check the shielding performance and compare with the previous calculations, the case with the ordinary concrete as the shielding material for the back wall was also considered. The specification of the other materials can be found in Refs. [55, 57].

Table 5.1 Composition of heavy concrete and ordinary concrete (wt %)

Element	Heavy concrete	Ordinary concrete
H	0.3116	0.555
O	33.09	49.748
Si	2.578	31.471
Ca	7.11	8.283
Mg	0.9348	0.256
Al	2.351	4.691
S	0.1416	0.128
Fe	47.78	1.238
Ti	5.439	0
Cr	0.17	0
Mn	0.1983	0
V	0.3116	0
Na	0	1.708
K	0	1.922

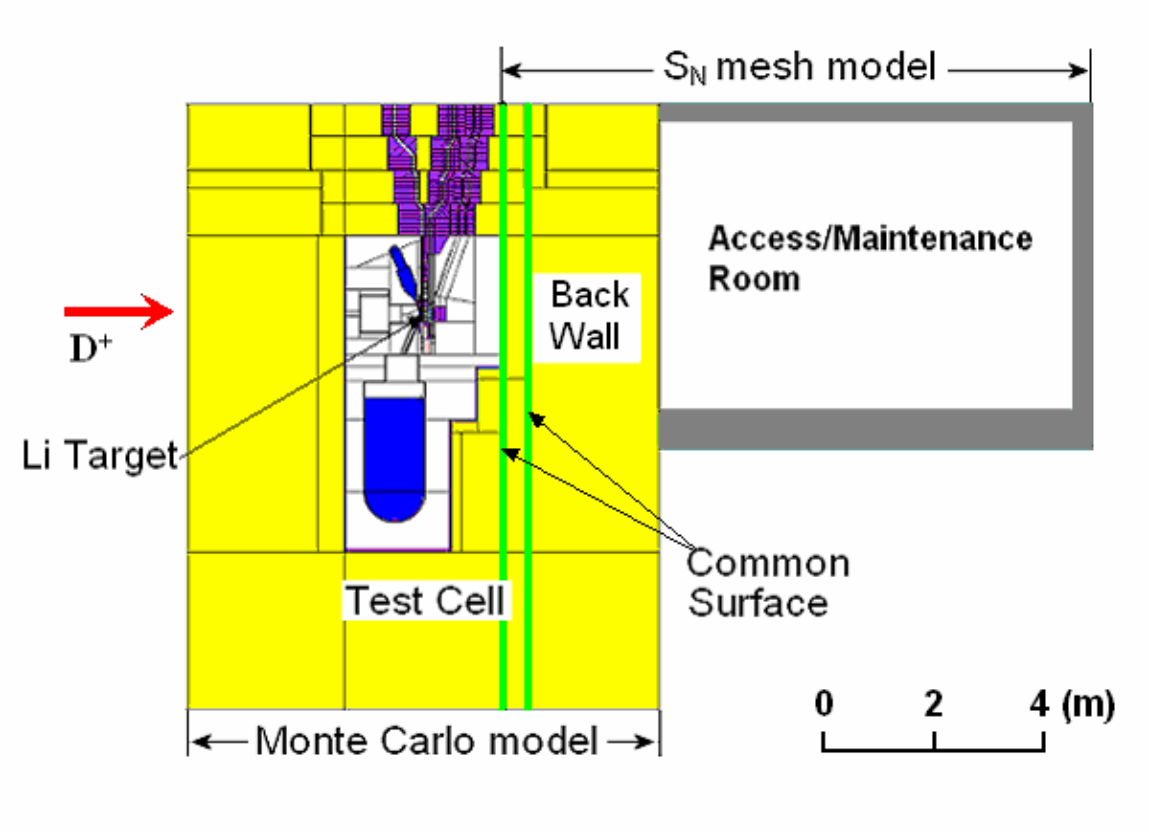

Fig. 5.3 Vertical cross section of the three-dimensional geometrical model of IFMIF: test cell and access/maintenance room

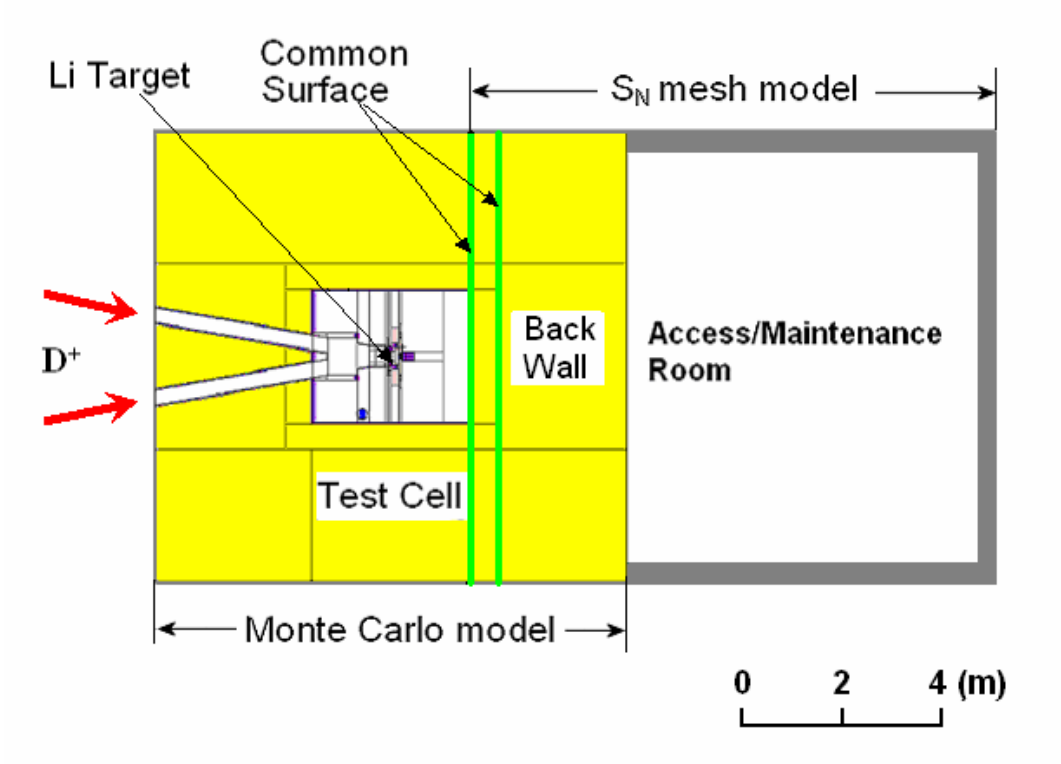

Fig. 5.4 Horizontal cross section of the three-dimensional geometrical model of IFMIF: test cell and access/maintenance room

5.3 Results and discussions

In the MC-S_N coupled analysis, the Monte Carlo simulations are first performed using McDeLicious. The SSW-format surface source files are created to record the neutron and photon tracks crossing the common surfaces CSA and CSB. The surface source file for CSA contains ~13 million neutron tracks and ~3 million photon tracks. For CSB, two cases are considered: CSB1 with 0.7 million neutron tracks and 0.3 million photon tracks, CSB2 with 10 million neutron tracks and 4.2 million photon tracks. The surface source files are read and processed by the interface program with the TORT input file and the user input file. Next the surface (boundary) surface file of TORT is generated. Using this surface source, coupled neutron/photon transport calculations are performed by TORT to obtain the three-dimensional neutron and photon flux distributions in the back wall and access/maintenance room. The dose rates are obtained by multiplying the neutron/photon fluxes by flux-to-dose rate conversion factors [58]. In the TORT calculations, a S_8 angular quadrature set, a P_3 Legendre series approximation of the scattering kernel and the 256-neutron and 49-photon energy group structure are used. It should be noted that most calculations are performed with CSA. The calculations with CSB are only performed for comparison and verification as discussed in Section 5.3.2.

5.3.2 Neutron and photon fluxes

The neutron and photon fluxes across the back wall of the test cell and in the access/maintenance room are calculated using the coupled MC-S_N program system. In addition, the neutron and photon fluxes across the back wall are calculated by the McDeLicious code while creating the surface source file for the coupled calculations. It was found that it is not possible to obtain statistically reliable results in the access/maintenance room with the direct Monte Carlo calculations despite the use of various variance reduction techniques.

Figs. 5.5 and 5.6 display the comparisons of the neutron and photon fluxes calculated by McDeLicious and the coupled approach with the common surfaces of CSA, CSB1 and CSB2, respectively. Heavy concrete is used as the shielding material of the back wall in these cases. Both the neutron and photon fluxes show an approximate exponential attenuation profile across the back wall. The neutron flux decreases by about 9 orders of magnitude across the

3m thick back wall and the photon flux by about 8 orders of magnitude. The attenuation of the neutron and photon fluxes in the access/maintenance room is shown to be very small.

As shown in Figs 5.5 and 5.6, satisfactory agreement between the neutron/photon fluxes across the back wall calculated by the Monte Carlo approach and the coupled scheme can be obtained. Slight discrepancies appear in the deep part of the back wall. This disagreement is partly due to the fact that surface estimators (tallies) are used in the Monte Carlo simulation while the results of the S_N calculations are cell-averaged. Additionally, in the Monte Carlo simulation fewer particles are tracked with the increasing depth of the shielding wall and the associated uncertainties of the tally estimators are correspondingly larger.

The comparison of the coupled calculations using the common surfaces CSA, CSB1 and CSB2 show good agreement. However, for the results with CSB1 and CSB2, slight underestimations are observed compared to the results with CSA. This is because fewer Monte Carlo particle tracks are considered in the cases of CSB1 and CSB2 than in the case of CSA. Consequently, the particle distribution on CSA is more accurately represented than that of CSB. When more Monte Carlo particle tracks are considered in the case of CSB2 compared to CSB1, the agreement with the case of CSA is improved from ~20% to ~5%. It should be noted, however, that in order to obtain more particle tracks in the case of CSB2, the corresponding Monte Carlo computing time is considerably increased. For instance, the computing time for the Monte Carlo simulation with CSA and CSB1 is about 2000 CPU minutes, and it is increased to as much as 20000 CPU minutes for CSB2 which is inefficient for most applications. The results indicate that the problem solution is independent on the selection of common surface. The common surface should thus be specified to obtain a source particle distribution with high statistical accuracy within reasonable computing times.

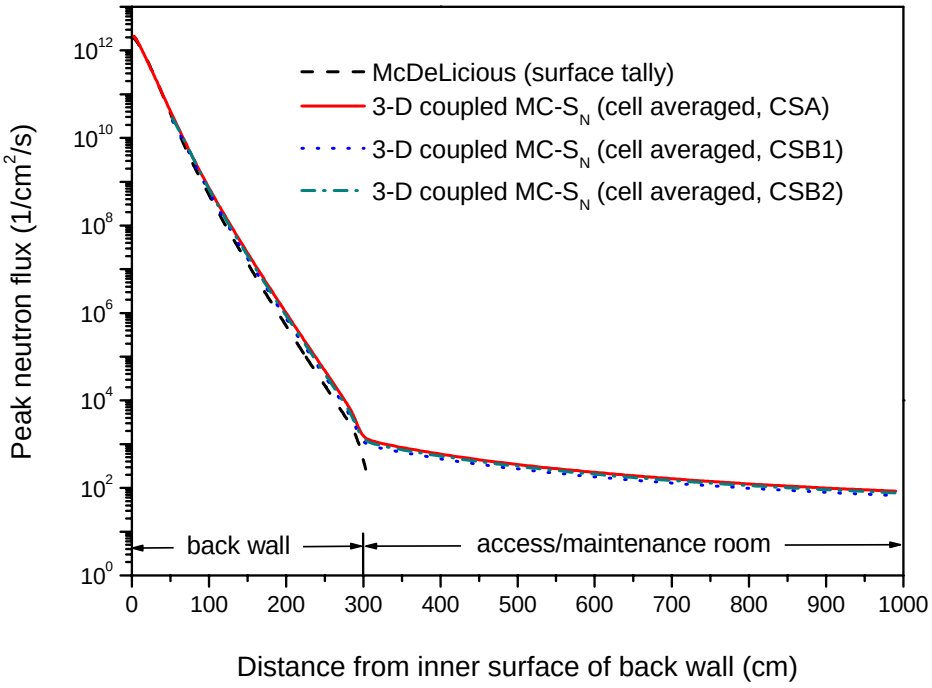

Fig. 5.5 Neutron flux across the back wall of the IFMIF test cell

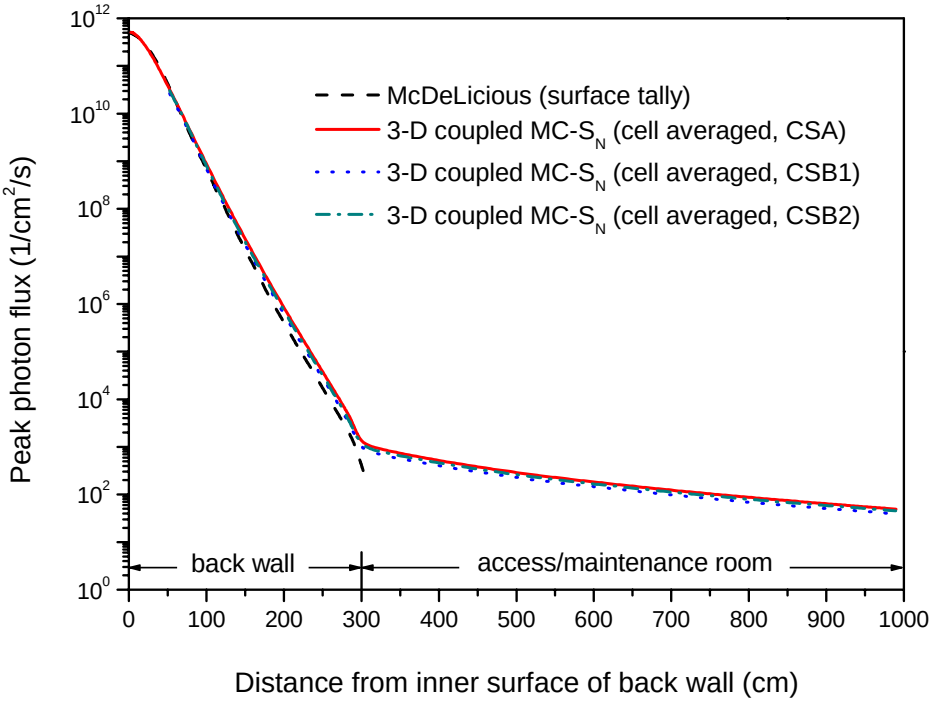

Fig. 5.6 Photon flux across the back wall of the IFMIF test cell

5.3.3 Neutron and photon spectra

The neutron and photon spectra in the back wall and the access/maintenance room are calculated with TORT starting from the source distribution at the common surface CSA.

Fig. 5.7 shows the neutron spectra in the back wall at the locations of 5, 145, and 300 cm and in the middle of the access/maintenance room. The profiles of the calculated neutron spectra are similar except in the high energy range (> 20 MeV). A peak of neutron flux in the energy range around 40 MeV becomes apparent as the distance increases from the back wall. This is because the mean free path of high energy neutrons in the shielding material is considerably larger than that of low energy neutrons. Therefore, the fraction of high energy neutrons increases with increasing penetration depth of the wall. For instance, at a distance of 5cm from the inner surface, the fraction of high energy neutrons is only ~0.3%. This fraction increases to 4.2% and 9.9% at distances of 145 and 300 cm, respectively. Correspondingly, the fraction of dose rate due to high energy neutrons increases from 1.7% at 5 cm depth to 15.3% and 25.2% at penetration depths of 145 and 300 cm, respectively. These results indicate that the high energy neutrons play a significant role for the shielding performance in spite of its small fraction in the virgin D-Li source neutron spectrum. The photon spectra at the locations of 5, 145, and 300 cm of the back wall and in the middle of the access/maintenance room are given in Fig. 5.8. It is observed that the profiles of photon fluxes at different depths of the back wall are similar. The energy of photons extends up to 60 MeV due to the scattering and reactions of high energy neutrons.

The accuracy of the calculated neutron/photon spectra has crucial influence on the evaluation of dose rate and materials activation. It has to be noted that the accurate calculation of neutron/photon spectra with fine group structure in optically thick media only becomes possible with the use of the coupled program system. The Monte Carlo method fails in this calculation due to the tremendous computing time. The S_N method, because of the approximations of source term and geometry of the target region, is also not able to provide reliable neutron/photon spectra.

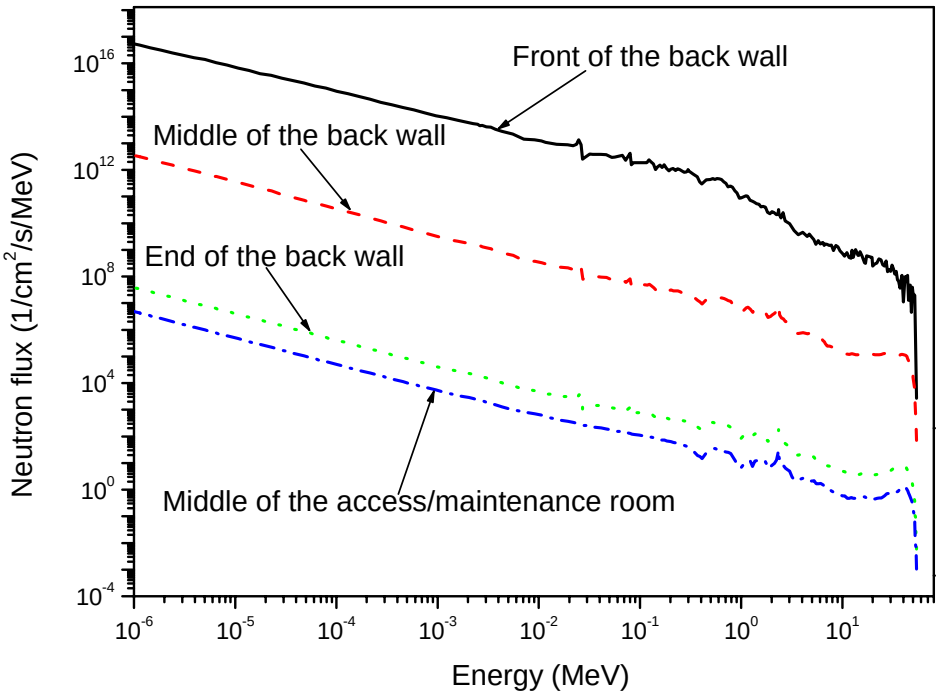

Fig. 5.7 Neutron spectra in the back wall and the access/maintenance room

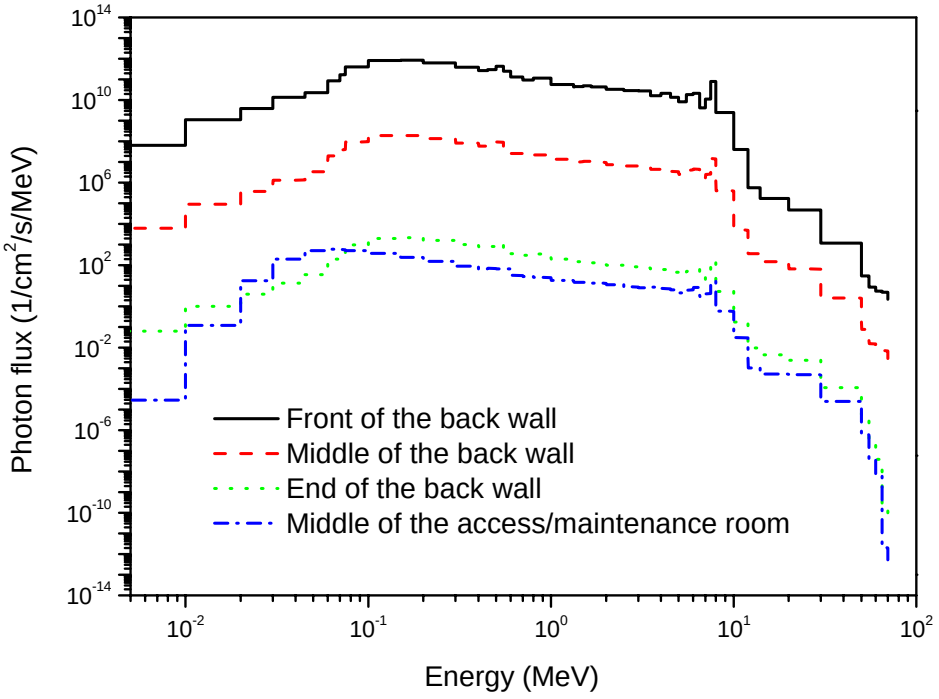

Fig. 5.8 Photon spectra in the back wall and the access/maintenance room

5.3.4 Dose rate distribution

The dose rates as a function of distance from the inner surface of the back wall are shown in Fig. 5.9. The results show that heavy concrete has a better shielding performance than ordinary concrete in this application. The dose rate attenuates across the back wall by about 9 orders of magnitude in the case of heavy concrete and about 8 orders of magnitude in the case of ordinary concrete. The dose rate decreases by a factor of ~25 in the access/maintenance room along the beam direction in both cases. The dose rate is dominated by the contribution from neutrons while the contribution from photons is less than 15% in both cases. The peak dose rate in the access/maintenance room exceeds the design limit of 10 μSv/h by about 3 orders of magnitude for ordinary concrete and by about 2 orders of magnitude for heavy concrete. To reduce the dose rate level in the room to the design limit, the thickness of the back wall would have to be about 400cm for the case of heavy concrete and about 450cm for the case of ordinary concrete.

Figs. 5.10 and 5.11 show the three-dimensional dose rate distribution in the back wall with heavy concrete and ordinary concrete as shielding materials, respectively. Note that the profiles of the dose rates are still very similar to the beam profile. The three-dimensional dose rate distributions in the access/maintenance room are shown in Figs. 5.12 and 5.13 for heavy concrete and ordinary concrete in the back wall, respectively. The results demonstrate that dose rate level in the room exceeds the design limit.

It should be mentioned that the results of three-dimensional distributions are of great benefit for the shielding analyses. In addition, the distribution in the access/maintenance room can be used to arrange and configure the radiation-sensitive devices and related equipments. The Monte Carlo method is incapable of providing such a complete solution as a three-dimensional distribution. This weakness limits the application of the Monte Carlo method in shielding analysis to some extent.

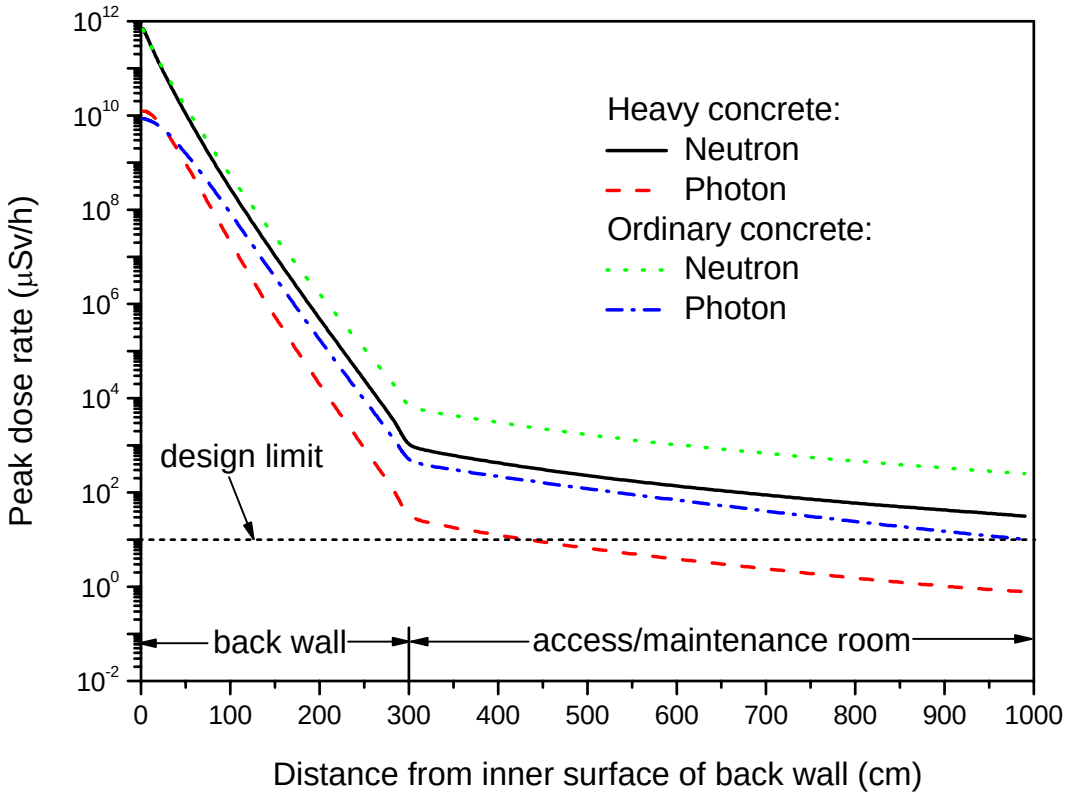

Fig. 5.9 Dose rate as a function of distance from the inner surface of back wall

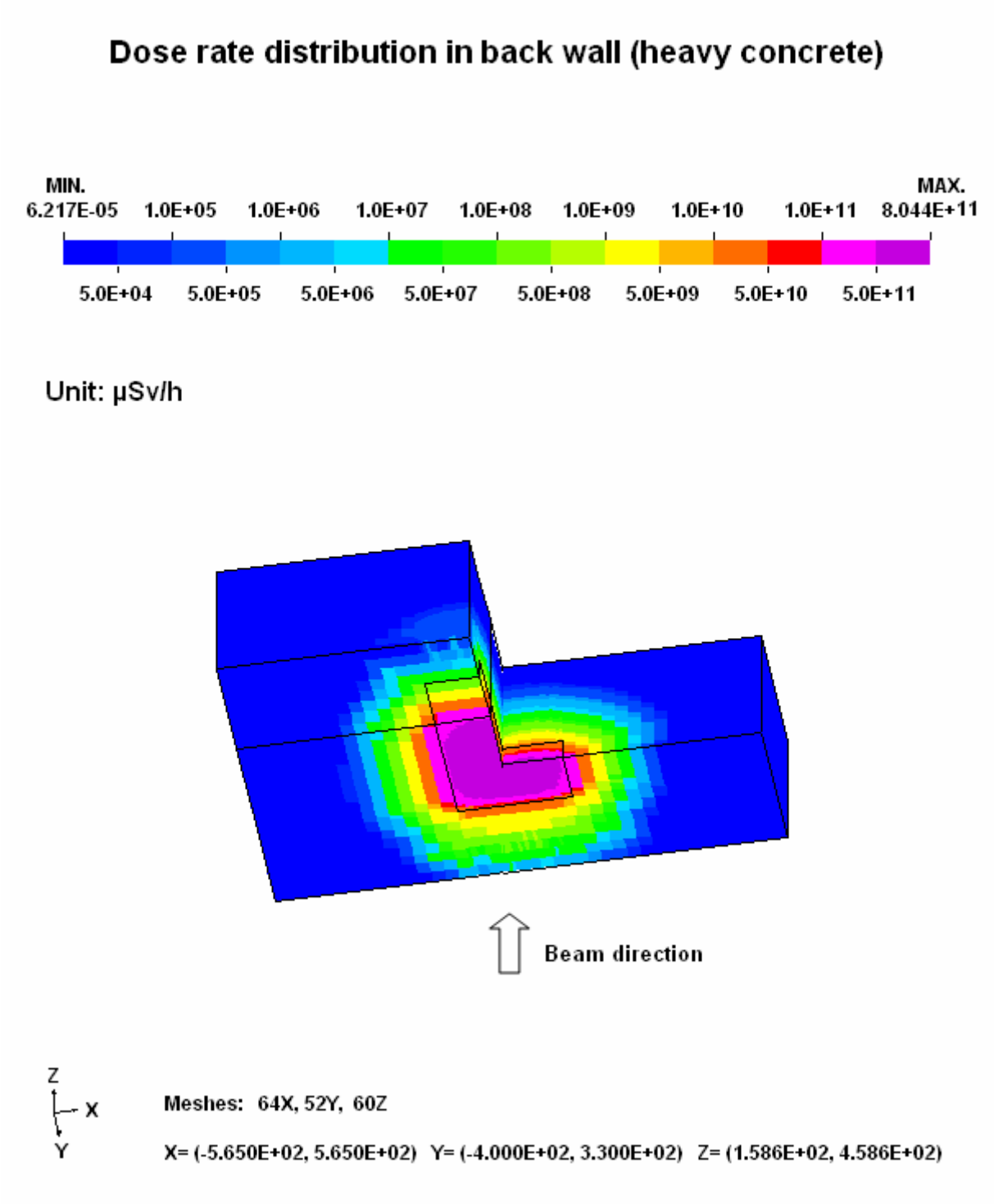

Fig. 5.10 Three-dimensional dose rate distribution in the back wall with heavy concrete

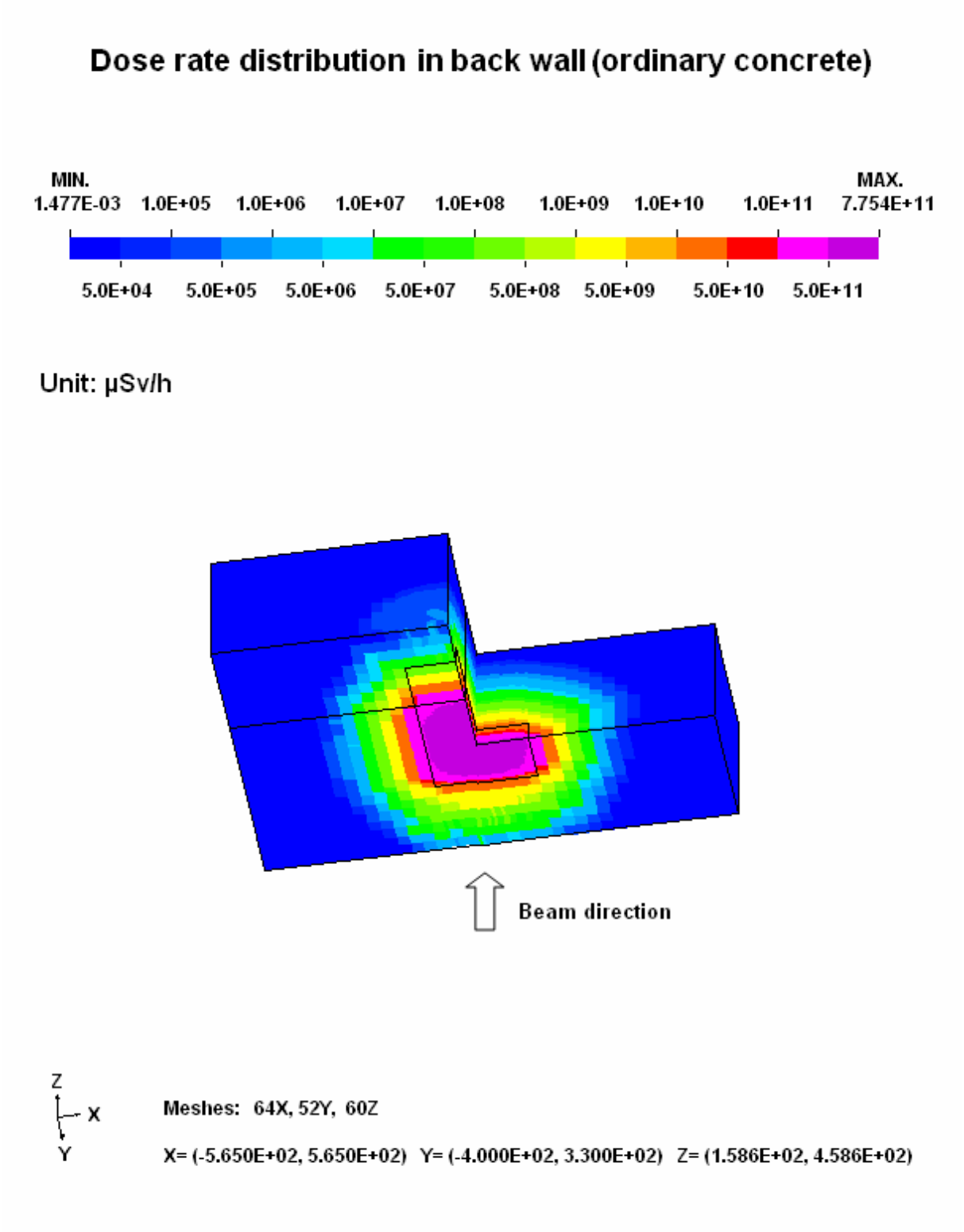

Fig. 5.11 Three-dimensional dose rate distribution in the back wall with ordinary concrete

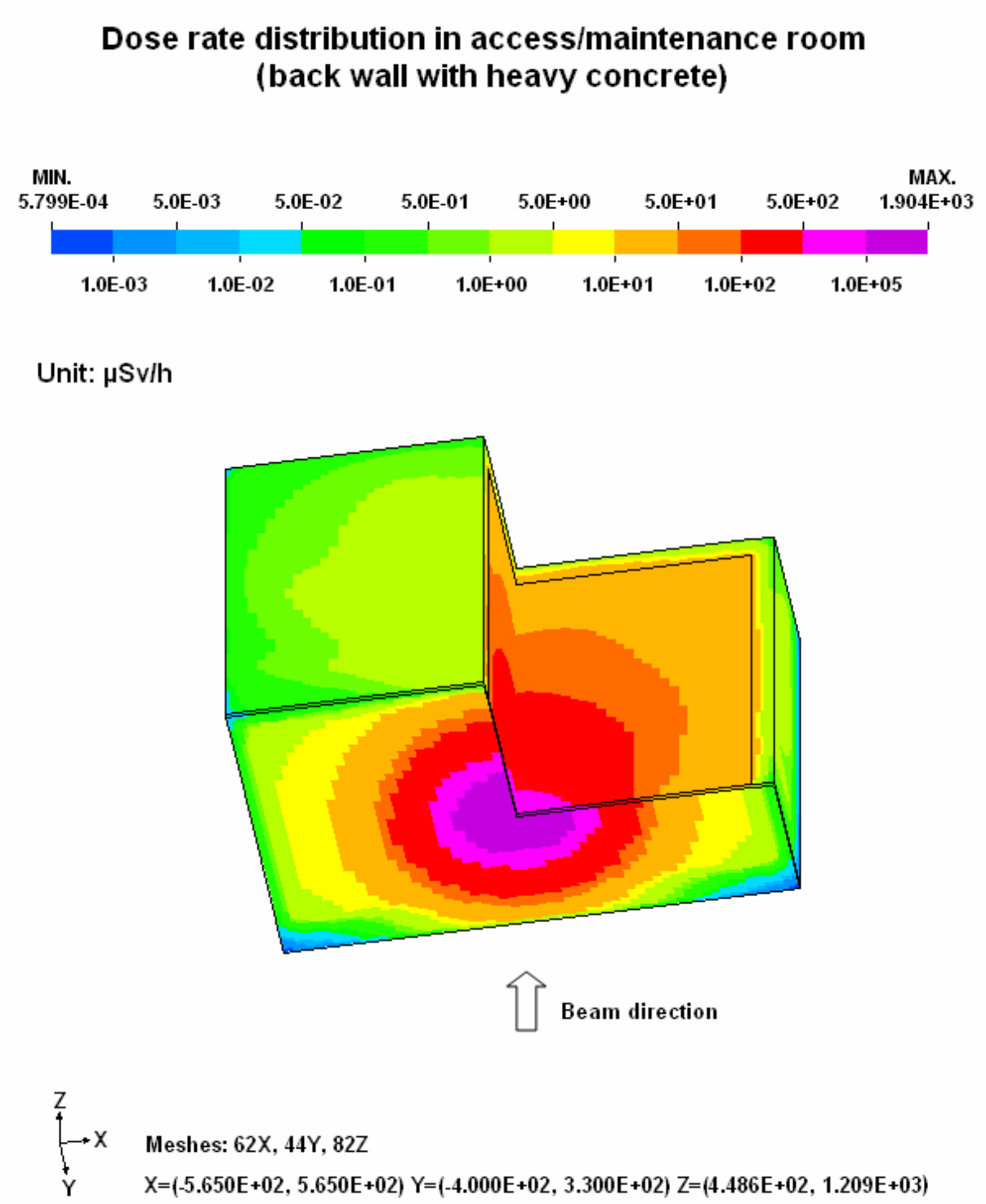

Fig. 5.12 Three-dimensional dose rate distribution in access/maintenance room with heavy concrete in back wall

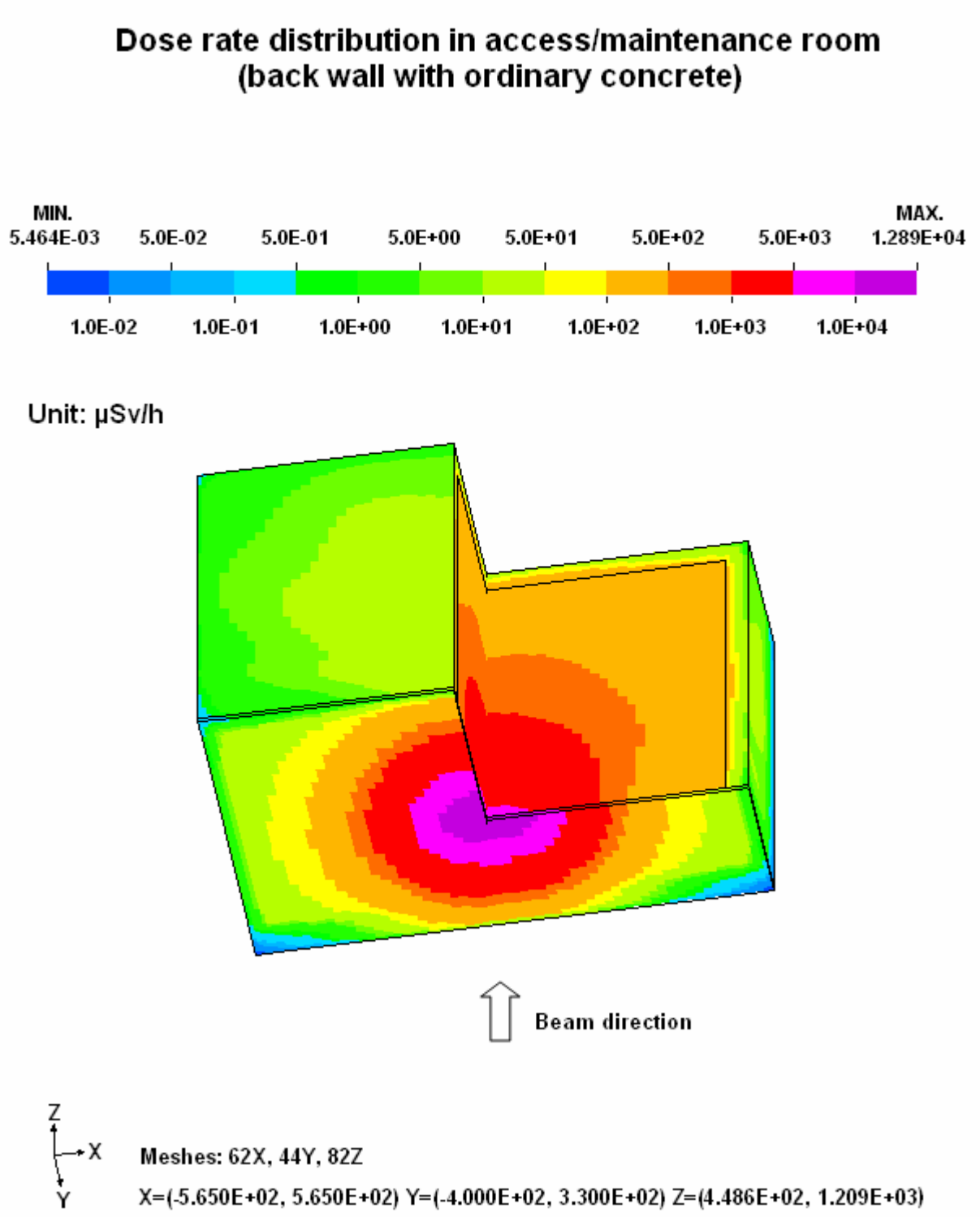

Fig. 5.13 Three-dimensional dose rate distribution in access/maintenance room with ordinary concrete in back wall

5.3.4 Comparison with previous calculations

In the previous shielding analyses of IFMIF, a group at the Japan Atomic Energy Research Institute (JAERI) performed three-dimensional calculations with MCNPX based on a simplified geometry model [49]. Heavy concrete was used as shielding material for the back wall. A point neutron source was used with a typical neutron spectrum for a given orientation. The dose rates were calculated at selected locations with surface tallies and point detectors. In addition, a group at the Italian National Agency for New Technologies, Energy and the Environment (ENEA) performed the shielding calculations with a one-dimensional discrete ordinates code [50]. A boundary neutron source was used in their calculations and ordinary concrete was used as shielding material for the back wall.

Table 5.2 compares the peak dose rates on the end surface of the back wall calculated by the coupled MC-S_N approach of this work, the MCNPX code by the JEARI group and the one-dimensional S_N code by the ENEA group. It can be seen that MCNPX overestimates the result by a factor of 2.6 compared to the coupled MC-S_N scheme. In the MCNPX solution, the gamma contribution to dose rate is about 4% and this is consistent with the MC-S_N coupled calculations. The one-dimensional S_N solution underestimates the dose rate by about 3 orders of magnitude compared to the three-dimensional coupled MC-S_N approach. This big difference is due to the simplified geometric treatment and the very approximate neutron source representation employed in the one-dimensional S_N solution. In addition, the gamma contribution to the dose rate in the one-dimensional S_N solution is almost the same as that of the neutron radiation. This is in contrast to the coupled MC-S_N calculations in which the gamma contribution is only about 7%.

Fig. 5.14 shows the comparison of dose rate profiles across the back wall calculated by the different approaches. Near the inner surface the JAERI and ENEA calculations overestimate the dose rates by a factor of ~2 as compared to the coupled MC-S_N calculations. It is noted that MCNPX systematically overestimates the results compared to the MC-S_N coupled calculation. But the attenuation profiles of the dose rates of these two approaches are similar. The attenuation profile calculated by the one-dimensional S_N code is completely different from that calculated by the MC-S_N coupled scheme. This is most probably due to the poor representation of the angular distribution of the neutron source in the one-dimensional S_N calculation.

Table 5.2 Comparison of peak dose rates at the end surface of the back wall calculated by different approaches

Method	Neutron dose rate (μSv/h)	Gamma dose rate (μSv/h)	Total dose rate (μSv/h)
3-D coupled MC-S_N (heavy concrete, FZK)[b]	1.05E+03[a]	3.30E+01	1.09E+03
MCNPX (heavy concrete, JAERI)[c]	2.69E+03	1.22E+02	2.81E+03
3-D coupled MC-S_N (ordinary concrete, FZK)[b]	6.98E+03	5.16E+02	7.50E+03
1-D S_N (ordinary concrete, ENEA)[d]	1.65E+00	1.59E+00	3.24E+00

[a] Read as 1.05×10^{3}, [b] current work, [c] ref. [49], [d] ref. [50].

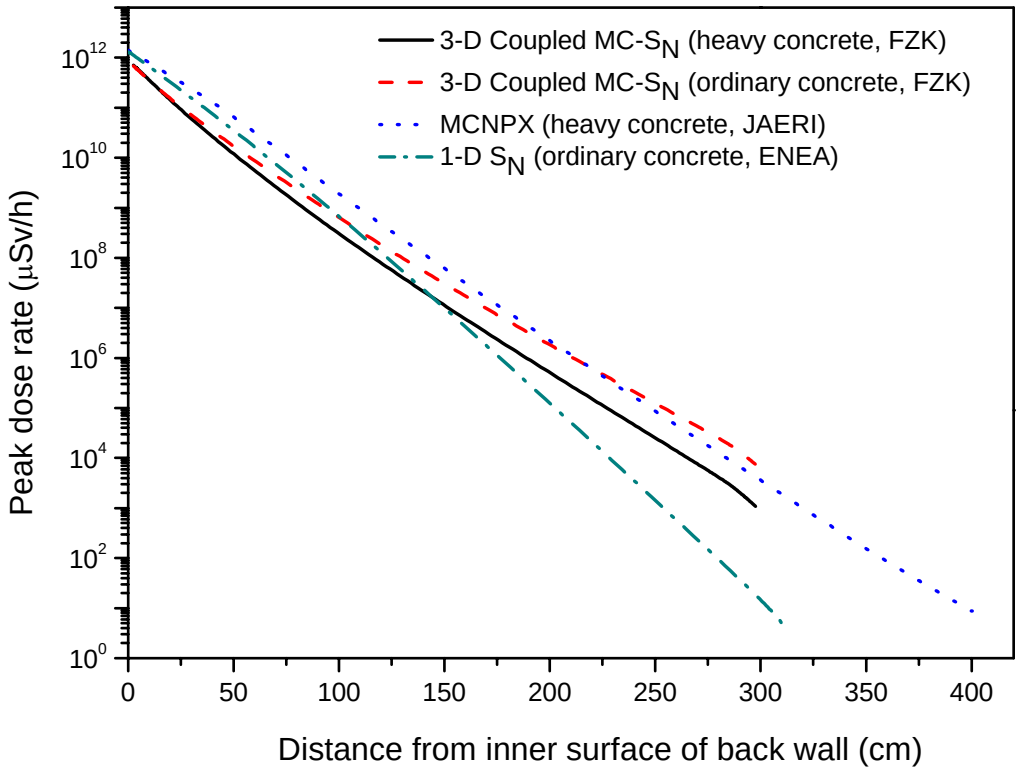

Fig. 5.14 Comparison of dose rates calculated by different approaches

6 Summary

Shielding analyses of advanced nuclear facilities, such as accelerator based neutron sources, require the use of dedicated computational approaches. This is due to the fact that conventional methods are not capable of solving shielding problems with complex geometry and bulk shielding with sufficient accuracy. In this work, a coupled Monte Carlo-Deterministic computational scheme was proposed that can satisfy the challenges in the shielding design of large and complex nuclear facilities. This coupled scheme was implemented in a program system and was validated through test calculations. As an illustrative application example, the coupled scheme was used for shielding calculations of the accelerator based IFMIF neutron source. The results demonstrate that this coupled scheme is a useful tool for the shielding analysis of large and complex nuclear facilities.

6.1 Coupled scheme and program system

The coupled scheme combines the advantages of the Monte Carlo and the Discrete Ordinates methods. The Monte Carlo method is used to deal with the source/target region with complex geometry, and the discrete ordinates method is used to solve the deep penetration problem in the bulk shield region with relatively simple geometry. In order to couple these two different approaches, a mapping approach was developed to calculate the angular flux distribution based on the Monte Carlo simulation and then pass it over to the discrete ordinates code. This mapping approach was implemented in a module. Its functionality was shown by means of numerical validation calculations.

The program system for the coupled shielding analysis integrates the Monte Carlo transport code MCNP, the three-dimensional discrete ordinates code TORT, and the mapping module. The entire program system was validated by comparison with direct Monte Carlo simulation calculations. The test calculations show that the program system for coupled shielding calculations is capable of providing reliable results for the relevant nuclear responses in three-dimensional geometries.

6.2 IFMIF shielding analysis

Due to the complexity of the shielding problem of the IFMIF neutron source, it is difficult to perform reliable shielding calculations on the basis of the conventional methods. Therefore, the coupled program system developed in this work was used to treat this problem. The IFMIF-dedicated Monte Carlo code McDeLicious was used to simulate the D-Li neutron generation and neutron/photon transport in the test cell with a detailed geometric model. The three-dimensional discrete ordinates code TORT was used to solve the deep penetration problem in the bulk shield region and to calculate the dose rate distribution.

The neutron/photon fluxes and spectra and the dose rate distribution across the back wall and in the access/maintenance room were calculated. The results confirm that heavy concrete has a better shielding performance than ordinary concrete in this application. With the option of heavy concrete, the thickness of the back wall should be about 400 cm in order to reduce the dose rate level to the design limit in the access/maintenance room next to the test cell. The dose rate is dominated by the contribution from neutrons and the contribution from photon is less than 15%. In addition, the results indicate that high energy (> 20 MeV) neutrons play a significant role in the shielding problem.

The results calculated by the coupling scheme were compared with those from previous shielding calculations. Considerable differences were observed. The differences are mostly caused by the approximation of the geometric models and the neutron source representation used in the previous analyses. Compared with the direct Monte Carlo approaches and discrete-ordinates methods, the coupled scheme is capable of not only employing the accurate modeling of the neutron source and geometry, but also solving the deep penetration problem and providing complete results.

6.3 Future Developments

The program system for the coupled Monte Carlo-Discrete Ordinates calculations developed in this work enables to conduct full three-dimensional shielding calculations for large and complex nuclear facilities. For the shielding analysis of nuclear facilities, besides the operational dose rate, the dose rate induced by decay gammas emitted from the activated materials is also an important issue. An MCNP based rigorous 2-step (R2S) method for three-dimensional decay gamma induced dose rate calculations has been developed recently [59,

60, 61]. It has been validated against an irradiation experiment and is applied for large and complex fusion tokamak devices. This method still suffers from the insufficient treatment of the deep-penetration radiation when large scale bulk shields are involved. The integration of the R2S method with the coupled Monte Carlo-Discrete Ordinates program system will also allow accurate calculations of the decay gamma induced dose rate for such cases. Therefore, an interface program to combine the R2S method and the coupled Monte Carlo-Discrete Ordinates program system of this work needs to be developed.

Shielding problems frequently involve the calculation of a dose rate distribution in a region outside the thick bulk shield including a complex geometric configuration with, e.g. gaps and penetrations. In such a case, it is beneficial to enable another Monte Carlo calculation for this region using the fluxes provided by the S_N calculation as input source. Such an application requires to extend the program system for coupled MC-S_N-MC calculations.

Another further application of the coupled MC-S_N program system may be in the field of transport problems with a strongly localized neutron source (e.g. a point source) surrounded by a weak scattering medium. For such problems, the multi-dimensional S_N approach suffers from the ray effect. With the mapping approach developed in this work, it is possible to overcome this limitation since the neutron source for the S_N calculation is provided by the Monte Carlo simulation.

Bibliography

[1]. B.G. Carlson and K.D. Lathrop, Transport Theory: The Method of Discrete Ordinates, in H. Greenspan, C.N. Kelber, and D. Okrent, eds., Computing Methods in Reactor Physics, pp. 167-266, Gordon and Breach, New York (1968).

[2]. W.W. Engle, Jr., ANISN, A One-Dimensional Discrete Ordinates Transport Code with Anisotropic Scattering, ORNL Report, K-1693 (march 1967)

[3]. R. Douglas O'Dell, et al., Revised User's Manual for ONEDANT – A Code Package for One-Dimensional, Diffusion-Accelerated, Neutral-Particle Transport, LA-9184-M, Rev. Manual (UC-705 Issued: December 1989).

[4]. W. W. Engle, Jr., M. A. Boling, and B. W. Colston, DTF-II, A One-Dimensional, Multi-group Neutron Transport Program, NAA-SR-10951 (March 1966).

[5]. W.A. Rhoades and R.L. Childs, The DORT Two-Dimensional Discrete Ordinates Transport Code, Nuclear Science and Engineering 99, 1, pp. 88-89 (May 1988).

[6]. R.E. Alcouffe, et al., User's Guide for TWODANT – A Code Package for Two–Dimensional Diffusion-Accelerated Neutral-Particle Transport, LA-10049-M (Revised Feb. 1, 1990).

[7]. Y.Y. Azmy, F.X. Gallmeier, D.A. Lillie, TORT Solution for the 3D Radiation Transport Benchmarks for Simple Geometries with Void Region, Progress in Nuclear Energy, Vol.39, No. 2, pp.155-166, 2001.

[8]. Y.Y. Azmy, J.O. Johnson, R.A. Lillie, M.J. Rennich, R.T. Santoro, Computing the Three-Dimensional Distribution of the Gamma Dose Rate in the Target Service Cell of the Spallation Neutron Source Using the DOORS Package, Progress in Nuclear Energy, Vol. 39, No. 3-4, pp. 321-333, 2001.

[9]. W.A. Rhoades and D. B. Simpson, The TORT Three-Dimensional Discrete Ordinates Neutron/Photon Transport Code, ORNL/TM-13221 (October 1997).

[10]. Sjoden, G. and Haghighat, A., PENTRAN™: Parallel Environment Neutral-particle TRANsport in 3-D Cartesian Geometry, Proceedings of the International Conference on Mathematical Methods and Supercomputing for Nuclear Applications, Saratoga Springs, NY, 1997, pp. 232-234.

[11]. Kucukboyaci, V., Haghighat, A., Sjoden, G. E., and Petrovic B., "Modeling of BWR for Neutron and Gamma Fields Using PENTRAN™," Reactor Dosimetry, ASTM STP 1398, John G. Williams, David W. Vehar, Frank H. Ruddy, and David M. Gilliam, Eds., American Society for Testing and Materials, West Conshohocken, PA, 2000.

[12]. J.F. Briesmeister (ed.), MCNP - A General Monte Carlo N-Particle Transport Code, Version 4C, Los Alamos National Laboratory, Report LA-13709-M, April 2000.

[13]. John S. Hendricks et al., "MCNPX, Version 2.5.E" Los Alamos National Laboratory report, LAUR-04-0569 (February 2004)

[14]. J.P. Both, H. Derriennic, B. Morillon, and J.C. Nimal, A Survey of TRIPOLI-4, Proceedings of the 8th International Conference on Radiation Shielding, pp. 373-380, Arlington, TX USA, April 24-28 (1994).

[15]. S. CHUCAS, I. CURL, T. SHUTTLEWORTH, and G. MORRELL, Preparing the Monte Carlo Code MCBEND for the 21st Century, Proceedings of the 8th International Conference on Radiation Shielding, pp. 381-390, Arlington, TX USA, April 24-28 (1994)

[16]. M.B. Emmett, MORSE-CGA: A Monte Carlo Radiation Transport Code With Array Geometry Capability, ORNL-6174, Martin Marietta Energy Systems, Inc., Oak Ridge National Laboratory, (April 1985).

[17]. J.C. Wagner, Acceleration of Monte Carlo shielding Calculations with an automated Variance Reduction Technique and Parallel Processing, Ph.D. Thesis, Nuclear Engineering Department of The Pennsylvania State University (1997).

[18]. J.C. Wagner, A. Haghighat, Automated variance reduction of Monte Carlo shielding calculations using the discrete ordinates adjoint function, Nuclear Science and Engineering (1998) 128 (2): 186-208.

[19]. K.A. VAN RIPER et al., AVATAR – Automatic Variance Reduction in Monte Carlo Calculations, Proc. Joint Int. Conf. Mathematical Methods and Supercomputing for Nuclear Applications, pp. 661-670, Saratoga Springs, New York, October 6-10, 1997, American Nuclear Society.

[20]. R.E. Alcouffe, F.W. Brinkley, D.R. Marr, User's Guide for THREEDANT: A Code Package for Three-Dimensional, Diffusion-Accelerated, Neutral-Particle Transport, Los Alamos National Laboratory, Report LA-10049-M, Feb. 1990.

[21]. Technical Basis for the ITER Final Design Report, Cost Review and Safety Analysis (FDR), ITER EDA Documentation Series No. 16, IAEA, Vienna, 1998.

[22]. IFMIF International Team, "IFMIF-KEP, International Fusion Materials Irradiation Facility key element technology phase report", JAERI-Tech 2003-005, March 2003.

[23]. M. Martone (Ed.), IFMIF – International Facility Conceptual Design Activity – Final Report, ENEA Frascati Report RT/ERG/FUS/96/11, 1999.

[24]. H. Lendeler, The European Spallation Source Study, Nucl. Instr. Meth., B139, 82 (1998).

[25]. National Spallation Neutron Source Conceptual Design Report, Oak Ridge National Laboratory, MSNS/CDR-2/VI, 1997.

[26]. S. Nagamiya, JAERI-KEK Joint Project on High Intensity Proton Accelerators, J. Nucl. Sc. Technol., Sup. 1, 40 (2000).

[27]. Franz X. Gallmeier, Ronald E. Pevey, Creation of a set of interface utilities to allow coupled Monte Carlo/discrete ordinates shielding analysis, Proc. Int. Top. Meet. Nucl. Appl. Accel. Technol., 3rd (1999), 404-409, American Nuclear Society, La Grange Park, III.

[28]. T.A. Gabriel at al., CALOR: A Monte Carlo Program Package for the Design and Analysis of Calorimeter Systems, Oak Ridge National Laboratory, ORNL/TM-5619 (1977).

[29]. J.O. Johnson, Shielding design of the spallation neutron source (SNS), Shielding Aspects of Accelerators, Targets and Irradiation Facilities, SATIF 4, Workshop Proceedings, Knoxville, Tennessee, September 1998, pp. 89-100, OECD Nuclear Energy Agency.

[30]. J.O. Johnson, R.T. Santoro, R.A. Lillie, J.M. Barnes and G.S. McNeilly, The SNS Target Station Preliminary Title I Shielding Analyses, Journal of Nuclear Science and Technology, Supplement 1, p.35-39 (March 2000).

[31]. D. Filges et al., Procedures and Data for Shielding Calculations of Spallation Target Stations and Accelerators in the Medium Energy Range, Proc. Specialist's Meeting of Shielding Aspects of Accelerators, Targets and Irradiation Facilities, Arlington, Texas, April 1994, pp. 253-270

[32]. P. Cloth, et al., HERMES, A Monte Carlo Program System for Beam-Materials Interaction Studies, KFA-Report Juel-22-3 (1988).

[33]. Weston M. Stacey, Nuclear reactor physics, John Wiley & Sons Inc., New York (2001), ISBN 0-471-39127-1.

[34]. DOORS 3.2, One-, Two- and Three-Dimensional Discrete Ordinates Neutron/Photon Transport Code System, RSICC Computer Code Collection, CCC-650, (1998).

[35]. R.L. Childs and D.E. Cullen, GROUPBAND-ANISN: A Code to Perform Multiband Calculations, Informal Notes, ORNL, (June 1994).

[36]. R.L. Childs, The FALSTF Last-Flight Computer Program, ORNL/TM-12675 (January 1996).

[37]. R. E. MacFarlane and D. W. Muir, The NJOY Nuclear Data Processing System Version 91, LANL report, LA-12740-M (October 1994).

[38]. R. E. MacFarlane, TRANSX 2: A Code for Interfacing MATXS Cross-Section Libraries to Nuclear Transport Codes, LANL report, LA-12312-MS (July 1992).

[39]. SCAMPI: Collection of Codes for Manipulating Multigroup Cross Section Libraries in AMPX Format, RSIC CODE PACKAGE PSR-352 (September 1995).

[40]. DANTSYS 3.0, One-, Two- and Three-Dimensional, Multigroup, Discrete-Ordinates Transport Code System, RSICC Computer Code Collection, C00547, (1997).

[41]. ENDF/B-VI: Cross Section Evaluation Working Group, ENDF/B-VI Summary Document, Report BNL-NCS-17541 (ENDF-201) (1991), edited by P.F. Rose, National Nuclear Data Center, Brookhaven National Laboratory, Upton, NY, USA.

[42]. J. E. White, R. Q. Wright, D. T. Ingersoll, R. W. Roussin, N. M. Greene and R. E. MacFarlane, “VITAMIN-B6: A Fine-Group Cross Section Library Based on ENDF/B-VI for Radiation Transport Applications”, from Proceedings of the International Conference on Nuclear Data for Science and Technology, Gatlinburg, Tennessee, USA, pp. 733-736, May 1994, J. K. Dickens (Ed.), American Nuclear Society, La Grange Park Illinois, 1994.

[43]. SCAMPI: Collection of Codes for Manipulating Multigroup Cross Section Libraries in AMPX Format, Radiation Safety Information Computational Center, RSIC Code Package PSR-352, Sept. 1995.

[44]. N. M. Greene, W. E. Ford Ill, L. M. Petrie, and J. W. Arwood, AMPX-77: A Modular Code System for Generating Coupled Multigroup Neutron-Gamma Cross-Section Libraries from ENDF/B-IV and/or ENDF/B-V, ORNL/CSD/TM-283, Oct. 1992.

[45]. SCALE: A Modular Code System for Performing Standardized Computer Analyses for Licensing Evaluation, NUREG/CR-0200, Rev. 4 (ORNL/NUREG/CSD-2R4), Vols. I, 7II, and III (April 1995).

[46]. Chikara Konn, Hiroshi Nakashima, Richard A. Lillie, Comment to VITAMIN-B6, proc. 2002 Symposium on Nuclear Data, Japan Atomic Energy Research Institute (JAERI), JAERI-CONF-2003-006, pp. 213-218, Tokai, Nov. 21-22, 2002.

[47]. Charles O. Slater, Hamilton T. Hunter, Validation of the VITAMIN-B6 and BUGLE-96 Cross-Section Libraries for Moderate-Energy Neutron and Photon Transport Calculations, Nuclear Technology Vol. 129, 201-217, Feb. 2000.

[48]. S. Monti, IFMIF CDA-Shielding Design and Dose and Neutron Induced Activation Calculation, ENEA-CT.FBC.00013, Oct. 1996.

[49]. M. Ida, M. Sugimoto, H. Takeuchi, Verification of the Design of Radiation Shielding, IFMIF-KEP, International Fusion Materials Irradiation Facility Key Element Technology Phase Report, p 486-492, IFMIF International Team, JAERI-Tech 2003-005, Japan Atomic Energy Research Institute, March 2003.

[50]. D.G. Cepraga, G. Cambi, M. Frisoni, Nuclear Safety and Shielding, IFMIF-KEP, International Fusion Materials Irradiation Facility Key Element Technology Phase Report, p 401-407, IFMIF International Team, JAERI-Tech 2003-005, Japan Atomic Energy Research Institute, March 2003.

[51]. S.P. Simakov, U. Fischer, et al., Advanced Monte Carlo procedure for the IFMIF d-Li neutron source term based on evaluated cross section data, Journal of Nuclear Materials 307-311 (2002) 1710-1714.

[52]. A. Yu. Konobeev, Yu.A Korovin, P.E. Pereslavtsev, et al., Development of methods for calculation of n+Li and d+Li cross sections for energies up to 50 MeV, Nucl. Sci. and Eng. 139 (2001) 1-23

[53]. Chadwick, M.B., Young, P.G., Chiba, S., Frankle, S.C., Hale, G.M., Hughes, H.G., Koning, A.J., Little, R.C., MacFarlane, R.E., Prael, R.E. and Waters, L.S., Cross-Section Evaluations to 150 MeV for Accelerator-Driven Systems and Implementation in MCNPX, Nucl. Sci. Eng. 131, 293-328 (1999).

[54]. Frisoni, M, Cepraga, D.G. and Cambi, G., New computational tools and data libraries for IFMIF shielding calculations, ENEA report, FUS-TN-SA-SE-R-034, June 2002.

[55]. F. Wasastjerna, unpublished report, Forschungszentrum Karlsruhe, June 2003.

[56]. W. A. Rhoades and D. B. Simpson, Splicing and Bootstrapping Methods for DORT/TORT-To-TORT Coupling (TORSET Section), Oak Ridge National Laboratory, ORNL/TM-13350 (to be published).

[57]. M. Ida, M. Sugimoto, H. Takeuchi, Verification of the Design of Radiation Shielding, IFMIF-KEP, International Fusion Materials Irradiation Facility Key Element Technology Phase Report, p 486-492, IFMIF International Team, JAERI-Tech 2003-005, Japan Atomic Energy Research Institute, March 2003.

[58]. ICRP Publication 74: Conversion coefficients for use in radiological protection against external radiation, Vol. 26, No. 3, Pergamon Press, 1996. ISBN: 0-08-042739-1.

[59]. Y. Chen, U. Fischer, Rigorous MCNP Based Shutdown Dose Rate Calculations: Computational Scheme, Verification Calculations and Application to ITER, Fusion Engineering and Design 63-64 (2002) 107-114.

[60]. Y. Chen, U. Fischer, M. Loughlin, P. Pereslavtsev, H. Tsige-Tamirat, Programme System for Monte Carlo Based Shutdown Dose Rate Calculations with Applications to ITER and JET", Jahrestagung Kerntechnik 2003, Berlin, 20.-22. Mai 2003, INFORUM GmbH, 2004 S. 421-24.

[61]. Yixue Chen, Yican Wu, Qunying Huang, Monte Carlo Based Operational and Shutdown Dose Rate Calculations of HT-7U Tokamak, Fusion Engineering and Design 70 (2004) 155-162.

ACKNOWLEDEGEMENTS

Herein I would like to thank all those people who have supported me throughout the development of this work. While I cannot list them all here, certain groups and individuals are deserving of special acknowledgements.

This work was carried out in the Institut für Reaktorsicherheit (IRS) at the Forschungszentrum Karlsruhe (FZK). I gratefully acknowledge the assistance of all my IRS colleagues, in particular the Fusion and Radiation Physics group.

Prof. Dr.-Ing. D. G. Cacuci is deserving of particular recognition for guidance while presiding over my research and for allowing me to carry out the research in the above institute. Also for Prof. E. Borie, whose careful reading of and feedback on this dissertation are invaluable.

Special thanks are due to Dr. U. Fischer, whose day-to-day support and feedback have guided me throughout and helped keep the goals of this work in focus. Discussion with Dr. H. Tsige-Tamirat has led to many new insights.

Finally, a very special thanks to my wife, Ya Liu.

APPENDIX

A. Sample of input files for the program system

The sample files of user.inp and sn.inp are used in the test calculations to validate the program system. In this example of test calculations, the Cartesian (X-Y-Z) geometry was used and the k-boundary source file was generated. A 20×20×30 mesh model, a coupled 199-neutron groups and 42-gamma groups cross section library and S_8 quadrature sets are used in the coupled calculations.

A.1 user.inp

```
! ------------------------------------------------------------------------------------------
!
!  user.inp
!
!  Purpose:    specify relevant files and provide data about
!              geometry, boundary source, etc.
!
!  NOTICE:     no blanks allowed to precede or be imbedded  in
!              the specification
!
!           !:    for comments
!         end:    signify the end of file
!
! ------------------------------------------------------------------------------------------
!
!  file specification:
!
!  MCNP SSW format binary file
mcnpssw=p1ssinw
!
!  TORT input file
tortdat=ts8np241d
!
!  User specified input file
userinp=userinp
!
!  the output TORT source file
srctort=s2np241u
!
! ------------------------------------------------------------------------------------------
!
```

```
!  geometry and source file specification:
!
!  to generate TORT boundary source
ifbfxi=0
ifbfxj=0
ifbfxk=0
!
!  igeomt = 0:          Cartesian (X-Y-Z) geometry
!  igeomt = 1:          cylindrical (R-Thita-Z) geometry (only for i-
!                       bndy src: ifio=0)
igeomt=0
!
!  ifio ( or ifjo,ifko) = 0:       i ( or j,k ) boundary source
!  ifio ( or ifjo,ifko) = 1:       not i ( or j,k ) boundary source
!
ifio=1
ifjo=1
ifko=0          !  k-bndy src
!
! ------------------------------------------------------------------------------------------------
end
!
```

A.2 sn.inp

```
! ------------------------------------------------------------------------------------------------
!
!  sn.inp
!
!  Purpose:    provide data about the geometric mesh, energy
!              group structure, quadrature set, etc.
!
!  NOTICE:     no blanks are allowed between ** and array
!              (parameter) name
!
!          ! :     for comments
!    end:          signify the end of file
!
! ------------------------------------------------------------------------------------------------
!
!  arrays for geometry
!
!        2**:      i-interval boundaries by i-set
!        3**:      j-interval boundaries by j-set
!        4**:      k-interval boundaries
!
im
 20
jm
 20
```

```
km
 30
2**
 -1.000000e+01  -9.000000e+00  -8.000000e+00  -7.000000e+00
 -6.000000e+00  -5.000000e+00  -4.000000e+00  -3.000000e+00
 -2.000000e+00  -1.000000e+00   0.000000e+00   1.000000e+00
  2.000000e+00   3.000000e+00   4.000000e+00   5.000000e+00
  6.000000e+00   7.000000e+00   8.000000e+00   9.000000e+00
  1.000000e+01
3**
 -1.000000e+01 -9.000000e+00 -8.000000e+00 -7.000000e+00
 -6.000000e+00 -5.000000e+00 -4.000000e+00 -3.000000e+00
 -2.000000e+00 -1.000000e+00  0.000000e+00  1.000000e+00
  2.000000e+00  3.000000e+00  4.000000e+00  5.000000e+00
  6.000000e+00  7.000000e+00  8.000000e+00  9.000000e+00
  1.000000e+01
4**
  1.000000e+01  1.100000e+01  1.200000e+01  1.300000e+01
  1.400000e+01  1.500000e+01  1.600000e+01  1.700000e+01
  1.800000e+01  1.900000e+01  2.000000e+01  2.100000e+01
  2.200000e+01  2.300000e+01  2.400000e+01  2.500000e+01
  2.600000e+01  2.700000e+01  2.800000e+01  2.900000e+01
  3.000000e+01  3.100000e+01  3.200000e+01  3.300000e+01
  3.400000e+01  3.500000e+01  3.600000e+01  3.700000e+01
  3.800000e+01  3.900000e+01  4.000000e+01
!
! ----------------------------------------------------------------------------------------------
! arrays for energy group
!
!    igm:        number of energy groups
!    ener:       top energy boundary of group ig
!    emin:       bottom energy boundary of group igm
!    neut:       last neutron group (0 if all groups are photons)
!    eneut:      bottom energy boundary of group neut (0 if neut=0)
!
igm
       241
neut
       199
emin
       1.0000E+03
eneut
       1.0000e-05
ener
       1.9640E+07  1.7332E+07  1.6905E+07  1.6487E+07
       1.5683E+07  1.4918E+07  1.4550E+07  1.4191E+07
       1.3840E+07  1.3499E+07  1.2840E+07  1.2523E+07
       1.2214E+07  1.1618E+07  1.1052E+07  1.0513E+07
       1.0000E+07  9.5123E+06  9.0484E+06  8.6071E+06
       8.1873E+06  7.7880E+06  7.4082E+06  7.0469E+06
       6.7032E+06  6.5924E+06  6.3763E+06  6.0653E+06
```

5.7695E+06 5.4881E+06 5.2205E+06 4.9659E+06
4.7237E+06 4.4933E+06 4.0657E+06 3.6788E+06
3.3287E+06 3.1664E+06 3.0119E+06 2.8651E+06
2.7253E+06 2.5924E+06 2.4660E+06 2.3852E+06
2.3653E+06 2.3457E+06 2.3069E+06 2.2313E+06
2.1225E+06 2.0190E+06 1.9205E+06 1.8268E+06
1.7377E+06 1.6530E+06 1.5724E+06 1.4957E+06
1.4227E+06 1.3534E+06 1.2874E+06 1.2246E+06
1.1648E+06 1.1080E+06 1.0026E+06 9.6164E+05
9.0718E+05 8.6294E+05 8.2085E+05 7.8082E+05
7.4274E+05 7.0651E+05 6.7206E+05 6.3928E+05
6.0810E+05 5.7844E+05 5.5023E+05 5.2340E+05
4.9787E+05 4.5049E+05 4.0762E+05 3.8774E+05
3.6883E+05 3.3373E+05 3.0197E+05 2.9849E+05
2.9721E+05 2.9452E+05 2.8725E+05 2.7324E+05
2.4724E+05 2.3518E+05 2.2371E+05 2.1280E+05
2.0242E+05 1.9255E+05 1.8316E+05 1.7422E+05
1.6573E+05 1.5764E+05 1.4996E+05 1.4264E+05
1.3569E+05 1.2907E+05 1.2277E+05 1.1679E+05
1.1109E+05 9.8037E+04 8.6517E+04 8.2503E+04
7.9499E+04 7.1998E+04 6.7379E+04 5.6562E+04
5.2475E+04 4.6309E+04 4.0868E+04 3.4307E+04
3.1828E+04 2.8501E+04 2.7000E+04 2.6058E+04
2.4788E+04 2.4176E+04 2.3579E+04 2.1875E+04
1.9305E+04 1.5034E+04 1.1709E+04 1.0595E+04
9.1188E+03 7.1017E+03 5.5308E+03 4.3074E+03
3.7074E+03 3.3546E+03 3.0354E+03 2.7465E+03
2.6126E+03 2.4852E+03 2.2487E+03 2.0347E+03
1.5846E+03 1.2341E+03 9.6112E+02 7.4852E+02
5.8295E+02 4.5400E+02 3.5357E+02 2.7536E+02
2.1445E+02 1.6702E+02 1.3007E+02 1.0130E+02
7.8893E+01 6.1442E+01 4.7851E+01 3.7266E+01
2.9023E+01 2.2603E+01 1.7604E+01 1.3710E+01
1.0677E+01 8.3153E+00 6.4760E+00 5.0435E+00
3.9279E+00 3.0590E+00 2.3824E+00 1.8554E+00
1.4450E+00 1.3000E+00 1.1253E+00 1.0800E+00
1.0400E+00 1.0000E+00 8.7643E-01 8.0000E-01
6.8256E-01 6.2506E-01 5.3158E-01 5.0000E-01
4.1399E-01 3.6680E-01 3.2500E-01 2.7500E-01
2.2500E-01 1.8400E-01 1.5000E-01 1.2500E-01
1.0000E-01 7.0000E-02 5.0000E-02 4.0000E-02
3.0000E-02 2.1000E-02 1.4500E-02 1.0000E-02
5.0000E-03 2.0000E-03 5.0000E-04
3.0000E+07 2.0000E+07 1.4000E+07 1.2000E+07
1.0000E+07 8.0000E+06 7.5000E+06 7.0000E+06
6.5000E+06 6.0000E+06 5.5000E+06 5.0000E+06
4.5000E+06 4.0000E+06 3.5000E+06 3.0000E+06
2.5000E+06 2.0000E+06 1.6600E+06 1.5000E+06
1.3400E+06 1.3300E+06 1.0000E+06 8.0000E+05
7.0000E+05 6.0000E+05 5.1200E+05 5.1000E+05
4.5000E+05 4.0000E+05 3.0000E+05 2.0000E+05

```
      1.5000E+05  1.0000E+05  7.5000E+04  7.0000E+04
      6.0000E+04  4.5000E+04  4.0000E+04  3.0000E+04
      2.0000E+04  1.0000E+04
! ------------------------------------------------------------------------------------------------
! arrays for directions
!
!  w:           quadrature weights
!  emu:         first-direction consines
!  eta:         last-direction consines
!  xzi:         second-direction consines
!
mm
     96
w
     0.00000E+00 1.51235E-02 1.51235E-02 0.00000E+00 1.13425E-02
     1.13425E-02  1.13425E-02 1.13425E-02 0.00000E+00 1.13425E-02
     1.15740E-02  1.13425E-02 1.13425E-02 1.15740E-02  1.13425E-02
     0.00000E+00 1.51235E-02 1.13425E-02 1.13425E-02  1.51235E-02
     1.51235E-02  1.13425E-02 1.13425E-02 1.51235E-02 0.00000E+00
     1.51235E-02  1.51235E-02 0.00000E+00 1.13425E-02 1.13425E-02
     1.13425E-02  1.13425E-02 0.00000E+00 1.13425E-02 1.15740E-02
     1.13425E-02  1.13425E-02 1.15740E-02 1.13425E-02 0.00000E+00
     1.51235E-02  1.13425E-02 1.13425E-02 1.51235E-02  1.51235E-02
     1.13425E-02  1.13425E-02 1.51235E-02 0.00000E+00 1.51235E-02
     1.51235E-02  0.00000E+00 1.13425E-02 1.13425E-02 1.13425E-02
     1.13425E-02  0.00000E+00 1.13425E-02 1.15740E-02 1.13425E-02
     1.13425E-02  1.15740E-02 1.13425E-02 0.00000E+00 1.51235E-02
     1.13425E-02  1.13425E-02 1.51235E-02 1.51235E-02  1.13425E-02
     1.13425E-02  1.51235E-02 0.00000E+00 1.51235E-02 1.51235E-02
     0.00000E+00 1.13425E-02 1.13425E-02 1.13425E-02  1.13425E-02
     0.00000E+00 1.13425E-02 1.15740E-02 1.13425E-02  1.13425E-02
     1.15740E-02  1.13425E-02 0.00000E+00 1.51235E-02 1.13425E-02
     1.13425E-02  1.51235E-02 1.51235E-02 1.13425E-02  1.13425E-02
     1.51235E-02
emu
     -3.08610E-01 -2.18220E-01  2.18220E-01 -6.17210E-01
     -5.77350E-01 -2.18220E-01  2.18220E-01  5.77350E-01
     -8.16500E-01 -7.86800E-01 -5.77350E-01 -2.18220E-01
      2.18220E-01  5.77350E-01  7.86800E-01 -9.75900E-01
     -9.51190E-01 -7.86800E-01 -5.77350E-01 -2.18220E-01
      2.18220E-01  5.77350E-01  7.86800E-01  9.51190E-01
     -3.08610E-01 -2.18220E-01  2.18220E-01 -6.17210E-01
     -5.77350E-01 -2.18220E-01  2.18220E-01  5.77350E-01
     -8.16500E-01 -7.86800E-01 -5.77350E-01 -2.18220E-01
      2.18220E-01  5.77350E-01  7.86800E-01 -9.75900E-01
     -9.51190E-01 -7.86800E-01 -5.77350E-01 -2.18220E-01
      2.18220E-01  5.77350E-01  7.86800E-01  9.51190E-01
     -3.08610E-01 -2.18220E-01  2.18220E-01 -6.17210E-01
     -5.77350E-01 -2.18220E-01  2.18220E-01  5.77350E-01
     -8.16500E-01 -7.86800E-01 -5.77350E-01 -2.18220E-01
      2.18220E-01  5.77350E-01  7.86800E-01 -9.75900E-01
```

```
      -9.51190E-01 -7.86800E-01 -5.77350E-01 -2.18220E-01
       2.18220E-01  5.77350E-01  7.86800E-01  9.51190E-01
      -3.08610E-01 -2.18220E-01  2.18220E-01 -6.17210E-01
      -5.77350E-01 -2.18220E-01  2.18220E-01  5.77350E-01
      -8.16500E-01 -7.86800E-01 -5.77350E-01 -2.18220E-01
       2.18220E-01  5.77350E-01  7.86800E-01 -9.75900E-01
      -9.51190E-01 -7.86800E-01 -5.77350E-01 -2.18220E-01
       2.18220E-01  5.77350E-01  7.86800E-01   9.51190E-01
eta
      -9.51190E-01 -9.51190E-01 -9.51190E-01 -7.86800E-01
      -7.86800E-01 -7.86800E-01 -7.86800E-01 -7.86800E-01
      -5.77350E-01 -5.77350E-01 -5.77350E-01 -5.77350E-01
      -5.77350E-01 -5.77350E-01 -5.77350E-01 -2.18220E-01
      -2.18220E-01 -2.18220E-01 -2.18220E-01 -2.18220E-01
      -2.18220E-01 -2.18220E-01 -2.18220E-01 -2.18220E-01
      -9.51190E-01 -9.51190E-01 -9.51190E-01 -7.86800E-01
      -7.86800E-01 -7.86800E-01 -7.86800E-01 -7.86800E-01
      -5.77350E-01 -5.77350E-01 -5.77350E-01 -5.77350E-01
      -5.77350E-01 -5.77350E-01 -5.77350E-01 -2.18220E-01
      -2.18220E-01 -2.18220E-01 -2.18220E-01 -2.18220E-01
      -2.18220E-01 -2.18220E-01 -2.18220E-01 -2.18220E-01
       9.51190E-01  9.51190E-01  9.51190E-01  7.86800E-01
       7.86800E-01  7.86800E-01  7.86800E-01  7.86800E-01
       5.77350E-01  5.77350E-01  5.77350E-01  5.77350E-01
       5.77350E-01  5.77350E-01  5.77350E-01  2.18220E-01
       2.18220E-01  2.18220E-01  2.18220E-01  2.18220E-01
       2.18220E-01  2.18220E-01  2.18220E-01  2.18220E-01
       9.51190E-01  9.51190E-01  9.51190E-01  7.86800E-01
       7.86800E-01  7.86800E-01  7.86800E-01  7.86800E-01
       5.77350E-01  5.77350E-01  5.77350E-01  5.77350E-01
       5.77350E-01  5.77350E-01  5.77350E-01  2.18220E-01
       2.18220E-01  2.18220E-01  2.18220E-01  2.18220E-01
       2.18220E-01  2.18220E-01  2.18220E-01  2.18220E-01
! ------------------------------------------------------------------------------------------------
!      end of data file
end
!
```

B. Interface files specification

The specifications for the interface files (i.e., DIRFLX, GIP and VARBND) which are used in the program system are given in the following sections.

B.1 Format DIRFLX

```
------------------------------------------------------------------------------------------------
-
-   name:       dirflx
-
-   purpose:    cell-average directional flux and interpretive data
-
-   notes:      order of energy groups is by decreasing energy
-               neutrons, then photons.
-
-       i is the first -dimension index, i=l,,,ims(j,k)
-       j is the second-dimension- index, j=l,,,jms(k)
-       k is the third -dimension index, k=l,,,km
-       m is the overall direction index, m=l,,,mset(ig)
-       mx is the quadrant direction index, mx=l,,,mdim
-       ig is the energy group index, ig=l,igm
-
-       mult=l if word length is 8 bytes; mult=2 if 4 bytes.
-
-       the "output patch" refers to a compact region of the space
-       mesh in which the directional flux is to be output.
-
-       flux records for a group are not present if no iterations
-       are done on that group. the user must provide for this
-       possibility.
------------------------------------------------------------------------------------------------
-   file structure
-
-       record type                              present if
-       -----------                              ----------
-       file identification                        always
-       file label                                 always
-       indexing arrays                            always
-       real arrays                                always
-
-       . . . . . . . . . repeat for ig=l,igm
-       .
-       .  . . . . . . . . repeat all k=km,l,-1
-       .  .
-       .  . . . . . . . . repeat all j=jms(k),l,-1
-       .  . . in, downward directional flux
```

```
-       . . . . . . . . end j loop
-       . .
-       . . . . . . . . repeat all j=l,jms(k),l
-       . . . out, downward directional flux
-       . . . . . . . . end j loop
-       . .
-       . . . . . . . . end k loop
-       .
-       . . . . . . . . repeat all k=l,km
-       . .
-       . . . . . . . . repeat all j=jms(k),l,-1
-       . . . in, upward directional flux
-       . . . . . . . . end j loop
-       . .
-       . . . . . . . . repeat all j=l,jms(k)
-       . . . out, upward directional flux
-       . . . . . . . . end j loop
-       . .
-       . . . . . . . . end k loop
-       .
-       . . . . . . . . . end ig loop
-
-------------------------------------------------------------------------------------------------
-   file identification
-
-       hname, (huse(i),i=1,2),ivers
-
-       number of words= 4*mult
-
-       hname       file name                  - (a8)
-       huse(i)     user file identification   - (a8)
-       ivers       file version number        - (a8)
-
------------------------------------------------------------------------------------------------
-   file label:
-
-       date,user,charge,case,time,(titl(i),i=l,9)
-
-       number of words= 14*mult
-
-       date        as provided by timer option 4          - (a8)
-       user        as provided by timer option 5          - (a8)
-       charge      as provided by timer option 6          - (a8)
-       case        as provided by timer option 7          - (a8)
-       time        as provided by timer option 8          - (a8)
-       titl(i)     title provided by user                 - (a8)
-
------------------------------------------------------------------------------------------------
-   integer parameters:
-
-       igm,im,jm,km,mmdnup, nun,mmsmsm,msm,ipchl,ipch2
```

- jpchl,jpch2,kpchl,kpch2, (idum(n),n=l,ll)
-
- number of words= 25
-
- igm number of energy groups
- im maximum number of cells in any row
- jm maximum number of rows in any plane
- km number of planes
- mmdnup max. no. of down/up directions in any m-set
-
- mm max. no. of directions in any m-set
- mmsmsm sum of no. of directions over m-set
- msm number of m-sets
- ipch1 first i in output patch, first i-set
- ipch2 last i in output patch, first i-set
-
- jpch1 first j in output patch, first j-set
- jpch2 last j in output patch, first j-set
- kpch1 first j in output patch, first k-set
- kpch2 last j in output patch, first k-set
- idum array set to 0
-

- indexing arrays:
-
- (mmbms(ms),ms=l,msm), (mset(ig),ig=l,igm)
- , (mmdn(ms),ms=l,msm), (mmdu(ms),ms=l,msm)
-
- number of words= 3*msm+igm
-
- mmbms no. of directions by m-set
- msets no. of m-set by group
- nundn no. of downward directions by m-set
- mmdu max. no. of down/upward directions by m-set
-

- real arrays:
-
- (w (m,ms),m=l,mmbms(ms)),ms=l,msm)
- ,(emu(m,ms),m=l,mmbms(ms)),ms=l,msm)
- ,(xzi(m,ms),m=l,mmbms(ms)),ms=l,msm)
- ,(eta(m,ms),m=l,mmbms(ms)),ms=l,msm)
- ,(pchbn(l),l=1,6)
-
- number of words = 4*mmsmsm+6
-
- W direction weight
- emu direction cosine with x axis
- xzi direction cosine with y axis
- eta direction cosine with z axis
- pchbn left/right,inside,outside,bottom,top patch bound

```
-
-------------------------------------------------------------------------------------------
-
-   directional flux:
-
-         ((dirf(i,mx),i=l,ims(j,k)),mx=l,mdim)
-         number of words = ims*mdim
-         dirf      cell-average directional flux
-
-------------------------------------------------------------------------------------------
-
-   end
```

B.2 Format GIP

```
-------------------------------------------------------------------------------------------
-
-   name: gip
-
-   purpose:   cross sections group-ordered for transport codes;
-              this format is compatible with anisn and dot requirements.
-
-   notes:
-
-         Groups are normally ordered from high neutron energy to
-         low, then from high photon energy to low, if any. igm is
-         the number of groups.
-
-         In a forward (non-adjoint) calculation, scatters appearing
-         before ihs are upscatter; Scatters appearing after ihs are
-         downscatter. Position ihp contains total upscatter, if any.
-
-         If upscatter data are not present, ihp position is missing
-         and ihs.eq.iht+l.
-
-         Each component of a pl set is treated as a separate
-         material in this format.
-
-         Transfers from groups .lt.l or .gt.igm are 0. Positions
-         .le.iht are 0 for pl components other than O'th.
-
-         For adjoint calculations, reverse the scattering; i.e.
-         where the format asks for scattering from ig-1 to ig, for
-         example, supply physical data for scattering from ig to
-         ig-1. Next, reverse the ordering of the group data so that
-         data for the highest neutron energy is last, not first,
-         etc. If ihs-l.gt.iht, the position ihp has its same formal
-         definition, but the physical data it describes are
-         different--it now describes total upscatter into a group,
-         in physical terms.
```

```
-
-------------------------------------------------------------------------------------------
-
- file structure:
-
-                record type                          present if
-                -----------                          ----------
-
-        . . . . . . do ig=l,igm
-        .  cross section data                         always
-        . . . . . . enddo
-
-------------------------------------------------------------------------------------------
-
- cross section data:
-
-        ((sig(ih,mt),ih=l,ihp),mt=l,mtm)
-
-        number of words = ihp*mtm
-
-        sig(ih,mt)      cross section data by table position, then
-                        by nuclide. table positions contain - -
-
-        1 to iht-5  arbitrary data, specified by user, or absent
-        iht-4       fission yield fraction (recommended)
-        iht-3       fission cross section (recommended)
-        iht-2       absorption cross section
-        iht-1       neutron production cross section
-        iht         total cross section
-        iht+l       scatter from group ig+(ihs-1-iht) to ig
-        ihs-1       scatter from group ig+l to ig
-        ihs         self scatter for group ig
-        ihs+l       scatter from group ig-1 to ig
-        ihm         scatter from group ig-(ihm-ihs) to ig
-        ihp         total scatter from group g to groups l,...,g-1
-
-------------------------------------------------------------------------------------------
```

B.3 Format VARBND

```
-------------------------------------------------------------------------------------------
-
-   name: varbnd
-
-   purpose:   boundry source and associated interpretation data
-
-   notes:     order of energy groups is by decreasing energy
-              neutrons, then photons.
-
-        i is the first -dimension index.
```

```
-       j is the second-dimension index.
-       k is the third -dimension index.
-       m is the direction index.
-       zero is a word set to zero used in padding to full length.
-
-       mult=l if word length is 8 bytes; mult=2 if 4 bytes.
-
-       When im.gt.O, the mesh is a regular (continuous) mesh with
-       im cells in each row and jm rows in each plane.
-       ism=jsm=ksm=l. ims=im. jms=jm. ima=im.
-
-       When im.lt.O, the mesh is discontinuous. Each plane
-       contains jms rows, where jms=jmbjs(jset(k)). Each row
-       contains ims cells, where ims=imbis(iset(j'k)). (j'k)
-       denotes j + sum of jms(kk) over kk=l, . . ..k-1.
-       ima=iabs(im). ism is the number of i-sets. jms is the
-       number of j-sets.
-
-       When mm.gt.0, mm directions are used in the directional
-       quadrature of flux in each energy group. msm=l. mms=mma.
-
-       When mm.lt.O, the number of directions in the directional
-       quadraturevaries by group. mms=nunbms(mset(ig)) is the
-       number of directions used in group ig. mma=iabs(mm). msm
-       is the number of direction sets.
-
-       mmsdu(ig) is the larger of the number of downward or
-       upward directions for the m-set used in ig. xmndnup is the
-       largest mmsdu for any ig.
-
-       For use by tort, ifbfxi=ifbfxj=ifbfxk=O.
-
-------------------------------------------------------------------------------------------
-
-   file structure:
-
-                  record type                      present if
-                  -----------                      ----------
-                  file identification                always
-                  file label                         always
-                  integer parameters                 always
-                  direction indexing arrays          always
-                  space indexing arrays              always
-                  real arrays                        always
-
-  . . . . . . . . do ig=l,igm
-  .
-  . . . . . . . . do k=km,l,-1
-  . . i-boundary directional data    if ifbfxi.eq.O
-  . . j-boundary directional data    if ifbfxj.eq.O
-  . . . . . . . . enddo on k
```

```
-  .
-  . . . . . do j=l,jm
-  . . k-boundary source, top          if ifbfxk.eq.O
-  . . . . . enddo on j
-  .
-  . . . . . do j=l,jm
-  . . k-boundary source, bottom      if ifbfxk.eq.O
-  . . . . . enddo on j
-  .
-  . . . . . enddo on ig
-
-----------------------------------------------------------------------------------------------
-
-   file identification:
-
-         hname, (huse(i),i=1,2),ivers
-
-         number of words= 4*mult
-
-         hname        file name                    - (a8)
-         huse(i)      user file identification     - (a8)
-         ivers        file version number          - (a8)
-
----------------------------------------------------------------------------------------------
-
-   file label:
-
-         date,user,charge,case,time,(titl(i),i=l,9)
-
-         number of words= 14*mult
-
-         date         as provided by timer option 4     - (a8)
-         user         as provided by timer option 5     - (a8)
-         charge       as provided by timer option 6     - (a8)
-         case         as provided by timer option 7     - (a8)
-         time         as provided by timer option 8     - (a8)
-         titl(i)      title provided by user            - (a8)
-
----------------------------------------------------------------------------------------------
-
-   integer parameters:
-
-         igm,im,jm,km,mm,mmdnup,ism,jsm,imsism,jmsjsm,jmskm,msm,
-         mmsmsm,ifbfxi,ifbfxj, ifbfxk,(idum(n),n=l,9)
-
-         number of words= 25
-
-         igm          number of energy groups
-         im           +/- maximum number of cells in any i-set
-         jm           maximum number of rows in any j-set
-         km           number of planes
```

```
-       mm          +/- maximum number of directions in any m-set
-
-       mmdnup      maximum number of directions down or up in any
                    m-set
-       ism         number of i-sets
-       jsm         number of j-sets
-       imsism      sum of ims over is
-       jmsjsm      sum of jms over js
-
-       jmskm       sum of jms over km
-       mmsmsm      sum of mmbms over ms
-       msm         number of m-sets
-       ifbfxi      .eq.O if i-boundary flux is included, else 1
-       ifbfxj      .eq.O if j-boundary flux is included, else 1
-
-       ifbfxk      .eq.O if k-boundary flux is included, else 1
-       idum        array set to 0
-
-----------------------------------------------------------------------------------------------
-
-   direction indexing arrays:
-
-       (mmbms(ms),ms=l,msm), (mset(ig),ig=l,igm)
-
-       number of words= msm+igm
-
-       mrnbms      number of directions in m-set ms
-       mset        m-set assigned to energy group ig
-
----------------------------------------------------------------------------------------------
-
-   space indexing arrays:
-
-       (imbis(is),is=l,ism), (jmbjs(js),js=l,jsm)
-       , ((iset(j'k),j=l,jms),k=l,km), (jset(k),k=l,km)
-
-       number of words= ism+jsm+jmskm+km
-
-       imbis       number of cells in i-set is
-       jmbjs       number of cells in j-set js
-       iset        i-set assigned to row j in plane k
-       jset        j-set assigned to plane k
-
----------------------------------------------------------------------------------------------
-
- real arrays:
-
-       ((x(i,is),i=l,ims+l),is=l,ism),((y(j,js),j=l,jms+l),
-       js=l,jsm),(z(k),k=l,km+l), (ener(ig),ig=l,igm),emin,eneut,
-       (dumrl(i),i=1,8)
-
```

```
-       number of words = imsism+ism+jmsjsm+jsm+km+l+igm+2+8
-
-       i-interval      boundaries by i-set
-       j-interval      boundaries by j-set
-       k-interval      boundaries
-
-       ener            top energy boundary of group ig
-       emin            bottom energy boundary of group igm
-       eneut           bottom energy boundary of group neut
-                       (0 if neut=O)
-       dumrl           array set to 0.
-
-------------------------------------------------------------------------------------------
-
-  i-boundary source:
-
-       ((fio(m,j),m=l,mms),j=l,jms), (zero,l=l+mms*jms,mms*jm)
-
-       number of words = mms*jm
-
-       fio     i-boundary directional source
-
------------------------------------------------------------------------------------------
-
-  j-boundary source:
-       ((fjo(m,i),m=l,mms),i=l,ims), (zero,l=l+mms*ims,mms*ima)
-
-       number of words = mms*ima
-
-       fjo     j-boundary directional source
-
------------------------------------------------------------------------------------------
-
-  k-boundary source (top or bottom):
-
-       ((fko(m,i),m=l,mmsdu),i=l,ims),
-       (zero,l=l+mmsdu*ims,mmsdu*ima)
-
-       number of words = mmsdu*ima
-
-       fko     k-boundary directional source, downward or upwar-d
-               (for j.gt.jms, fko is filled with zero.)
-------------------------------------------------------------------------------------------
-
-  end
-
```